HYGROMECHANICAL RESPONSE OF FIBRE REINFORCED POLYMERS WITH VARYING FIBRE TOPOLOGIES

By

DEEPAK JAIN

Dissertation submitted to the

DEPARTMENT OF MECHANICAL ENGINEERING
THAPAR UNIVERSITY
PATIALA-147004

Advisory Committee:
Dr. Abhijit Mukherjee
Dr. Naveen Kwatra
Dr. S. K. Mohapatra
Dr. S. P. Nigam
Dr. V. P. Agrawal

Dedication

"If I have been able to see further,
It was only because I stood on the shoulders of giants"
Sir Issac Newton

I dedicate this dissertation to the memories of...

My Father ***Sh. Nath Kumar Jain***
[1940-1991]

My Mother ***Smt. Daya Rani***
[1941-1989]
&
My beloved sister ***Nisha***
[1978-2013]

Your memories will forever linger in my heart and continue to inspire me...

Certificate

DEPARTMENT OF MECHANICAL ENGINEERING
THAPAR UNIVERSITY
PATIALA-147004

This is to certify that the thesis entitled '*Hygromechanical Response of Fibre Reinforced Polymers with Varying Fibre Topologies*' submitted by ***Deepak Jain*** (Regn. No: 950808007) in partial fulfilment of the requirements for the award of Doctor of Philosophy in Mechanical Engineering to the Thapar University, Patiala is an authentic record of research work carried out by him under our supervision and guidance.

To the best of our knowledge, the work incorporated in this thesis has not been submitted elsewhere for the award of any degree.

Dr. Abhijit Mukherjee
Professor, Civil Engineering Department,
Curtin University, Bentley (Perth),
WA 6102, Australia.

Place: Bentley (Perth)
Date: 22-12-2014

Dr. Naveen Kwatra
Assoc. Prof. & Head, Civil Engineering Department,
Thapar University, Patiala,
147004, India.

Place: Patiala
Date: 22-12-2014

Abstract

Title of Document:

HYGROMECHANICAL RESPONSE OF FIBRE REINFORCED POLYMERS WITH VARYING FIBRE TOPOLOGIES

Deepak Jain
Ph.D. (Mechanical Engineering), 2015.

Directed By:

Dr. Abhijit Mukherjee
Professor, Civil Engineering Department,
Curtin University, Bentley (Perth),
WA 6102, Australia.

&

Dr. Naveen Kwatra
Associate Professor and Head,
Civil Engineering Department,
Thapar University, Patiala 147004,
India.

Vulnerability to environmental factors is a major concern for the reliability of fibre reinforced polymers (FRP). Life of FRP composites is limited to a great extent by the type and scale of service and environment factors viz. heat, moisture, mechanical load, alkalinity

etc. The microstructural damage is the initial site of failure. The multi-scale analysis using the computer based finite element methods are becoming increasingly popular. The dissertation presents the micromechanics of FRP composites subjected to diffusion and hygromechanical conditions. A comprehensive analysis is undertaken to analyse the effect microstructural topological arrangement of fibres inside the matrix. To accomplish this several microstructures have been created with the variable topologies. The diffusion process is modelled by Fickian phenomenon. Effect of fibre clustering is reported on the diffusion kinetics. Several algorithms are written to create the microstructures with clustered fibre architectures. A number of statistical measures are employed to quantify the extent of fibre clustering. The statistical measures were helpful to predict the global characteristics of microstructures. The results show that the diffusivity of composites can be controlled through careful design of topology. Stresses due to the transient moisture distribution have been estimated through finite element modelling using appropriate displacement boundary conditions. Some fundamental topologies have been studied. Most important topological parameters have been identified. Utilising the results of fibre neighbourhood, interpretation of large microstructures has been discussed. Considerable interactions among neighbouring fibres can be observed in the stress build up. A major part of this study is conducted considering 2-dimensional microstructures. However the analysis is further extended in 3D to promote the understanding of diffusion and hygromechanical stress behaviour along the fibre axis. The observations should be helpful in designing optimum filament geometry with minimised stress concentration and impeded moisture ingress for improving the durability of FRP's.

Acknowledgements

As I write this acknowledgement to thank all those who helped and supported me during my Ph.D. work, my train of thoughts takes me back to Dec. 2008. I was then working with 'Tata Consultancy Services (TCS) Ltd.'. I returned back to India after a long term project assignment from US on 12th of Dec. 2008. I appeared for the Ph.D. interview on the very next day, got selected and later on joined the Ph.D. programme at Thapar University. It was a tough decision for me as I had already started on the family track and settling down in my industrial career with TCS (that I worked for six years). Passion for research and motivation from my well wishers had a final win and boarded me on the journey of a great experience for next six years. Experience presented itself in varied colours. Happiness, persistence, devotion, hard work, knowledge and skills were accompanied by sadness, anxiety and disappointment. Nevertheless, it was a great experience of incredible intensity that will enlighten me throughout my life.

First and the foremost I wish my sincere gratitude to my supervisor ***Dr. Abhijit Mukherjee*** for his invaluable support and guidance. I am sincerely thankful to him for best judging my potential and providing me an interesting topic according to my ability. I am thankful for his constructive suggestions, problem modelling ideas and meticulous guidance that helped me to improve my ability to communicate, write scientific papers and carry out the meaningful research. His patience, understanding and motivation boosted me up to achieve my goal. I feel honoured to have worked and excelled under his mentorship throughout these years. I am also thankful to ***Dr. Naveen Kwatra*** who lately became my Ph.D. co-supervisor, for his insightful guidance, positive attitude and encouragement throughout my study.

I thank the members of advisory committee ***Dr. S. K. Mohapatra, Dr. S. P. Nigam*** and ***Dr. V. P. Agrawal*** for the feedback and reviews that were given regularly on the monitoring presentations. Their opinions were beneficial for me to improve on my research. I am also thankful to ***Dr. Tarun Nanda*** our Ph. D. Coordinator for his approachability and keeping me informed with all the relevant communications through E-mails and phone. I thank ***Mr. Sandeep Sharma*** for being a very good friend. I approached frequently him to seek his useful suggestions.

The research support provided by ***Indian Institute of Technology, Gandhinagar***-382424 (India) under its faculty fellowship program (SRIP-2013) during the summer of 2013 is gratefully acknowledged.

From the core of my heart, I thank my wife ***Samriti***, my charming son ***Sambhav*****,** my sisters ***Deepika, Veena, Prabha, Rashmi*** and ***Nisha*** and my parents-in-law ***Smt. & Sh. Shiv Kumar Jain*** for their never ending love, support and encouragement. I am especially thankful to my wife Samriti who acted selflessly to resign from her job for looking after Sambhav and his studies single-handedly. This immensely helped me to relieve from many household duties and focus on the research work since last couple of years. The joy I derive from the company of my son 'Sambhav' cannot be quantified. The analogy he gives on moisture diffusion in circular FRP's with the synthesis Rasgullas and all those tender and naive comments on my work kept me amused and enlightened. Thank you both to bear with me all through these six long years. I feel bestowed with the love and affection I get from my sisters, especially 'Veena Didi' who holds a special place in my life for raising me up selflessly after my father and mother. Space will not permit me to mention all the names of friends and families that have been a source of support to me in this journey. However, their kindness is greatly appreciated.

I thank '*The almighty* ***God*****'** for giving me strength, endurance and patience to achieve my goal.

Last I pay the heartfelt tributes to my beloved sister ***'Nisha'*** whom we lost on 23rd of sep. 2013. We grew up together and she always wished for my well-being. The Life of *Nisha* was cut short by cancer. Her dignity, strength, courage and above all that heart-warming 'angelic smile' will remain in my memories forever.

Deepak Jain

Contents

Nomenclature

Symbol	*Description*	*Units*
C	Mass Concentrations	%
D	Mass Diffusivity	m^2/s
ε_h	Hygral Strain	-
β_h	Coefficient of Moisture Expansion	m^3/g
μ, ν	Poission's Ratio	-
ζ	Shear Stress	MPa
M_∞	Saturation Mass	Mol
$\vec{J}$	Mass Flux Vector	Mol/s
$U_{1,2,3}$	X, Y and Z-components of Displacement	µm
K	Thermal Conductivity	$W\ m^{-1}\ K^{-1}$
C_P	Heat Capacity at Constant Pressure	$J\ kg^{-1}\ K^{-1}$
V_f	Fibre volume Fraction	-
V_m	Matrix Volume Fraction	-
σ_h	Hygral Stress	MPa
Δl	Mesh Element Size	µm
D_{eff}	Effective Diffusivity by Rule of Mixture	m^2/s
P	Mass Density	Kg/m^3
M_t	Mass at Time Instance (t)	Mol
Φ	Normalized Moisture Concentration	-
R	Fibre Radius	µm
Θ	Inter Fibre Angle	°
D	Inter Fibre Distance	µm
A_f	Cross-section area of Fibre	μm^2

Abbreviations

Abbreviation	*Expansion*
ACD	Average Cluster distance
AND	Average Neighbourhood
CCA	Concentric Cylinder Assemblage
FEM	Finite Element Method
FRP	Fibre Reinforced Polymer
OD	Ordered Fibre Arrangement
RMG	Random Microstructure Generation
RN	Random Fibre Arrangement
RVE	Representative Volume Element
UCM	Unit Cell Modelling

List of Figures

List of Tables

Chapter 1: Introduction

1.1 Background and motivation

The reinforced composites are being used in versatile engineering applications. Structural, marine, aerospace, wind energy and automobile are few such industries that have a wide usage of these materials. Apart from their superior Strength to weight characteristic the 'design flexibility' is an additional benefit presented by the composite materials. With the freedom to create wide array of shapes from 'simple to complex' by changing the reinforcement direction and volume fraction these materials can be easily tailored to suit the purpose.

Amidst the rising popularity of the fibre reinforced polymer (FRP) composites, there remain wider concerns about their vulnerability to the environmental factors. During their service life the composite materials are subjected to different loading and environmental conditions viz. Thermal (cyclic, freeze-thaw), moisture, alkalinity, fire etc. The synergistic effects of several environments can exacerbate the effect of individual environmental factor. As an example, the absorbed moisture causes temperature to have more severe effect as moisture. This is because the moisture diffuses through the gaps between polymeric chains and causes many irreversible changes into the polymeric structure. The setting of these defects during the working conditions leads to substantial loss of thermo-physical, mechanical and chemical properties. This in turn affects the long term durability of the composites. The inability of composites to deform plastically results in

energy absorption via the creation of matrix cracks and de-lamination. The principal mechanisms of failure in fibre-reinforced composites are:

- Matrix Cracking
- Fibre-Matrix Debonding: Debonding is separation of the fibre from the matrix.
- Delamination: Delamination is the failure mode in which cracks propagate between the layers (lamina) of the composite.
- Fibre Fracture: Fibre fracture is failure of the reinforcement and normally occurs across the diameter of the fibre.
- Fibre Pullout
- Micro-buckling
- Kink Bands
- Cone of Facture

Alongside the experimental studies it becomes important to develop and use the alternate capabilities of predicting the response of these materials. The computer based numerical methods are getting popular to simulate the response of composites for their numerous advantages. Apart from saving time and cost, the multi-scale analysis can be performed using different homogenization techniques. Coupling both linear and non-linear micromechanics with finite element analysis presents a powerful tool to analyse the local behaviour. Numerous micromechanical theories have been developed and utilized to calculate effective properties of a heterogeneous media and predict both elastic and inelastic response. Micromechanics is a recognized a tool to forecast the macroscopic constitutive response of heterogeneous composite microstructures. For a given macroscopic loading condition and constitutive properties, the objective is to measure the localized damage. The possibility to incorporate damage

processes and associated progressive degradation of the constituent properties has offered the researchers a good flexibility in choosing damage parameters (Bonora and Ruggiero, 2006; Ghosh *et. al.,* 2007; Mishnaevsky and Brøndsted, 2007; Böhm, 2012). Since the mechanical behaviour is modelled as a continuous mass (in absence of space and discontinuities), most of the times the micromechanics is also referred as 'Continuum Micromechanics'. The continuum micromechanics are studied following the different methods. These methods are broadly classified as Analytical and Numerical approaches. Many analytical micromechanical models exist from the simplest bounding methods (Voigt and Reuss) to complex yet more accurate mean field methods of homogenization (Hashin-Shtrikman, Eshelby, Mori-Tanaka, composite cylinder assemblage (CCA) etc.). Within a restricted realm of application each approach has its obvious strength and weakness (Jacob, 2012). On the other hand a numerical approach is more accurate yet computationally intense way to solve the micromechanics problems. The increase in computational and therefore numerical resources allows considering periodic homogenizations. These periodic homogenizations are also called representative volume element (RVE). The RVE captures close microstructure and represents the topological arrangement of the different phases. A numerical approach in general considers a single representative volume element (RVE). The appropriate load and boundary conditions are applied to approximate the macroscopic response.

The variation of reinforcement architecture has a great influence on the residual strength and damage mechanism of the reinforced polymer composites. At the time of fabrication, the final fibres layup is influenced by the manufacturing technology, resin flow, mould

geometry, applied pressure etc. Lack of manufacturing control results in the formation of resin rich zones due to fibre clustering. This in turn contributes to the variability of bulk properties.

In presence of geometric topology variations it becomes necessary to analyse the effect of fibre orientations to characterize the fibre matrix system. The present work studies the effect of microstructural fibre arrangement on the moisture diffusion and mechanical (Moisture induced stresses) response of FRP composites. A dedicated effort is made to simulate and interpret the diffusion and hygromechanical characteristics of different fibre matrix architectures at various length scales. The work presented in this thesis is carried out to accomplish the following objectives:

1. Perform spatial characterization of composite microstructure.
2. Study moisture diffusion response of different classes of microstructure.
3. Study mechanical response of different classes of microstructure.
4. Evaluate combined mechanical and moisture diffusion response

The proposed micromechanical models integrate various aspects of geometry of microstructures, diffusion mechanism, hygromechanical behaviour at different length scales. This should be helpful to describe the local behaviour and predict the overall system response with time. The in-house codes are written for the automatic generation of different microstructures. It takes into account the arrangement of fibres (Ordered, random and clustered). Solutions are implemented in FE software.

1.2 Outline of the thesis

The remainder of this thesis is organized as follows:

Chapter 2 is an extended review of literature that includes the studies related to hygromechanical behaviour, qualitative and quantitative characterization of composites and micromechanical modelling techniques. The application of micromechanical theories to solve the heterogeneous media problems comprising two or more phases with different materials is also discussed.

Chapter 3 discusses the finite element governing theories. Expressions are discussed for finite element stress-strain relationships and Fick's law of diffusion. These theories are utilized in subsequent chapters while evaluating the microstructural response.

In *Chapter 4* a detailed micromechanical diffusion modelling framework is presented. The analysis begins by taking simplistic single fibre and neat resin models. Fickian diffusion is simulated along the two-dimensional models using FEM. The fibre and Matrix are modelled explicitly. The influence of fibre and its neighbourhood is discussed on the diffusion response in terms of moisture evolution. The results lead to identification of neighbourhood topologies for the better diffusion response. The results show that the diffusivity of composites can be controlled through careful spatial design of filaments.

Chapter 5 reports the moisture propagation inside the clustered fibre-matrix architectures. The algorithms are to generate the random and uniform architectures are discussed. The novel heuristics are presented for the faster generation of clustered fibre matrix microstructures. For a quantitative characterization of microstructures, the different statistical descriptors of clustering are proposed. The statistical measures that depict the global characteristics of the microstructure are found to have a better correlation with time to saturate the representative volume element.

Chapter 6 presents the micromechanical stresses inside the composite due to the fibre topology. Stresses due to the transient moisture distribution have been estimated using a finite element model. Some fundamental topologies have been studied. Most important topological parameters have been identified. Utilising the results of fibre neighbourhood, interpretation of large microstructures has been discussed.

Chapter 7 reports an extended analysis of composites by 3-dimensional moisture diffusion followed by stress behaviour. A three-dimensional (3D) micromechanical model is developed to study diffusion both across and along the fibre. The well-known 2D plane strain condition is modelled and validated as a special case of the 3D model. The utility of 3D modelling is further demonstrated to analyse the stress along the fibre length. It is demonstrated that the variation of boundary conditions along the fibre length has a dramatic effect on the stresses.

Major conclusions of this thesis are given in *chapter 8*.

Chapter 2: Literature Review

This chapter presents the background of the issues and objective that are taken up in this thesis. The relevance of present study is also emphasized. The present study deals in various aspects of environment effects on polymer composites with a special reference to their hygromechanical characteristics. This review includes the available research reports:

- On the failure of composites due to environment exposure
- On the moisture diffusion inside polymer composites
- On the stresses due to the hygromechanical loading
- On the effect of microstructural fibre distribution
- On the geometric characterization of microstructures
- On the modelling and simulation procedures

2.1 Failure of composite due to environment exposures

A composite material is required to perform under versatile conditions of tensile, compression, shear, impact and flexural loadings under different surrounding environments. While under tensile loading the major part of load is borne by high modulus fibres and they tend to fail first. It further leads to evolution of localized stress fields due to significant mismatch between the mechanical properties of the fibre and matrix. This mismatch leads to stress localization in composites (Lee and Peppas, 1993; Ray, 2006; Romanov *et. al.,* 2013) and lead to matrix cracking. The reverse happens in a brittle system where the matrix starts cracking at low stress levels. With an increase in the load, the matrix becomes fully saturated with cracks and sheds the entire load to the fibres (Murthy *et. al.,* 1997). The exposed resins are

susceptible to microcracks at the early stages of service loading (Gamstedt and Andersen, 2001; Karbhari *et. al.,* 2003). These microcracks act as precursors to other forms of damage such as Matrix Delamination, Fibre fracture and Fibre-Matrix Debonding due to the lack of plastic deformation characteristics. Due to the cyclic nature of service loads these microcracks coalesce and increased crack displacements reduce the resin to a fragmented state (Yang and Cox, 2005). The fibre fracture occurs with the further accumulation of damage whose shape depends upon the interfacial strength. A weak interface may result in broom-failure whereas a strong interface results in much planar surface (Gamstedt and Sjögren, 1999). Apart from the discussed failure elastic and plastic Micro-buckling of fibre and Kink-band formations are the failure mechanism under compression (Edeson *et. al.,* 2010; López and Pellegrino, 2012). The matrix allows fibres to micro-buckle that lead to strain softening and the bulk of the system drops to lower energy state. Most of the times there are multiple criterions of failure under mechanical loads acting in combination. Thus, the failure analysis under mechanical loading is a complex field.

Thermal exposures are also the usual service conditions. The curing process of polymers and thermal cycling environments can induce thermal stress and strain. It alters the mechanical properties when one substrate is bonded to stiffer elastic substrate (Loh *et. al.,* 2005; Boualem *et. al.,* 2011). Hygrothermal effects induce the residual stress (Kundu *et. al.,* 2007). The residual stress can lead to damage and de-bonding and thus affect the durability of composites. Exposure to lower temperatures may cause brittleness whereas higher temperatures lead to decrease in modulus because of thermal

softening (Ray, 2006). In epoxy resins the glass transition temperatures is the point at which polymer goes from glassy solid to rubbery solid. At higher temperatures, the polymers go through glass transition and lose their semi-crystalline nature. It is mainly the susceptibility of resin to deteriorate under the described conditions has hindered their wider use especially in the outdoor applications.

2.2 Diffusion mechanism in polymer composites

The mass transfer is due to random molecular motion and it is independent of the state of the phase (liquid or gaseous) (Crank, 1956; Sahimi, 1994). In the non-steady state conditions, the concentration of diffusing mass goes up with the time. The mass due to water builds up due to the exposure to moist environment. The driving force is concentration gradient. In this work the term "absorption" is used to describe the process of moisture (vapours + liquid) diffusion due to the exposure to humid and wet environments. In many cases the term "adsorption" has been used to exactly describe the same content especially in case of porous materials (Lin et. al., 2006; Wu *et. al.*, 2014) where water vapours gets adsorbed on the wall surface of pores due to the capillarity. In composites, the moisture diffusion is mainly inside the resin. This is due to the space available between the polymeric chains. Flux is the mass of water particles crossing the unit cross sectional area per unit time. The traditional diffusion theories are applied in mass transfer analysis assuming that medium is homogeneous, whereas the fibres are generally hydrophobic. Fick's law of diffusion is arguably and important and most common method in analysing the moisture diffusion inside the composites (Vaddaddi *et. al.,* 2003(a,b); Tang *et. al.,* 2005; Loh *et. al.,* 2005; Boukhoulda *et. al.,*

2006; Wang *et. al.* 2006; Youssef *et. al.,* 2008; Karalekas *et. al.,* 2009; Joliff *et. al.,* (2012, 2013)). The law is applied under a set of assumptions related to constituent properties. The Langmuir model represents a wider class of diffusion phenomenon in comparison the Fick's model. The Langmuir model considers the free and bound phases of water molecules (Carter and Kibler, 1978). The Langmuir model considers the physiochemical changes due to moisture absorption. A free to move molecule becomes a bonded molecule due to reversible chemical reaction. This results in faster absorption at the earlier time history and a delayed absorption during the later time intervals. In such circumstances, Langmuir model captures moisture uptake more accurately.

2.3 Stresses due to hygromechanical loading

Although fibre reinforced polymers (FRP) are generally durable, exposure to moisture and temperature can limit their lives considerably. It was pointed out in the early days of development of FRPs that their moisture and temperature sensitivity are resin dominated and they can lead to a change in failure mode, while fibre dominated properties show very little environmental sensitivity (Whitney, 1978). The polymer matrix absorbs moisture and tends to swell. The fibres, on the other hand, remain largely unaffected by moisture. Thus, interfacial stresses develop in the FRP causing deformation. Alternating wetting and drying accelerates ageing of FRP. Moisture distribution inside any composite structure can prove harmful as it leads to altered stress states because of matrix plasticization, degraded interface strength and mechanical properties of the constitutive materials (Tang *et. al.,* 2005; Yagoubi *et. al.,* 2012).

It can also cause stress build-up due to significant mismatch in the moisture induced volumetric expansion between the matrix and the fibres (Lee and Peppas, 1993). Sometimes moisture may carry deleterious matters that attack the fibre causing severe damages (Fig. 2.1) (Mukherjee and Arwikar, 2005a,b). Such concerns have hindered the wider use of composites in construction industry.

Fig. 2.1. Damage in FRP bars in concrete after 12 months in hot water bath (Mukherjee and Arwikar, 2005b)

The effect of moisture diffusion on the stresses is mostly identical to the thermal stresses. Effective diffusivity calculations have been reported (Bond, 2005; Li, 2002; Vaddadi *et. al.,* 2003b) and the suggested parameters are used to compute the mechanical stresses.

2.4 Effect of microstructural fibre distribution

It is generally believed that a well-controlled manufacturing process would ensure uniform fibre distribution and optimum performance. However, some topological variation is inevitable and allowable tolerances for the intended performance must be ascertained. Fig. 2.2 illustrates various composite micrographs that exhibit different fibre topologies reported in literature. In these manufactured specimens different geometrical patterns can be attributed to the chosen manufacturing procedures. Thus, estimation of moisture diffusion and

stresses in presence of topological irregularities is imperative for ensuring the design life performance of the composites.

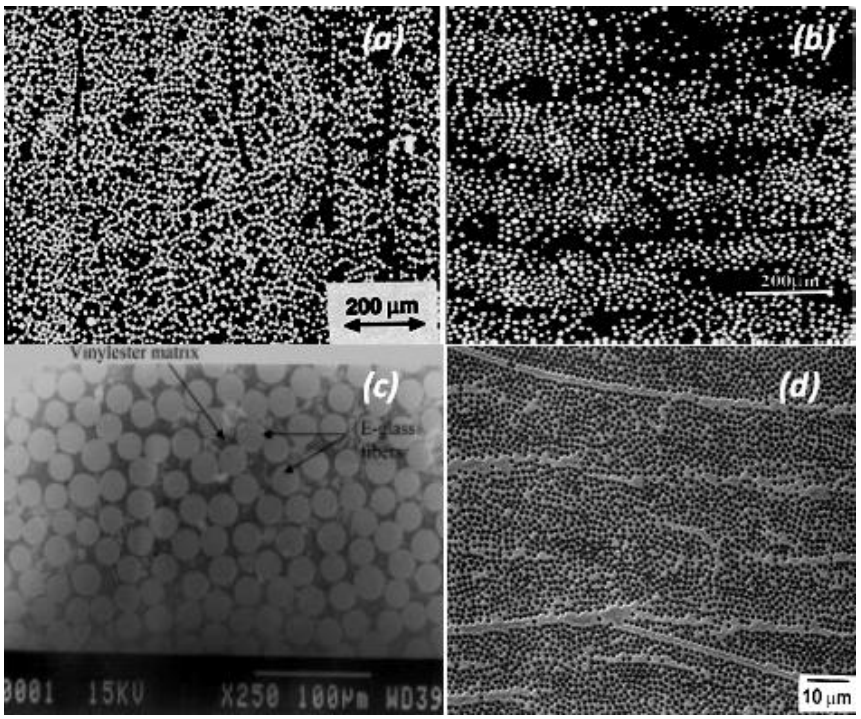

Fig. 2.2. Topological variation in microstructures (a) Resin pockets (Boccaccini et. al., 1998) (b) Fibre segregation (Shan and Gokhale, 2002) (c) Dense packing with occasional matrix damage (Mukherjee and Arwikar, 2005b) (d) Resin flow channels (Ramamurty and Seshacharyulu, 1999)

There are a few prior reports on the effect of reinforcement topology on particle reinforced composites (Steglich *et. al.,* 1999; Segurado *et. al.* 2003; Chawla *et. al.,* 2006). Understandably, the microstructural aspects, such as fibre fraction, size, shape, and distribution play an important role in the ageing process.

Effect of fibre distribution was found to be quite significant when fibres are in contact (Joliff *et. al.,* 2012). It is also pointed out that the polymer and the filament develop an interphase that has considerably higher diffusion than the bulk resin (Joliff *et. al.,* 2013). If a diffusion coefficient based on rule of mixture is used, fibre tortuosity is observed

to considerably alter the diffusion rate of a composite from Fickian predictions, especially at large moisture concentrations (Tsai *et. al.,* 2009).

Geometry variations viz. Fibr orientation, aspect ratio, and boundary conditions play an important role on these characteristics (Singh and Verma, 2009). Interfacial degradation due to hygral and thermal effects has been investigated in unit cells with uniformly arranged fibres (Lee, 2000). Among several notable ways to study the effect of different fibre arrangements, regular fibre arrangements namely the hexagonal and the square are the fundamental models (Curtin and Takeda, 1998; Jiang *et. al.,* 2002; Biwa *et. al.,* 2004; Fiedler *et. al.,* 2006; Thomas *et. al.,* 2008). Statistically equivalent representative volume elements (RVE) with random and clustered arrangement have also been attempted (Kondo and Taki, 1982; Lee *et. al.,* 2000; Vaddadi *et. al.,* 2003a; Hrach *et. al.,* 2006; Fiedler *et. al.,* 2006; Thomas *et. al.,* 2008).

2.5 Geometric characterization of microstructures

An essential quality of the chosen statistical approach is that it should closely capture the non-homogeneity in distribution through study of key topological aspects viz. fibre layout, randomness of arrangement, fibre clustering etc. Nearest neighbour statistics, Poisson point distribution, Voronoi tessellations have been extensively used for quantitative characterization of different types of microstructures. Following are some notable works in this area:

- Two dimensional shape and geometrical locations have been shown as the variants for automated clustering classification (MacSlyene *et. al.,* 2008) whereas composite samples of varying strength and

type of clustering were analysed by developing functional shape, size and volume fraction metrics (Okabe and Takeda, 2002; Wilding and Fullwood, 2011).

- The clustered microstructures were used for quantitative analysis of physical property relationship in composites when subjected to elastic (Okabe and Takeda, 2002; Segurdao *et. al.,* 2003; Raghavan *et. al.* 2004; Sevostianov and Kushch, 2009; Vaughan and McCarthy, 2011), thermal (Okabe and Takeda, 2002; Sevostianov and Kushch, 2009; Vaughan and McCarthy, 2011), diffusion (Carter and Kibler, 1978; Bond 2005; Boukhoulda, 2006) and Electric (Ramamurty and Seshacharyulu, 1999) fields.
- Heterogeneity of fibre distribution has been characterized by the coefficient of variation (C_v) of the centre-to-centre distances between interacting fibres and correlated with mechanical stress field (Pyrz and Bochenek, 1998) and moisture induced damage parameter (Abhilash *et. al.,* 2011) where a cut-off radius around a fibre is employed to define the neighbourhood .
- Voronoi cells and Dirchlet tessellations have been used for quantitative characterization of different cluster models representing directional fibre-matrix composites (Ghosh *et. al.,* 1996; Raghavan *et. al.,* 2004; Ghosh *et. al.,* 2007). In all these investigations a random fibre distribution has been considered.

2.6 Modelling & simulation methods

Now a day most of the physical effects viz. mechanical, thermomechanical, hygral, chemical etc. are simulated employing the suitable set of governing equations to the multi-scale problems (Meso, Micro or even Nano structural levels).

Meanfield and periodic microfield studies are the fundamental modelling approaches for the composite materials. A meanfield approach averages out the properties but ignores the fibre distribution (Böhm and Rammerstorfer, 1993). Various averaging mean field theorems normally assume a random and homogeneous reinforcement distribution and provide the volume averaged stress and strain fields.

A periodic microfield approach on the other hand assumes that the reinforcements are placed at prescribed (periodic) locations in space. The macroscopic properties are determined from the numerical or analytical simulation of the mechanical response of a representative volume element (RVE) having proportionate volume fraction of the constituents. Periodic boundary conditions are employed to respect the microstructural symmetries (Noda *et. al.,* 2005; Bonora and Ruggiero, 2006). Therefore the periodic microfield approach can be regarded as a more detailed investigational approach in terms of the topological fibre distribution (Böhm *et. al.,* 1993). Unit cell method, Random and periodic microstructures, cohesive zone model are some of the popular microfield approaches.

Unit cell Modelling (UCM) is a simplistic modelling approach that studies the effects of shape, and fibre volume fraction. Assuming a periodic arrangement of voids, fibres or particles, the unit cells can be constructed with different shapes (e.g. square, circular, hexagonal, etc.) and differently positioned inclusions in a representative volume element (RVE). Micromechanical unit cell models have been widely applied to the analysis of the composite failure under the tensile

loading along the fibre direction, or off-axis loading (Zhang *et. al.,* 1997; Benzarti *et. al.,* 2001; Haj-Ali and Kilic, 2003; Zulkifli, 2009; Vaughan and McCarthy, 2011). For the non-homogeneous materials like composites while numerical prediction of the parameters representative volume element can be taken (RVE) to represent the approximate volume (or area) fraction of the constituent parts which is typically equivalent to a unit cell (Segurado and LLorca, 2006; Li *et. al.,*2010). Fig. 2.3 shows the typical representative volume element (RVE) that considers different arrangement of circular fibres inside the resin. All the four RVE's are statistically identical with a fibre volume fraction (V_f) of 0.4 (or 40%) but geometrically different. One quarter of the region around the circular fibre having similar fibre volume fraction can considered as a unit cell. In order to model a field problem with the unit cell, the boundary conditions can be set in manner that the compatibility of the unit cell with neighbouring cells in the infinite composite can be satisfied.

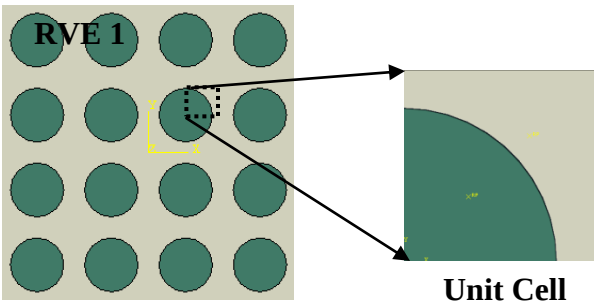

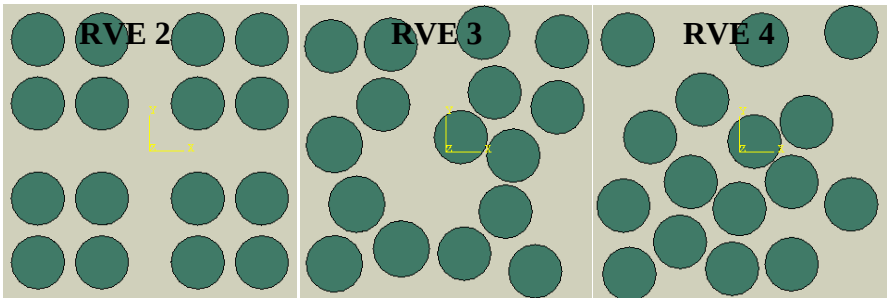

Fig. 2.3. Illustration of a typical 2 dimensional RVE's with different fibre arrangements and a unit cell

Depending on the arrangement of fibres the unit cells can be constructed with various shapes. The effect of thermal residual stresses in composites was modelled was modelled (Tsai and Chi, 2008) considering different fibre packings and then choosing an appropriate unit cell from different fibre arrays (Fig. 2.4).

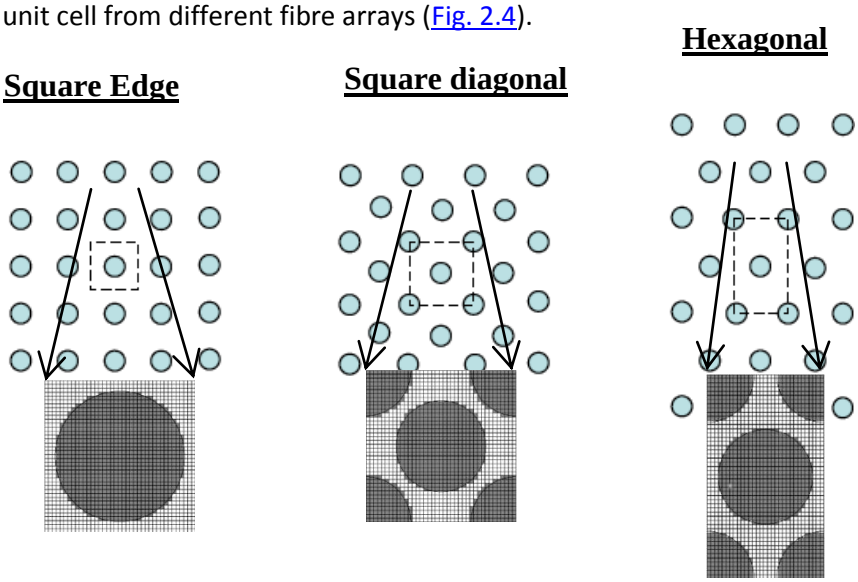

Fig. 2.4. Different fibre packings and corresponding unit cells (Tsai and Chi, 2008)

Many a times the 3-dimensional axi-symmetric cylindrical unit cells are used along with 2-dimensional unit cells to extend the study under three dimensional loading conditions (Kuna and Zun, 1996; Noda and Nisitani, 2005).

In case the shape and topology of inclusions is changed the results given by unit cell models may vary drastically. Therefore it is very important to clarify the effect of topology in a close if not real microstructure. In order to model the two phase composites, the effect of topology is studied by choosing representative volume

elements with periodic and random fibre inclusions. This approach provides full control of the constituent properties, spatial distribution and loading to assess the validity of the failure criteria (Mishnaevsky and Schmauder, 2001).

FRP's are being increasingly prepared outdoors such as in construction sites using hand layup technology where controlling the fibre arrangement can be challenging. Hence the fibre distribution is often clustered in composites leading to resin rich areas. These areas can be potential nucleation sites of moisture diffusion. It is important to understand the moisture diffusion through clustered microstructure to realistically estimate the life of such composites. To study the effect of clustering it is important to have microstructures with various clustering characteristics. Synthetic microstructures can closely replicate the real ones and at the same time can reproduce the desired clustering characteristics. In addition to statistical conformance the algorithm must be efficient in computation time. In order to generate the random fibres architecture simple random microstructure generation (RMG) algorithms work well up to a fibre volume fraction around 0.5. The modified RMG based on specially developed heuristics is able to generate random distributions with high fibres volume fractions (Melro *et. al.,* 2008). Strauss hard-core model (Pyrz, 1994) is equally popular in getting a uniform statistical distribution by maintaining certain minimum distance when the fibre volume fractions is limited to around 0.5 (Melro *et. al.,* 2008; Sevostianov and Kushch, 2009). Once a random microstructure is generated, it can be used as a starting point for generating representative clustered arrangements through controlled fibres movement.

In order to determine the effect of clustering, the clustered microstructures are modelled often by choosing different cluster shapes. The shape of the clusters is by and large decided by the requirement of the analysis. A variety of cluster structures such as line, circular, string or chain, and elliptical have been reported (MacSleyne *et. al.,* 2008; Sevostianov and Kushch, 2009; Wilding and Fullwood, 2011). In general, the architecture is controlled by randomly seeding centre points of the clusters followed by addition of new fibres around these centres. Composite samples of varying strength and type of clustering have been analysed by developing functional shape, size and volume fraction metrics (Okabe and Takeda, 2002; MacSleyne *et. al.,* 2008).

2.7 Summary of literature and research gap

From the studied literature it is concluded that it is matrix which is more susceptible to the deterioration under the moist environments. The diffusion and resulting stresses in a fibre-matrix system vary considerably with the topology and clustering of the fibres inside the polymer matrix. Thus it becomes imperative to study the effect of final fibre arrangements on the overall behaviour of FRP composites when they are subjected to service conditions. There are several gaps in the available literature which are summarized as follows:

(i) In several available literatures the effect of topology is studied adopting unit cell, periodic microfield and regular/random neighbourhood microarchitectures. There doesn't exist any topological models which analyze the effect of parameters viz. neighbourhood orientation/density/inter fibre gaps in a smaller localized field.

Adopting such approach should be helpful in understanding the effect of local microstructure in a more detailed manner.

(ii) The effect of fibre clustering is reported mainly in context of mechanical and thermal loading conditions, but there doesn't exist much literature on the effect of clustering over the hygromechanical response.

(iii) Although a number of statistical measures exists to characterize the microstructure. They have largely been used to describe the microstructure in the elastic fields. The existing and new statistical measures can be used to microstructure characterization and correlate it with mass diffusion characteristics.

Chapter 3: Finite Element Governing Theories

The finite element framework is employed to model diffusion and hygromechanical response. The material behaviour is studied for two phase composites at the microstructural level. The micromechanical behaviour is studied choosing appropriate for the considered microstructures subjected to various loading and boundary conditions.

3.1 Ficks's law of diffusion

For most of the fibre-reinforced polymer composites, diffusivity of the fibre is negligible as compared to that of the polymer matrix. Hence, it is entirely appropriate to consider moisture transport occurring only in the matrix. The moisture diffusion inside reinforced polymers can be attributed to the presence of either liquid or water vapour in respective wet or humid service conditions.

The Darcy flow is found more suitable at nano scale pores (Vlahinić *et. al.* 2012). In the micro scale models the Fick and Langmuir models are preferred. Most of the works in diffusion kinetics are based on either Fickian or Langmuir models. The majority of the models for diffusion kinetics in composite materials (Vaddaddi *et. al.,* 2003(a,b); Tang *et. al.,* 2005; Loh *et. al.,* 2005; Boukhoulda *et. al.,* 2006; Wang *et. al.,* 2006; Youssef *et. al.,* 2008; Karalekas *et. al.,* 2009; Joliff *et. al.,* (2012, 2013)) are based on Fick's law that states moisture sorption is a diffusion mechanism at a constant rate and constant solubility. Since the effort of this work is towards the effect of fibre topology and a majority of this thesis is dedicated to effect of fibre placement and clustering on

the diffusion and related stresses. Therefore a simplified Fick's model based on the restrictive assumption of constant diffusivity has been used. In the current work Fick's law of diffusion is applied under various set of assumptions.

Under the moisture boundary conditions diffusion is simulated through reinforced composites with one of its edges suddenly exposed from dry state to the ambient moisture (C_{amb}) that is maintained throughout the time of diffusion. The assumptions are:

1. The moisture diffuses through the gaps in polymer structure.
2. The mass transfer in the composite is due to exposure to the humid environment that results in concentration gradient across the plane.
3. The diffusivity of the fibre and the matrix remains unaffected during the moisture diffusion process.
4. The maximum moisture concentration in the entire domain does not exceed the concentration at the exposed edge (saturation concentration).

Fick's second law can be used to predict the change of mass concentration (C) of a diffusing material in time and space for a given diffusivity (D) of the medium and flux vector $(\vec{J})$. It represents a non-steady state diffusion. The governing equation for mass diffusion is:

$$\partial C/\partial t + \nabla.\vec{J} = 0 \tag{3.1}$$

Where ∇ is the generalized gradient operator. In steady state $\vec{J}$ does not change with time. When Eq. (3.1) is applied to inhomogeneous fibre-matrix regions, mass concentration (C) is not continuous across the interface between two different materials (Tang *et. al.,* 2005). To overcome this problem, the concept of normalized moisture concentration ϕ is used for composite material systems to maintain the interfacial continuity.

$$\phi = C/C^{\infty} \tag{3.2}$$

Here C^{∞} is the saturation mass concentration of the diffusing material within a particular material. Fick's first law combined with Eq. (3.1) and Eq. (3.2) can be solved by implicit finite element scheme with the normalized concentration as basic field variable. According to Fick's first law

$$\vec{J} = -D\frac{\partial C}{\partial x} \tag{3.3}$$

Taking D_m as diffusivity of matrix resin, and The Eq. (3.1) can be rewritten as in the form of 2nd order partial differential equation

$$\frac{\partial c}{\partial t} = D_m \frac{\partial^2 c}{\partial x^2} \tag{3.4}$$

Fig. 3.1 shows the schematic of a reinforced polymer domain exposed to the moisture. The initial and boundary conditions for moisture exposed surfaces are $C = 0 \quad (0 < x < a, \forall t = 0)$ and $= C_a \quad (x = 0, \forall t > 0)$ respectively. Rest of the edges in Fig. 3.1 are assumed as impermeable boundaries.

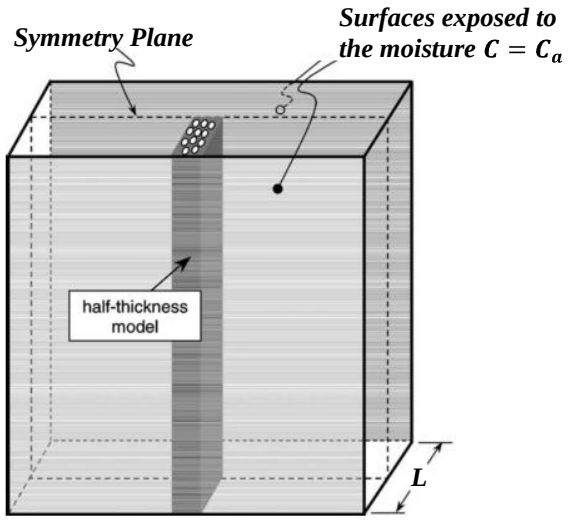

Fig. 3.1 Boundary conditions of a composite laminate subjected to humid environments

Under the restrictive assumption that diffusivity remains unaffected with moisture content, the solution to the Fickian equation under the boundary conditions described in Fig. 3.1 is given by (Jost; 1960)

$$\frac{c(t)-c_i}{c_a-c_i} = 1 - \frac{4}{\Pi}\sum_{j=0}^{n} \frac{1}{(2j+1)} sin\frac{(2j+1)\Pi x}{L} e^{\left[-\frac{D_m(2j+1)^2\Pi^2 t}{L^2}\right]} \quad (3.5)$$

Here *L* is the specimen thickness. *C(t)* is absorbed moisture % at time instance *t* and C_a, C_i are the ambient moisture and initial moisture concentration (if any) inside the specimen.

Since it is not possible to measure the moisture concentration at a point experimentally, the above expression is integrated over the area and the fractional mass uptake of the as a function of time as given by (Shen and Springer, 1976):

$$\frac{M_t}{M_\infty} = 1 - \frac{8}{\Pi^2}\sum_{n=0}^{\infty} \frac{1}{(2n+1)^2} e^{\left[-\frac{D_m(2n+1)^2\Pi^2 t}{L^2}\right]} \quad (3.6)$$

Here M_t is the mass of moisture after absorption time *t* and M_∞ is the mass of saturated lamina. Eq. (3.6) implies that the moisture mass of the matrix part exposed to a humid environment obeys an asymptotic behaviour, for which a saturation state exists. An approximation to equation (3.6) is given by the expression in following form (Jiang *et. al.,* 2012; Eslami *et. al.,* 2014)

$$M_t = M_\infty \left\{1 - e^{\left[-7.3\left(\frac{Dt}{L^2}\right)^{0.75}\right]}\right\} \quad (3.7)$$

Eq 3.8 thru Eq. 3.10 are the corresponding equations applicable for three-dimensional diffusion:

$$\frac{\partial c}{\partial t} = D_m\left(\frac{\partial^2 c}{\partial x^2} + \frac{\partial^2 c}{\partial y^2} + \frac{\partial^2 c}{\partial z^2}\right) \quad (3.8)$$

Here $\partial c/\partial x$, $\partial c/\partial y$, $\partial c/\partial z$ are the concentration gradients in the orthogonal axes.

$$\frac{c(t)-c_i}{c_{amb}-c_i} = 1 - \frac{64}{\pi^3}\sum_{i=0}^{\infty}\sum_{j=0}^{\infty}\sum_{k=0}^{\infty} \frac{(-1)^i(-1)^j(-1)^k}{(2i+1)(2j+1)(2k+1)} \boldsymbol{X}$$

$$\cos\frac{(2i+1)\Pi x}{a}\cos\frac{(2j+1)\Pi y}{b}\cos\frac{(2k+1)\Pi z}{c} \boldsymbol{X}$$

$$e^{\left[-\pi^2 t D_m\left(\left(\frac{2i+1}{a}\right)^2+\left(\frac{2j+1}{b}\right)^2+\left(\frac{2k+1}{c}\right)^2\right)\right]} \quad (3.9)$$

a, b, c are characteristic dimensions of 3D diffusion space along x, y, and z. The weight gain is calculated by the volume integration of Eq. 3.9. It results in the fractional mass uptake (Shen and Springer, 1976):

$$\frac{M_t}{M_\infty} = 1 - \left(\frac{8}{\Pi^2}\right)^3 \boldsymbol{X}$$

$$\sum_{i=0}^{\infty}\sum_{j=0}^{\infty}\sum_{k=0}^{\infty}\frac{1}{\left((2i+1)(2j+1)(2k+1)\right)^2} e^{\left[-\pi^2 t D_m\left(\left(\frac{2i+1}{a}\right)^2+\left(\frac{2j+1}{b}\right)^2+\left(\frac{2k+1}{c}\right)^2\right)\right]} \quad (3.10)$$

3.2 Hygromechanical stress-strain relationships

The moisture diffusion results in hygroscopic swelling. The induced body forces results due to expansion results in volumetric stresses. The analogy between the moisture diffusion and heat conduction laws can be exploited during the stress analysis. The hygral strain is assumed linearly proportional to moisture concentration:

$$\boldsymbol{\epsilon_h} = \beta_h C \quad (3.11)$$

Where $\boldsymbol{\epsilon_h}$ is the hygral strain tensor and β_h (mm^3/g) is the coefficient of moisture expansion. Eq. (3.1) can be solved at discrete time intervals with sufficiently small time steps. The generalised body forces due to moisture expansion can be obtained by employing the constitutive relationship on the strains.

$$\boldsymbol{\sigma_h} = \boldsymbol{D}\boldsymbol{\varepsilon_h} \quad (3.12)$$

$\boldsymbol{D}$ is the material constitutive matrix. In the present investigation stiffness based finite element technique with nodal displacements as field variables has been used. The mechanical stresses induced by the ingress of moisture can be obtained by solving energy invariant relationship for the deformable body

$$\delta\Pi\ (\boldsymbol{u}) = 0 \quad (3.13)$$

Where $\boldsymbol{u}$ is the displacement vector due to moisture expansion and $\Pi\ (\boldsymbol{u})$ is the total energy of the system. Thus, Eq. (3.13) can been rewritten as

$$\boldsymbol{Ku} - \int_v \boldsymbol{D\varepsilon_h}\, dv = 0 \tag{3.14}$$

$\boldsymbol{K}$ is the stiffness matrix. Eq. (3.1) and Eq. (3.14) are solved at successive time steps to obtain the moisture concentrations and displacements thereof. The stresses induced due to moisture build up can be obtained in finite element framework as

$$\boldsymbol{\sigma} = \boldsymbol{DBu} \tag{3.15}$$

Where $\boldsymbol{B}$ is the strain-displacement relationship matrix; and $\boldsymbol{\sigma}$ is the stress tensor. The hygroscopic mismatch strain has a significant impact at the interface. Therefore, in addition to aforesaid boundary conditions the nodes are tied at the fibre matrix interface to model the interfacial behaviour. Once boundary conditions are applied, the resulting linear simultaneous equations (Eq. 3.14) can be solved for nodal displacements and hence strains. For the plane strain problem the stress components along the plane are:

$$\begin{Bmatrix} \sigma_{hx} \\ \sigma_{hy} \\ \zeta_{hxy} \end{Bmatrix} = \frac{E}{(1+\mu)(1-2\mu)} \begin{bmatrix} 1-\mu & \mu & 0 \\ \mu & 1-\mu & 0 \\ 0 & 0 & \frac{1-2\mu}{2} \end{bmatrix} \begin{Bmatrix} \varepsilon_{hx} \\ \varepsilon_{hy} \\ \gamma_{hxy} \end{Bmatrix} \tag{3.16}$$

Chapter 4: Diffusion Micromechanics

Fibre distribution in a polymer matrix composite plays a key role in moisture transport which in turn affects its long term behaviour. In this chapter, effect of filament arrangement on moisture diffusion is studied. The emphasis is on the effect of neighbourhood filaments on a single filament placed in a polymer matrix. The effect of tortuosity has been analysed along transverse direction by considering arbitrary cross-sections with carefully controlled filament distribution. Influence of inter-filament distance, their angles and size of neighbourhood has been reported. Fickian diffusion has been simulated using finite element method. Several microstructures have been created using variable angular and spatial orientations of the filaments. Their saturation times have been recorded and analysed. Microstructures for most favourable saturation time have been identified. The results show that the diffusivity of composites can be controlled through careful spatial design of filaments. The observations should serve as a clue for designing optimum filament geometry for impeding moisture ingress and improving durability of composites. The results are fundamental building blocks for analysing the behaviour of large fibre topologies. They also indicate basic principles of designing optimum filament geometry for control of moisture ingress.

4.1 Finite element diffusion model

Fig.4.1 is an illustration of a cross-section of a uni-directional composite that is studied here.

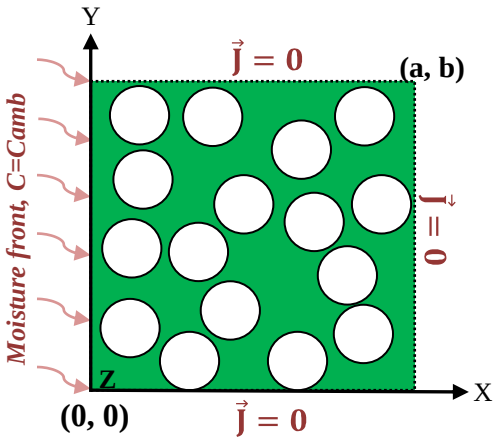

Fig. 4.1. Present diffusion problem

The left edge is exposed to a moist environment of specified concentration. At time *t=0* the entire representative model including its other three edges had zero moisture content, The boundary conditions for moisture exposed left edge are:

$$C = 0 \qquad (0 < x < a, \forall t = 0) \tag{4.4a}$$

$$C = C_{amb} \qquad (x = 0, \forall t > 0) \tag{4.4b}$$

The rest of edges in Fig. 4.1 are impermeable boundaries with no moisture flux entering or leaving them for the entire duration, the boundary conditions of these edges are:

$$\vec{J} = 0 \qquad (x = a, y = 0, y = b, \forall t \geq 0) \tag{4.5}$$

Using these boundary conditions diffusion is simulated through a two-dimensional lamina representing transverse section of a reinforced composite with one of its edges suddenly exposed from dry state to the ambient moisture (C_{amb}) that is maintained throughout the time of diffusion.

Moisture diffusion is modelled by Fickian diffusion based FE code ABAQUS (ABAQUS/STANDARD, 2011). All models of presented in this

chapter were meshed using quad-dominated (4-noded DC2D4) elements. One of the challenges of using a microstructure-based approach is that a large number of elements and a highly refined mesh are required to conform to the heterogeneous nature of the microstructure. A convergence study is carried out to determine the optimum mesh size and time step. Considering a typical filament radius (R) of 9µm, approximately 8,000 elements were used to mesh most of the geometric models. Each node has a single degree of freedom of moisture concentration. Properties used are listed in Table 4.1.

Table 4.1: Material properties of fibre and epoxy (Vaddadi *et. al.,* 2003a)

Property	Fibre	Matrix
Moisture Diffusivity	0	54.4×10^{-14} m^2/s
Solubility(S)	0	1

In transient mass diffusion analysis with second order elements there is a relationship between the minimum usable time step and the element size. A simple guideline to get the solution convergence is (ABAQUS MANUAL, 2011):

$$\Delta t \geq \Delta l^2 / 6D \tag{4.6}$$

Where Δt is the time increment, D is the diffusivity, and Δl is the typical element dimension (such as the length of a side of an element). If time increments smaller than this value are used, spurious oscillations can appear in the solution. In the present work Δt is chosen based on Eq. (4.6). Several analyses on varying filament topologies have been performed to study the effect of filament arrangement on moisture diffusion. The moisture concentration inside the domain increases gradually to finally reach the specified concentration of the left edge. When any point reaches the moisture concentration of the left edge it saturates, i.e. it holds no more moisture. The analysis ends

when the entire domain reaches saturation. Thus, saturation progresses from the left edge to the right. The progression of the saturation front is depicted as a ratio of the area that is saturated to the total area of the resin. Understandably, this progression is influenced by the presence of the fibres and their location. The time to full saturation is also noted to evaluate different microstructures.

4.2 Model validations

The present model is validated by comparing the rate of weight gain in a carbon fibre reinforced composite when moisture diffuses through one boundary. The parameters have been kept the same as the experimental (Vaddadi *et. al.,* 2003a). Two smeared models are compared with the present model. A microstructure of dimensions 600µm x 64µm with randomly distributed fibre is generated (Fig. 4.2). A finite element mesh is generated. One 64µm edge is exposed to the moisture.

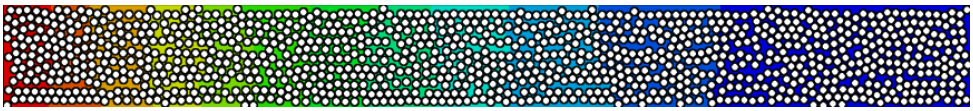

Fig. 4.2. Moisture diffusion through composite model

Two homogenized smeared models based on the Halpin-Tsai relationship (Halpin, 1984; Springer, 1984) and Rule of mixtures (Alger, 1997; Askeland, 2010) are also compared. If D_m and D_f are the diffusivities of the matrix and the fibre, and V_m and V_f are the corresponding volume fractions, then according to Halpin and Tsai relationship the effective diffusivity is:

$$D_{eff} = \frac{1-V_f}{1+V_f} D_m \tag{4.7}$$

Alternatively, when a general rule of mixtures by weighted mean is used to predict the effective diffusivity, the relationship is:

$$D_{eff} = V_m D_m + V_f D_f \tag{4.8}$$

The gain in weight due to moisture diffusion is calculated by integrating the moisture concentration in the entire domain. The weight of specimen at a given time $W(t)$ when measured with respect to weight of dry specimen $W(0)$ results in relative weight gain percentage (w_t):

$$w_t = [W(t) - W(0)]/W(0) \tag{4.9}$$

The present example has maximum moisture content of 1.48% and fibre volume fraction(V_f) is 0.58. Thus %moisture shall converge at 1.48 × (1-.58) = 0.62.

Weight gain due to diffusion was estimated for 600 hours using the smeared models and compared with the present analysis where the fibre and the matrix are modelled distinctly. Fig. 4.3 shows the weight gain with time. It is clear that the present analysis agrees reasonably well with the experimental results. It may be noted that the exact microstructure of the experimental specimen is not available. Thus, a randomly distributed fibre microstructure of the same volume fraction as in the experiment is created. Smeared models show similar trends of weight gain. However, the rate of moisture absorption is slower in the smeared models. This is due to the missed interactions of the fibres and the moisture in the smeared formulations.

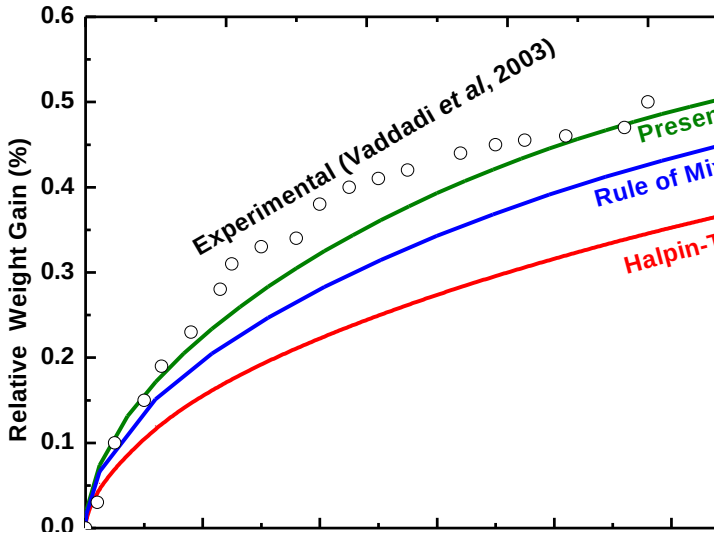

Fig. 4.3. Comparison between finite element and experimentally reported weight gain

The trend in weight gain is clearly Fickian for this class of problems. The example clearly highlights the importance of modelling the fibre and the matrix distinctly if one is interested in studying the propagation of moisture through the fibre composite. It may also be noted that the fibre topology in the experimental specimen is not available. It is modelled approximately by randomly distributing the fibre of the same volume fraction as in the experiment. Although the equivalent randomly distributed microstructure could predict overall trends very well there are local variations. There are bound to be local differences in fibre topologies of the experimental and the theoretical models. This mismatch is likely to cause local deviations of the present results from the experimental ones. This observation also establishes the influence of local fibre geometry on the moisture diffusion that is hitherto ignored in smeared models. The influence of fibre topology on moisture diffusion is presented.

4.3 Neighbourhood interactions

This section reports influence of topology of filaments on moisture diffusion. Both progression of moisture and saturation have been studied. Neat resin has been taken as the benchmark case. Effect of introduction of single reference filament is observed. Then new filaments are introduced around the reference filament to study their interactions.

4.3.1 *Reference filament*

Fig. 4.4 shows simulation snapshots taken at different stages of moisture progression. At first, a square domain of dimension 54µm has been considered for the neat resin. Moisture concentration (C) of 1.48 weight percentage of the polymer has been introduced at the left edge.

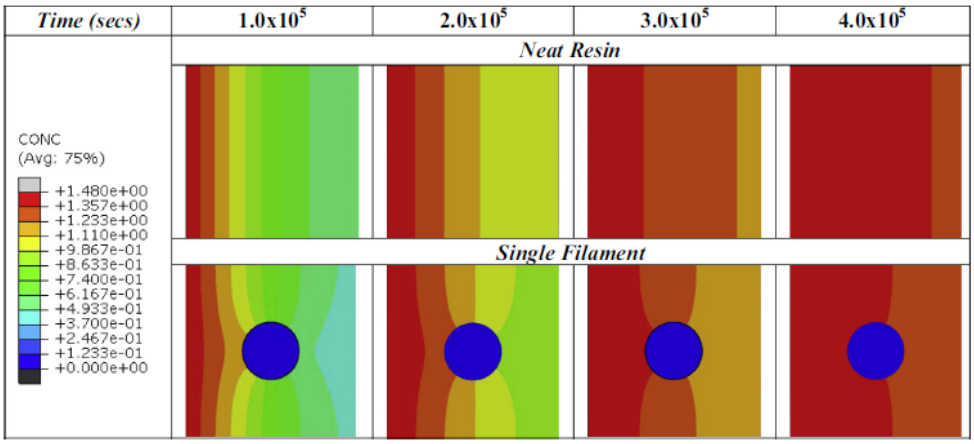

Fig. 4.4. Moisture isolines at different times

It's progression through the resin is observed at distinct time points. As evident from Fig. 4.4, moisture progresses uniformly along Y for neat resin.

To evaluate the effect of filaments on moisture progression a single filament of radius R= 9µm has been introduced at the centre of the domain. It is intuitive that the filament that does not absorb any moisture would act as a barrier and thus, would extend the time taken for saturation. It can be noticed in Fig. 4.4 that the isolines to the left of filament bend towards it. It illustrates that instead of acting as a barrier, the filament attracts moisture towards it. This phenomenon can be explained by studying the concentration gradient of the composite. The filament does not absorb any moisture thus it remains a dry island while moisture diffuses through the resin. Therefore, as a result of introduction of the filament in the neat polymer resin the largest concentration gradient (C) between the resin and the filament is created at the centre of the domain. As a result, the filament acts as an attractor of moisture rather than a barrier. Final saturation time of the neat resin and the single filament models are 4.04×10^5 s and 4.37×10^5 s respectively.

To estimate the rate of internal progression of moisture front a colour based spatial calibration technique has been used (Image J Analyzer, 2013). For the image shown in Fig. 4.5a, area fraction of saturated resin is almost 8.5 percent of total area. In a similar manner, fraction of area that is saturated has been measured for all time steps. In the neat resin the left edge attains the saturation first and it progresses in a straight line towards the right edge. The rate of progression of saturation front has been reported in Fig. 4.5b. It can be noted that saturation front moves exponentially in space. It is clear that the solution to Eq. (3.1) is exponential in *X*.

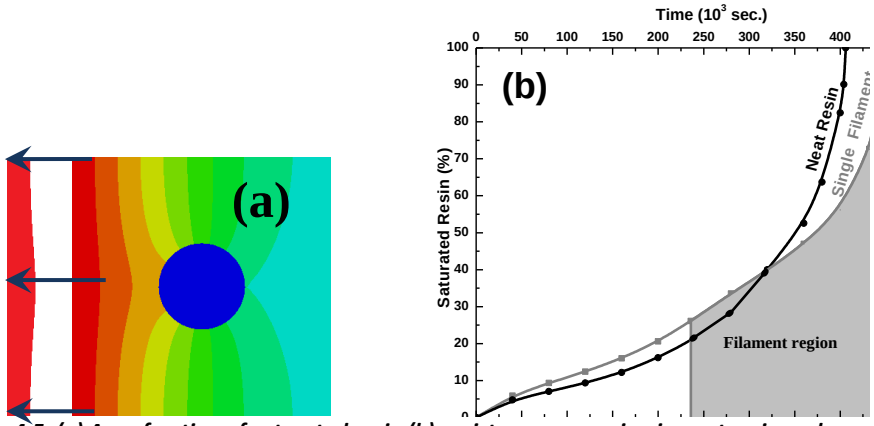

Fig. 4.5. (a) Area fraction of saturated resin (b) moisture progression in neat resin and single filament

In the case of the composite if we note the profile of concentration isolines (Fig. 4.4) on the right of the filament they too bend towards it. Therefore, it is clear that the filament starts to prevent moisture diffusion only after the water molecule has passed it and as a result, it slows down the progression of moisture front. This phenomenon is illustrated in a comparison of moisture progression between neat resin and single filament in Fig. 4.5b. Moisture diffusion starts from X=0. It progresses faster in the presence of filament than in the neat resin at the left side of the filament. This is somewhat counter-intuitive. However, it is easily understood that the higher moisture gradient is created in presence of fibre is responsible for faster progression of moisture. The two curves cross each other at the centre of filament. Beyond that point progression in composite slows down below that of the neat resin. Finally, the composite takes about 8.3% longer to completely saturate. Thus, the effect of embedding a non-absorbing and non-diffusive filament on a diffusive matrix is that moisture will be attracted towards the filament. It accelerates the progression of moisture front until it has reached the filament and deters the front from progressing further. The overall result is an increase in saturation

time. However, understanding the internal kinetics of the saturation front is as important as the final saturation time.

4.3.2 *Neighbourhood filaments*

In this section the effect of introducing other filaments in vicinity of the reference filament (reported earlier) is observed. The filaments surrounding reference filament are named as neighbourhood filaments. The neighbourhood is characterized by three parameters - angle *(θ)*, distance *(d)* and density *(N)* (Fig. 4.6). The neighbourhood filaments are located in a symmetrical fashion across the horizontal line bisecting the reference filament. Thus, neighbourhood filaments are introduced in a pair at $\pm\theta$ at the same distance (d) from the reference filament. The angle (θ) is varied in a range of 15° to 165° with an increment of 30°. It may be noted that for small distances (d) the increment of θ must be higher to avoid overlap between the filaments. In such cases the next feasible increment is chosen.

The distance *(d)* is varied in range 2R-4R where *R* is the radius of filaments. The theoretical limit of packing of filament is *2R* and from our experience It is observed that effect of neighbourhood is negligible beyond 4R. Thus, this range covers the entire zone of interest. The third parameter is density *(N)* that ranges from 2 to 12. For the filament radius *(R)* of 9μ, a representative square domain of 92μ dimension was sufficient to accommodate the neighbour arrangement of largest considered gap (d=4R). The effective volume fraction range is 9% (for N=2) to 40% (N=12). The entire neighbourhood matrix is presented in Table 4.2.

Table 4.2: Neighbourhood matrix with nomenclature.

θ-2R-N		*Orientation(θ)*					
		30°,-30°	***90°,-90°***	***150°, -150°***			
N	*2*	30-2R-2	90-2R-2	150-2R-2			
	4		90-2R-4	150-2R-4			
	6			150-2R-6			
θ-2.5R-N		***30°,-30°***	***90°,-90°***	***150°, -150°***			
N	*2*	30-2.5R-2	90-2.5R-2	150-2.5R-2			
	4		90-2.5R-4	150-2.5R-4			
	6			150-2.5R-6			
θ-3.5R-N		***30°,-30°***	***75°,-75°***	***120°, -120°***	***135°,-135°***	***150°, -150°***	
N	*2*	30-3.5R-2	75-3.5R-2	120-3.5R-2	135-3.5R-2	150-3.5R-2	
	4		75-3.5R-4	120-3.5R-4	135-3.5R-4	150-3.5R-4	
	6			120-3.5R-6	135-3.5R-6	150-3.5R-6	
θ-4R-N		***15°, -15°***	***45°,-45°***	***75°,-75°***	***105°, -105°***	***135°,-135°***	***165°,-165°***
N	*2*	15-4R-2	45-4R-2	75-4R-2	105-4R-2	135-4R-2	165-4R-2
	4		45-4R-4	75-4R-4	105-4R-4	135-4R-4	165-4R-4
	6			75-4R-6	105-4R-6	135-4R-6	165-4R-6
	8				105-4R-8	135-4R-8	165-4R-8
	10					135-4R-10	165-4R-10
	12						165-4R-12

The nomenclature of each model is defined in sequence θ-d-N. Table is divided in sub-domains of distance (d). Within each sub-domain each column corresponds to same θ and varying N while each row corresponds to same N and varying θ. This definition has been used consistently in the subsequent discussion.

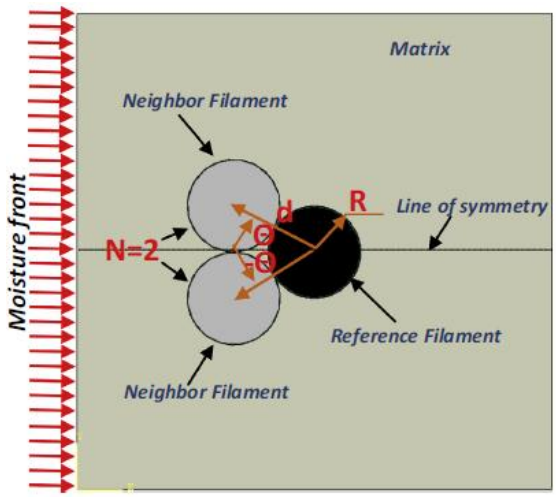

Fig. 4.6. Illustration of neighbourhood parameters (θ-d-N)

(i) Influence of θ

Fig. 4.7 illustrates the progression of moisture front for θ-2R-2 configuration with θ = 30, 90, 150.

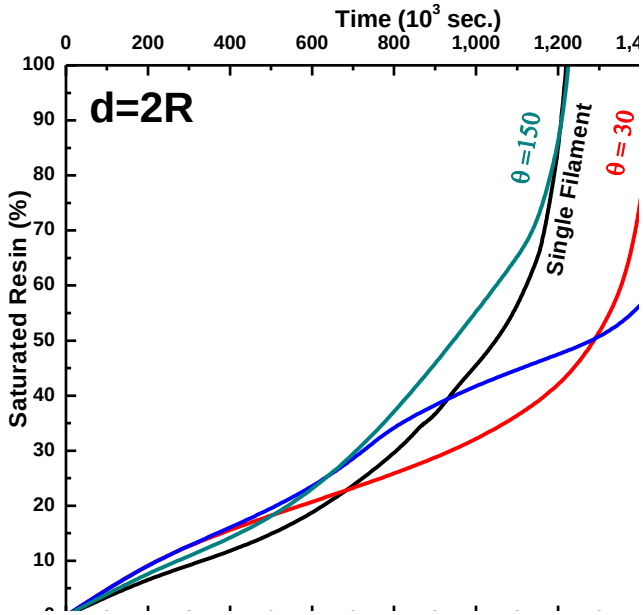

Fig. 4.7. Moisture progression in resin for θ-2R-2configuration

The curve for single filament is presented for comparison. It is noted that although the density is constant there is a substantial variation in the rate of diffusion with θ. While θ =90 increases the saturation time taken to 1.6 x 10^6 s if compared to 1.2 x 10^6 s (single filament), in case of θ = 150 there is no gain in saturation time even with the addition of 2 more filaments in the composite. The graph also demonstrates that there can be dramatic variation in moisture ingress due to change in angular orientation although density remains unchanged.

It is demonstrated in section 4.3.1 that filaments behave as attractors of moisture. Thus, introduction of neighbourhood filaments accelerates the ingress of moisture front towards it whereas retards the progression only when moisture moves towards right of filament.

Θ = 150 introduces 2 filaments at the back of reference filament thus, when the front has passed the reference filament, the retardation effect of reference filament is overcome by acceleration effect of two neighbourhood filaments. Therefore, there is no gain in introducing additional filaments. The reverse happens at θ = 30. In this case the two neighbourhood filaments are introduced in front of reference filament thus when moisture front passes over the reference filament the neighbour filaments retard the progression whereas reference filament pulls the front forward. As the pull of 2 neighbourhood filaments is more than the single reference filament. The moisture gets retarded and that result in increase in time to saturation. This point is further emphasized in case of θ = 90. In this case all 3 filaments attract or retard the front simultaneously. As a result, there is no counter-acting effect of the neighbourhood on the reference filament. This configuration results in highest saturation time.

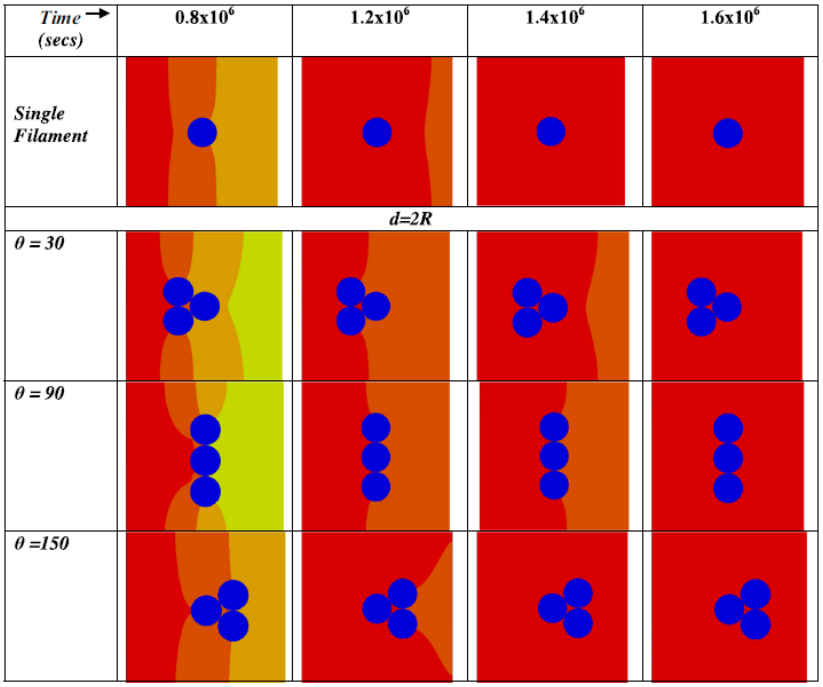

Fig. 4.8. Moisture profiles with N=2 at different θ

The diffusion phenomenon is illustrated through moisture isolines in Fig. 4.8. When the snapshots are compared at 0.8 x 10^6 s it is observed that the saturation front has reached the farthest at θ = 90. This demonstrates the highest attractive pull of this configuration. However, when on comparing the images at 1.2 x 10^6 s it is seen that the single filament has lost almost all its capacity to resist moisture. This is demonstrated by a flat isoline in that case. Among all N=2 configurations the moisture advances the most in θ=150 configuration while θ = 30 and 90 still resist the advancement of moisture. At 1.4 x 10^6 s both the single fibre and the θ = 150 configurations have been completely saturated and the moisture front has passed further for θ = 30 than θ = 90. This demonstrates the combined retardation for θ = 90 while the counter-acting effect of 2 neighbouring filaments and the reference filament that results in lower resistance for θ = 30. At 1.6 x 10^6 s all the microstructures are fully saturated. Thus, it is concluded that angular orientation of the neighbourhood has a profound effect on moisture diffusion in composites. The resistance is highest at θ = 90.

(ii) *Influence of d*

Effect of distance between the reference and the neighbourhood filaments (*d*) is demonstrated in Fig. 4.9. The graph for single fibre is plotted for reference. The saturation time varies inversely with d. The effect is most evident in θ=90 (Fig. 4.9a). The saturation time is maximum at the minimum theoretical limit of d=2R. As *d* increase, the neighbourhood effect diminishes and the filaments tend to behave as individual ones as a result the saturation curve comes closer to that of the single filament.

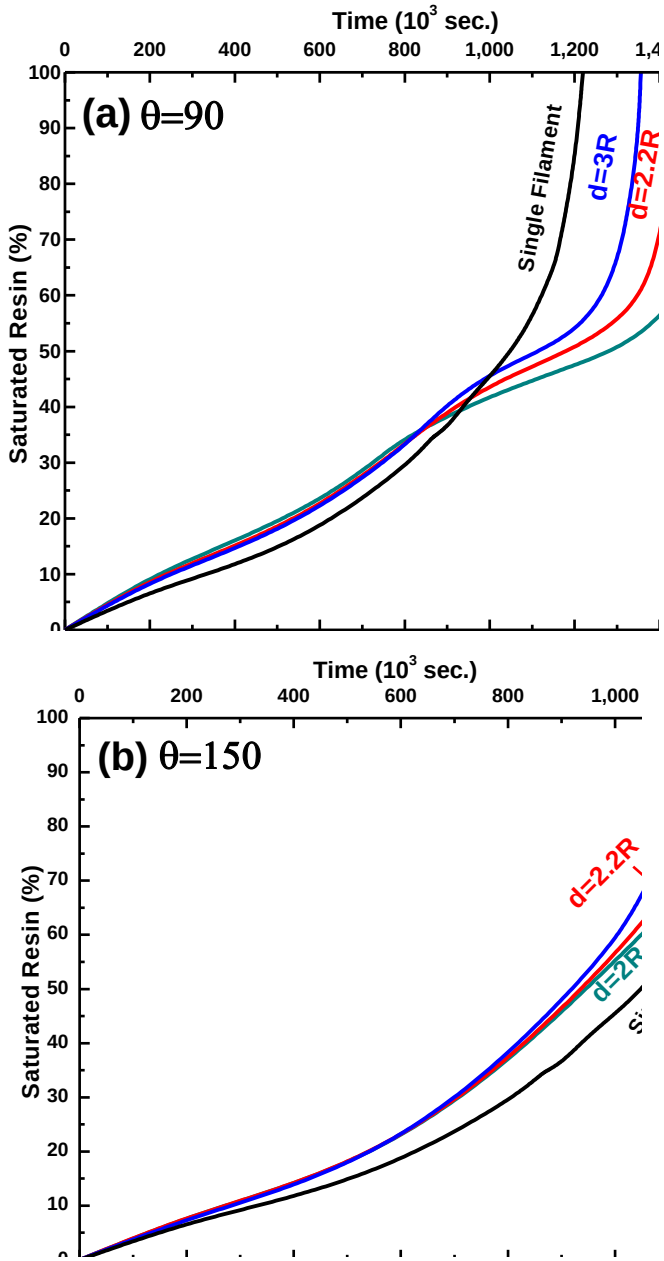

Fig. 4.9. Moisture progression in composite (a) θ = 90 (b) θ = 150

For θ = 150 (Fig. 4.9b) the effect of d is marginal. However, regardless of *d* all microstructures have lower saturation time than the single filament. Thus, it is clear that addition of filaments beyond θ=90 would accelerate the moisture diffusion rather than retarding it.

(iii) *Influence of* θ *and d*

Saturation times for the entire range of θ and *d* are plotted in Fig. 4.10. It is seen that although density remains unchanged the saturation time has ranged between 1.15 x 10^6 s and 1.6 x 10^6 s. This underlines the seminal effect of microstructural arrangement on moisture diffusion. The curve for single filament is used for reference. It is clear that introduction of neighbouring filaments may increase or reduce the saturation time depending on θ and d. For best retardation one should keep θ = 90 and d = 2R while θ > 150 would allow fastest ingress of moisture irrespective of d.

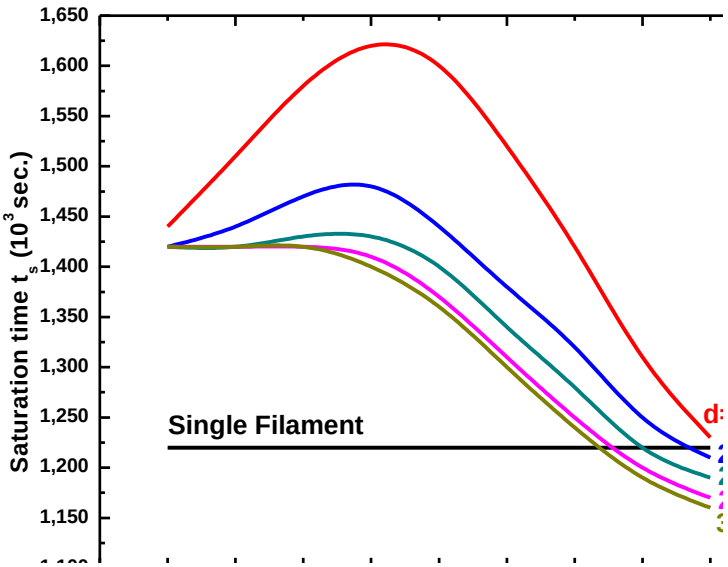

Fig. 4.10. Saturation duration vs. neighbourhood orientation

(iv) *Influence of* θ*, d, and N*

The combined effect of θ, *d*, and *N* is studied in this section. A matrix for a range of filament arrangements with varying θ, *d* and *N* was already generated (Table 4.2). The table has been divided into sections of constant d. In each section the rows have same N while the columns

have same θ. To explain the geometry, the section d=4R is illustrated here. The case of 15-4R-2 has two neighbourhood filaments at 15° angle at a radial distance of 4R from the reference fibre (Fig. 4.11a). As we move along the row θ increases gradually at an interval of 30° from 15 to 165 (Fig. 4.11b) resulting in a shift of the two neighbourhood filaments in a circular arc of radius 4R.

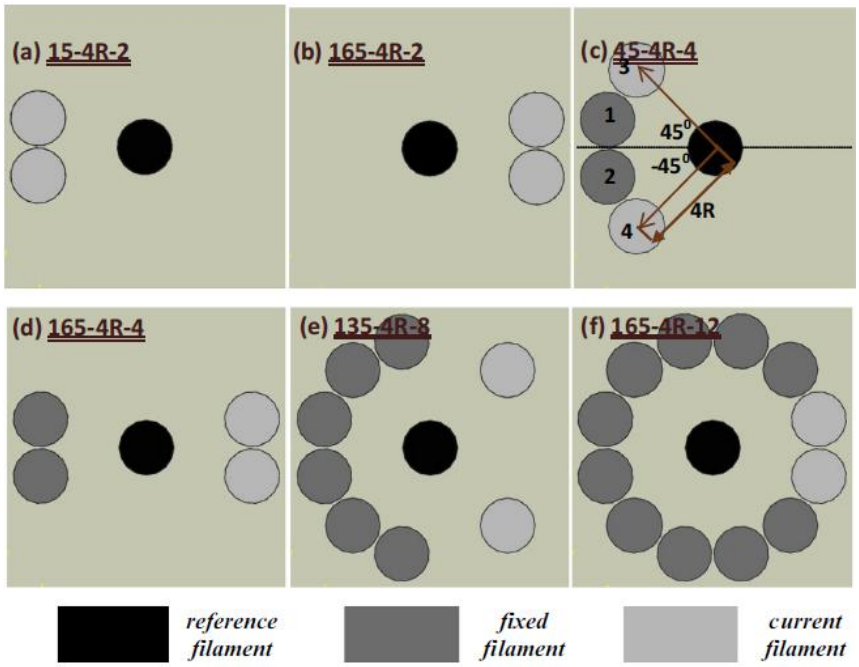

Fig. 4.11. Layouts featuring the nomenclature (θ-d-N) adopted to describe neighbourhoods

The density *(N)* is increased to 4 in the subsequent row of Table 4.2. In this case the first two neighbourhood filaments are fixed at 15°. Then two new filaments are introduced at an initial θ of 45° (Fig. 4.11c). The new filaments are moved in a circular arc of radius 4R at a step of 30° up to 165° (Fig. 4.11d). In this manner the density has been gradually increased in subsequent rows of Table 4.2 up to a maximum of 12. Fig. 4.11e illustrates an intermediate case of 135-4R-8. The densest configuration is 165-4R-12 (Fig. 4.11f). It may be noted that as d

reduces maintaining a 30° interval is not feasible as the filaments tend to overlap. Therefore, for a smaller d an interval higher than 30° has been used.

The saturation time for all the microstructures has been evaluated. Fig. 4.12 presents the variation of saturation time for different filament configurations. Each curve corresponds to a fixed density *(N)* whereas each marker point on a particular curve corresponds to the orientation (θ) of the rightmost filament when it moves in presence of a fixed number of filaments at its left at fixed orientations. Number of marker points on each graph is equal to the number of uniquely defined configurations in Table 4.2 for the particular distance *(d)*.

The results are presented for 3 different neighbourhood distances (d). For d=4R (Fig. 4.12a) the saturation times ranging from N=2 to 12 are presented. The curve for the single filament is drawn for reference.

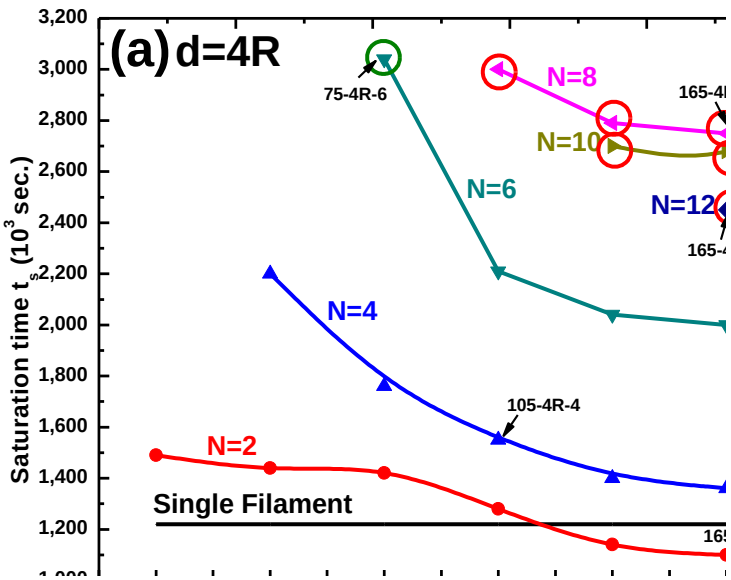

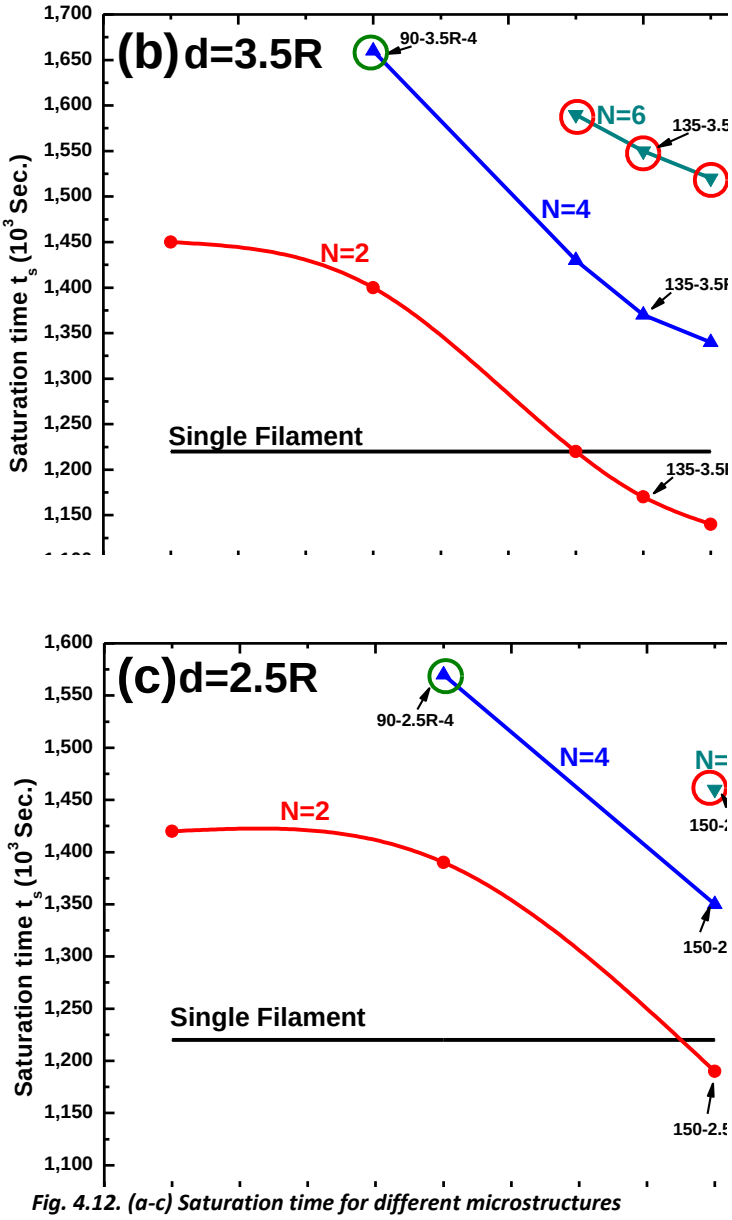

Fig. 4.12. (a-c) Saturation time for different microstructures

Fig. 4.12a corresponds to the θ-4R-N section of Table 4.2. It can be seen that as *N* increases the saturation time (t_s) also increases till N=8. Beyond that point $t_s$reduces with increase in *N*. Although the fraction of filament goes up in the composite, t_s goes down. It may be noted

from the 135-4R-N column of Table 4.2 that from this point the neighbourhood filaments start being positioned behind the reference filament. As discussed previously, such orientations reduce t_s due to their forward pull on the moisture front that accelerates moisture progression.

Among the 39 orientations reported in Fig. 4.12, 10 of the configurations show faster diffusion when new neighbourhood filaments have been included. Thus although the density and therefore the volume fraction goes up, the composite has a faster rate of diffusion. The corresponding marker points are encircled red in the graphs. 6 of these 10 cases correspond to d=4R (N=8, 10, 12), 3 are for d=3.5R (N=6, 8) and one for d = 2.5R (N=6). The orientations that took longer to saturate although their fibre volume fraction is less are encircled green. For example, 75-4R-6 contained 6 neighbouring filaments in comparison to 165-4R-8 that had a similar shape except 2 additional filaments at θ = 165. The saturation time in the former with 25% fewer filaments is 10.5% higher than the latter with a higher volume fraction. These results emphasize that the spatial distribution of filaments in terms of inter-filament distance and angular orientation is of far greater importance than the density or the volume fraction in moisture propagation characteristics of the composite. There are topological limits to filament geometry beyond which the effective diffusivity cannot be reduced through introduction of new filaments.

4.4 Diffusion in clusters

This section highlights the diffusion behaviour of different filament clusters with variable densities. A very closely packed cluster having d=2R with hexagonal orientation (theoretical limit of close packing) is

used (Fig. 4.13a). This is the arrangement with the largest number (19) of filaments (volume fraction=57%). We call it cluster A. The cluster of Fig. 4.13b (cluster B) is created by removing 10 filaments of Fig. 4.13a. Thus, cluster B has N=9 and volume fraction 27%. Two filaments have been added to cluster B to create the other two configurations. In Fig. 4.13c the two new filaments have been added at the back of the cluster, away from the diffusing edge (cluster C). While Fig. 4.13d shows the configuration where two new filaments have been added closer to the diffusing edge (cluster D). In terms of angular orientation, θ of the new filaments in cluster C was lower than 90° while that of cluster D was more than 90°.

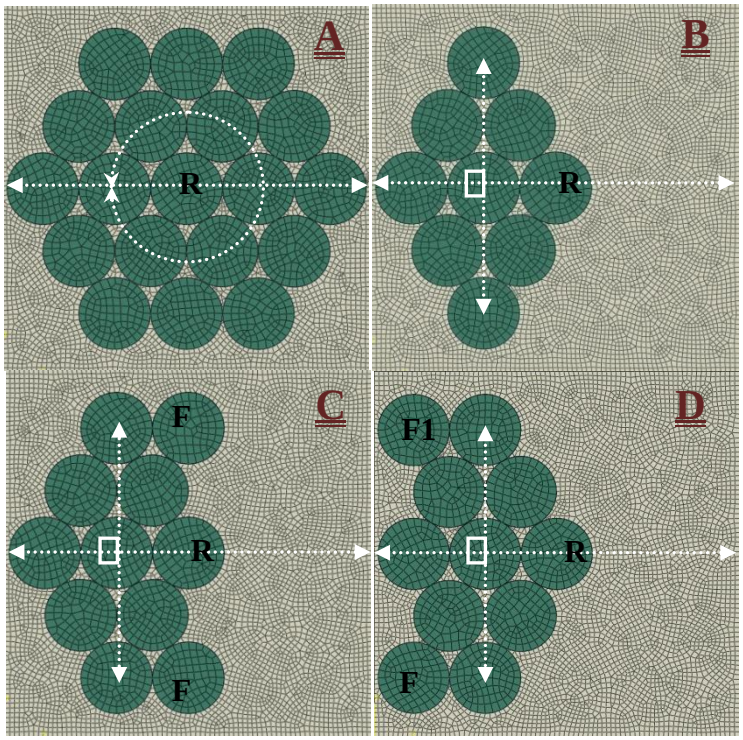

Fig. 4.13. Different cluster arrangements

Moisture progression snapshots at three different time points are presented in Fig. 4.14. At time 2×10^6s half of cluster A is saturated (spread of red color in the domain). Although the fibre density of

cluster B is less than half of A, at time 2 × 10^6s less than 20% is saturated. Although the density of clusters C and D is equal, moisture progresses slower in D. At time 3 × 10^6 s cluster A is fully saturated while the progress in the other three configurations is much slower. Cluster B is saturated at 4 × 10^6 s, but C and D are still resisting saturation.

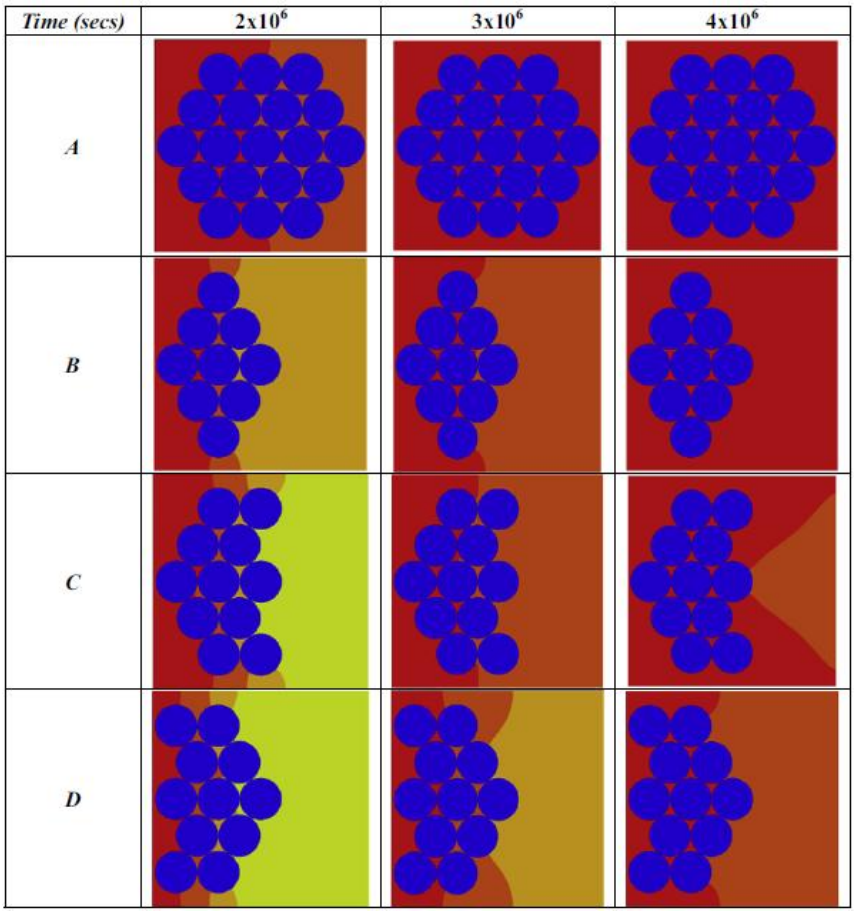

Fig. 4.14. Snapshots of moisture profiles for different clusters

Progression of saturation with time is plotted in Fig. 4.15. Cluster A with the highest density saturates faster than the other three configurations that have far lower density. The forward and back ward pull of the layers of filaments on the moisture counteract with each other and reduces the effect of the filaments. Configurations B, C and

D have much longer plateau region signifying the retardation effect of the filaments.

Clearly, the curves have three regions. Initially the moisture is attracted by the filaments. This is the build-up region. Once the saturation front reaches the cluster its progression is slowed down resulting in a plateau region. The efficacy of the cluster configuration in resisting moisture progression can be judged by the length of the plateau region. Once the moisture front has progressed beyond the effect of the cluster its progression is determined by the diffusivity of the matrix. This region is characterized by the sharp increase in diffusion rate. Although configuration A has the largest number of filaments the spatial arrangement of the filaments is not effective in slowing down the moisture. Configuration B that has less than half the number of filaments than A has been far more effective in retarding the moisture.

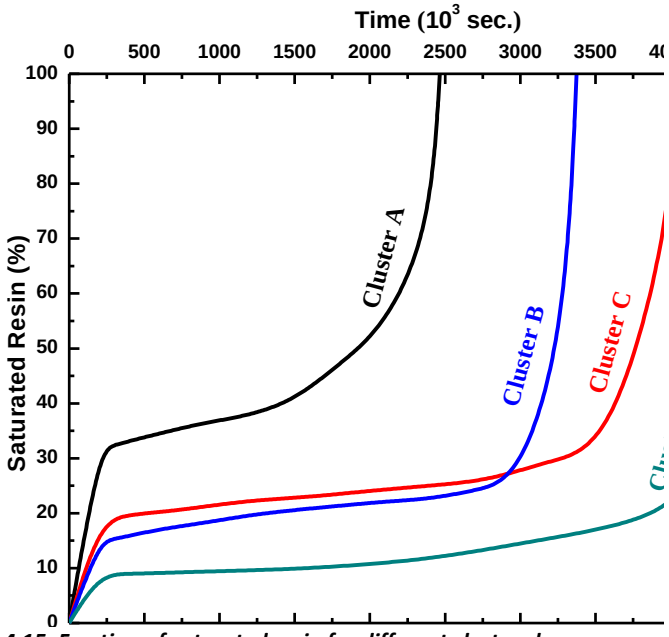

Fig. 4.15. Fraction of saturated resin for different cluster shapes

Configuration B has the least number of filaments. Addition of two filaments to the right of the basic configuration of B has resulted in a gain of more than 15% in saturation time. Comparison of B and C shows that addition of two more filaments has initially resulted in marginally faster of diffusion in C. Higher pull of the two extra filaments is responsible for it. However, those two filaments hold back the progression of moisture at later stages resulting in a longer plateau region. Thus, the red curve crosses the blue curve and finally reaches saturation at a later time. Configuration C and D has equal number of filaments. The only difference is that in C the new filaments are added at the back of the centre line of configuration B while in D the two new filaments are in front of the centre line. This subtle difference has a considerable impact on diffusion characteristics. In D the moisture front encounters the filaments earlier. As a result, it transitions into the plateau region quite early. The plateau region continues for the longest time in this case. Thus, it takes longest to saturate.

This study clearly illustrates that the fibre placement rather than the density is seminal in determining the diffusion characteristics of the composite. It should be possible to design cluster configurations for controlled diffusion in composites. The presented examples should be useful in designing the barrier layers to resist degradation and improve durability of composites.

Chapter 5: Diffusion in Clustered Microstructures

This chapter presents a numerical study of moisture propagation in fibre reinforced polymer (FRP) materials with spatial tortuosity. An algorithm for creation of microstructures with clustered fibre architecture is presented. Several controls for different characteristics of the clusters are described. Different statistical descriptors of geometry are used to quantify the clustering. The Fickian diffusion process has been modelled. The effect of clustering on moisture diffusion through the FRP is reported. It is observed that microstructures greatly affect the diffusion behaviour of the FRP.

The work assesses the relation between the statistical fibre distributions in clustered microstructures and moisture diffusion. An algorithm has been developed for creation of representative clustered microstructures. A simple and fast heuristic to create the clustered fibre arrangement is proposed. The generated fibre distributions are analysed for statistical spatial descriptors viz. nearest neighbour distance, cluster scatter and Ripley's-K function. This chapter provides an insight of the interplay between moisture diffusion behaviour and microstructural fibre distribution. Correlation between moisture diffusion and the statistical descriptors has been examined. The statistical measures that depict the global characteristics of the microstructure are found to have a better correlation with time to saturate the representative volume element. The results should help in prediction of macroscopic response and durability of clustered FRPs.

5.1 Microstructure generation

Generation of clustered microstructures has two steps. First an initial microstructure is generated. The initial microstructure is generated in two forms- ordered and random. The ordered microstructure represents total control at the time of manufacturing with no deviation from the desired arrangement while the random microstructure represents no control. The clustered microstructures have been created by moving the fibres from these two extreme initial conditions. All the micrographs are generated inside a rectangular lattice. The programming language MATLAB (MATLAB, 2013) is used for the implementation of the methodology.

5.1.1 *Initial Microstructures*

A 2-Dimensional square lattice representing the transverse section is considered. The region is defined by base vector $\vec{\mathrm{A}}$ joining origin to the bottom right corner $(X_{max}, 0)$ and height vector $\vec{\mathrm{B}}$ joining origin to the top left corner $(0, Y_{max})$ (Fig. 5.1). For a given fibre radius (r) the number of fibre insertions (n) inside the lattice is calculated from the fibre volume fraction$(\mathrm{v_f})$.

$$n = v_f \left\|\vec{A}\right\| \left\|\vec{B}\right\| / (A_f) \tag{5.1}$$

Where $\mathrm{A_f}$ is the cross-sectional area of the circular fibre.

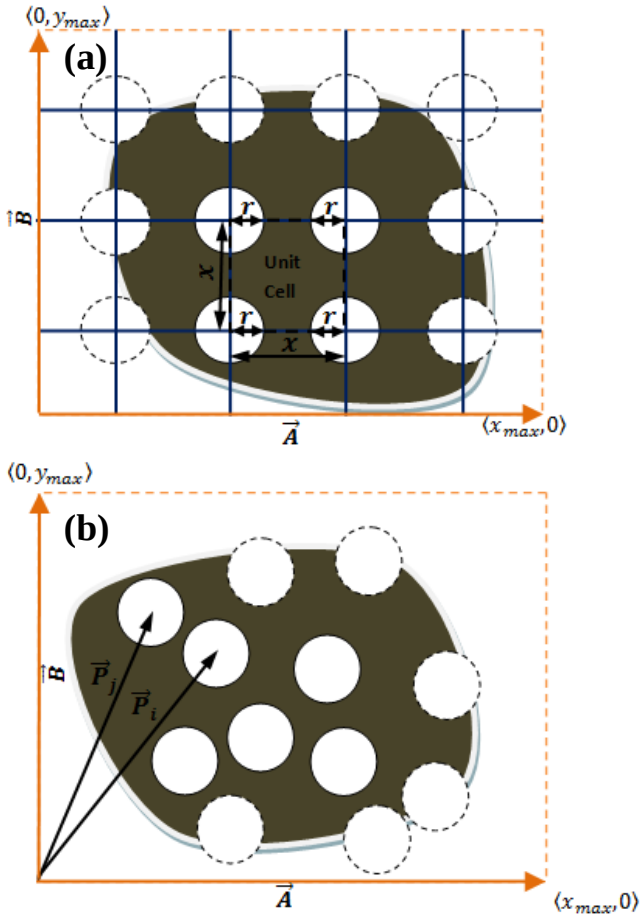

Fig. 5.1. Small representative regions to symbolize (a) Unit cell within an ordered fibre (OD) distribution (b) Random arrangement

Fig. 5.1a represents an ordered multi-fibre 2-D model of a unit cell. The ordered arrangement can be generated by seeding fibre centres at a defined interval. For a given fibre volume fraction (V_f) and fibre radius (r), the centre to centre (c-c) distance (x) can be computed as $\sqrt{r^2\pi/(V_f)}$. On the other hand, in order to generate a random architecture (RN) a unique non-overlapping location for a new fibre is determined. Position vector of the fibre centre $\vec{P}_i$ (it can also be read as $P(X_i, Y_i)$ is defined randomly inside the square array as:

$$\vec{P}_i = R_1\vec{A} + R_2\vec{B}\,,\ 0 < R_1, R_2 < 1 \qquad (5.2)$$

Subjected to the compatibility condition of minimum distance between any two fibres:

$$\left\|\vec{\mathrm{P}}_\mathrm{i} - \vec{\mathrm{P}}_\mathrm{j}\right\| \geq (2\mathrm{r} + \mathrm{G}), \forall_\mathrm{j} = 1.2.3 \ldots \mathrm{i} - 1 \qquad (5.3)$$

Here R_1, R_2 are the random numbers between 0 and 1. The minimum Euclidian distance between two fibres $\left\|\vec{P}_i - \vec{P}_j\right\|$ is maintained with G as the prescribed minimum circumferential gap. Generation of new fibres is terminated when the prescribed volume fraction is reached. Fig. 5.2 shows the results of the ordered (OD) and the random (RN) algorithms.

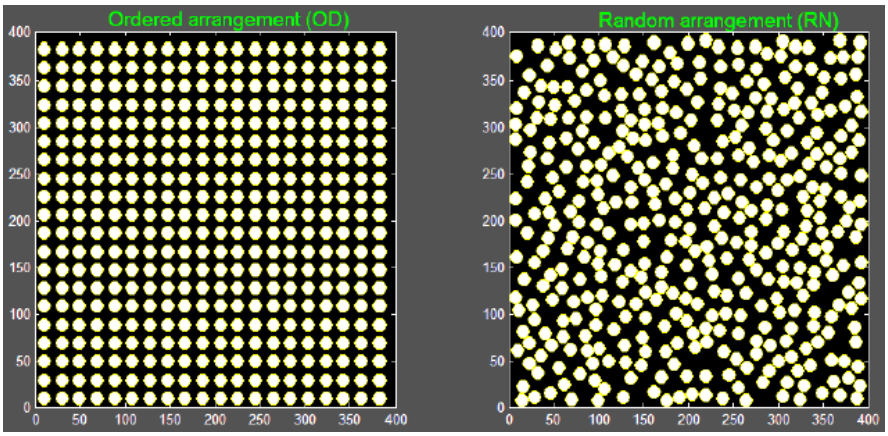

Fig. 5.2. Initial ordered (OD) and random (RN) fibre phase in matrix

5.1.2 *Clustered Microstructures*

In order to generate the clustered fibre architecture, the initial microstructure is processed through an iterative clustering algorithm. The centres of the clusters can be imagined as the poles in a gravity field. Due to the gravity field the fibres are attracted towards the poles in proportion to their distance from the poles. Thus, they gradually move towards the poles resulting in clustering. For the user defined

number of poles (m) with position vectors $\vec{C}_1, \vec{C}_2, \vec{C}_3 \ldots\ldots \vec{C}_m$ the pole nearest to a fibre with position vector $\vec{P}_i$ can be identified computing the Euclidean distance $\|\vec{D}_i\|$:

$$\|\vec{D}_i\| = min\left(\|\vec{C}_k - \vec{P}_i\|\right), \forall_k = 1,2, \ldots . m \qquad (5.4)$$

The fibres are moved towards the poles, subject to condition (3), starting from the nearest fibre. Fig. 5.3 shows the shaded gravity field and illustrates the fibre pull towards the nearest pole $\vec{C}_k$ within it. $\vec{M}_i$ is referred as 'Movement Vector' directed from the current fibre centre to the pole. The magnitude of movement of a fibre $\left(\|\vec{M}_i\|\right)$ is limited by the locations of other intermediate fibres that trespass its line of movement. The fibre orientation (θ_i) in respect to the pole is calculated as $\theta_i = tan^{-1}[(P_i j - C_k j)/(P_i i - C_k i)]$. Once the orientation is calculated, the fibre is moved towards pole along $\vec{M}_i$. The magnitude $\left(\|\vec{M}_i\|\right)$ is the Euclidean distance between the fibre and the pole.

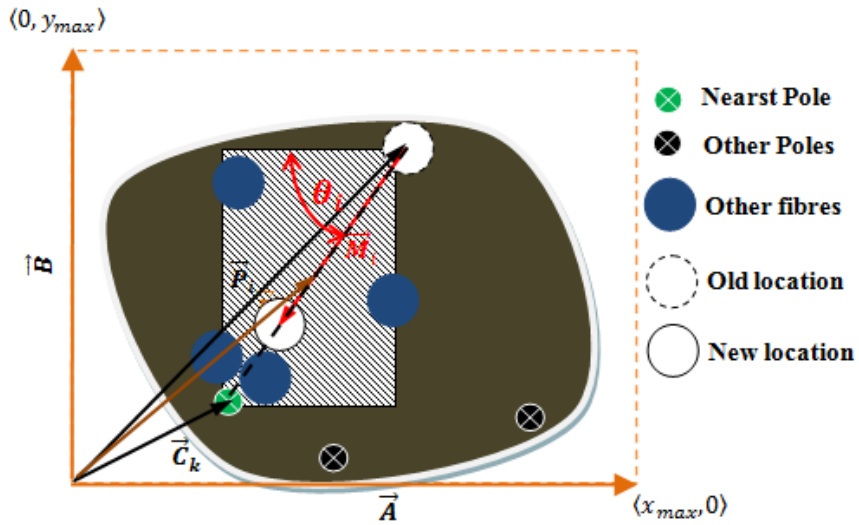

Fig. 5.3. Movement of fibres for clustered microstructure

A square domain of size 300µm x 300 µm with a fibre volume fraction $\left(V_f\right)$ of 30% is considered for clustering with both ordered (OD) and

random (RN) arrangements. Three pole points are taken at (100, 100), (100, 200) and (200, 150) respectively. The results of clustering are presented for both OD and RN arrangements (Fig. 5.4). The figure illustrates the snapshots at different instants of progression of clustering. The clustering percentage of a frame is the fraction of fibres that have been moved towards the pole with respect to the total number of fibres. The blue circles show the fibres that have been moved in the most recent iteration. The initial and the final microstructures are referred as 0% and 100% clustered microstructures in subsequent sections.

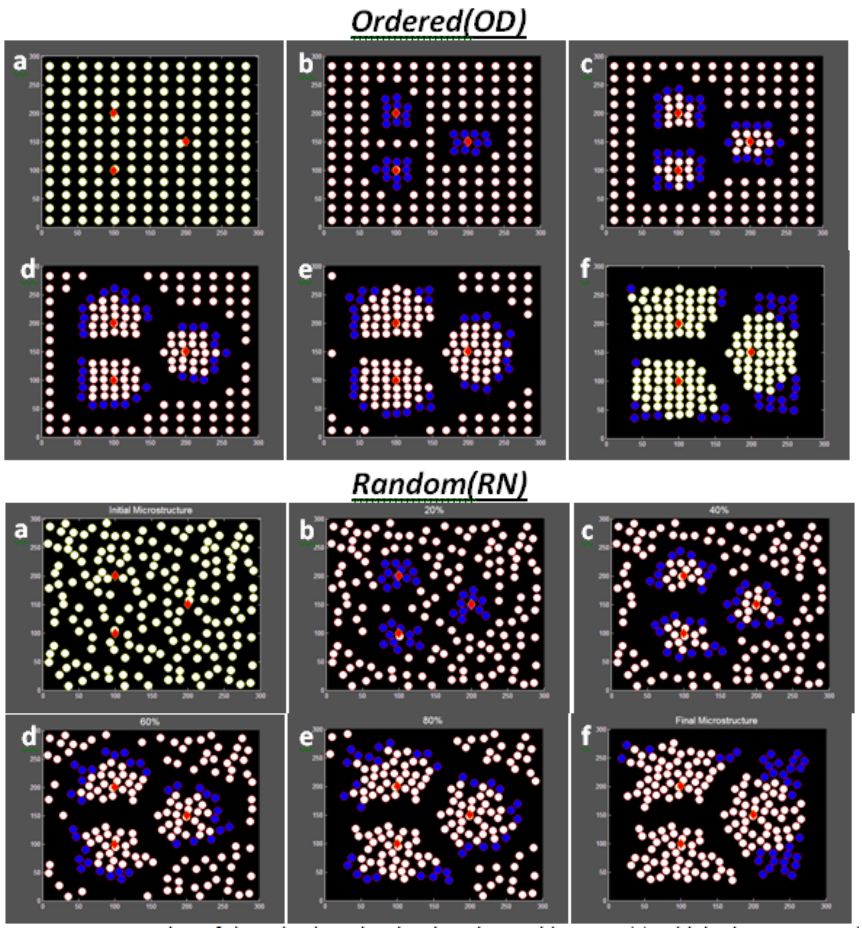

Fig. 5.4. Progression of clustering in ordered and random architectures (a) Initial microstructure (b) 20% (c) 40% (d) 60% (e) 80% (f) final cluster shapes

It can be noted that OD produces clusters of similar shapes and sizes while RN retains its initial randomness in the clustered microstructure. OD has symmetry in both Axes in its initial configuration. In the present example the pole points too are symmetric to *X-axis.* Thus, clustered structure of OD maintains the symmetry in x-axis (except in the case of fibres that are equidistant from two poles. In that case, the fibres are attracted to one of the poles). In case of RN although the pole points are symmetric to x-axis the initial configuration has no symmetry at all. As a result, the resulting clustered structure does not exhibit any ordered formation. OD may be useful in theoretical studies where effect of different parameters can be studied. RN may be useful in analysing more realistic clustered structures. Although OD and RN start from very different initial conditions the shape and number of fibres in each snapshot are similar. RN produces a distorted version of the clusters produced by OD. Both structures have been statistically characterised and correlated for moisture diffusion in this chapter.

5.2 Statistical characterization of microstructure

In this section, the microstructures presented in Fig. 5.4 are statistically characterised. Three statistical functions have been used. They are measures of how densely the cluster is crowded. However, they are different in the method of measurement. This section describes the algorithms.

5.2.1 *Average neighbourhood distance (AND)*

Average Neighbourhood Distance is one of the most common measures to describe spatial clustering (Clark and Evans, 1954;Torquato, 1995; Zangenberg *et. al.,* 2012). AND is defined as the

average distance of each fibre from its neighbours. The average distance is divided by the diameter of a fibre to give a non-dimensional expression ($\bar{d}_n$).

$$\bar{d}_n = \sum d_{ij} / r \qquad (5.5)$$

Here d_{ij} is the distance between the i^{th} and the j^{th} fibres in a neighbourhood. The neighbourhood of a fibre is defined by drawing a circle of a specific radius with the fibre at its centre. The fibres whose centres lie within the circle constitute the neighbourhood. In case the line joining the two fibres under consideration crosses another fibre then that pair of fibres are excluded from the calculation. An example neighbourhood is shown in Fig. 5.5. For the i^{th} fibre, the fibres j_1 through j_5 lie within the cut-off radius. Since the line joining the centres i-j_5 passes through fibre j_1, the distance between i and j_5 is excluded from the computation.

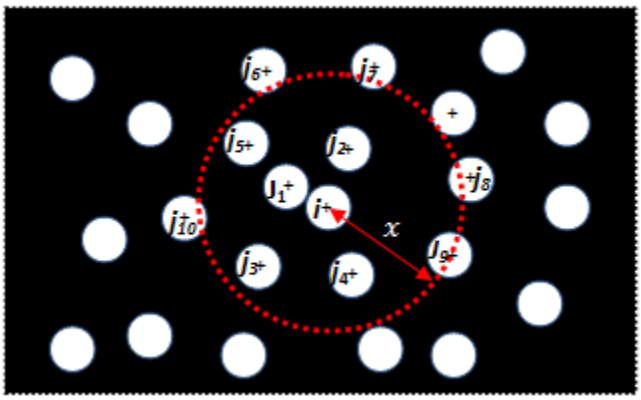

Fig. 5.5. An illustration of fibre neighbourhood

It may be noted x = 2r is the minimum limit of cut-off radius that describes two fibres whose boundaries are in contact. Three different cut-off radii (x) = 3r, 4r and 5r (r=radius of a fibre) are chosen. This is an extreme case of clustering with little practical significance.

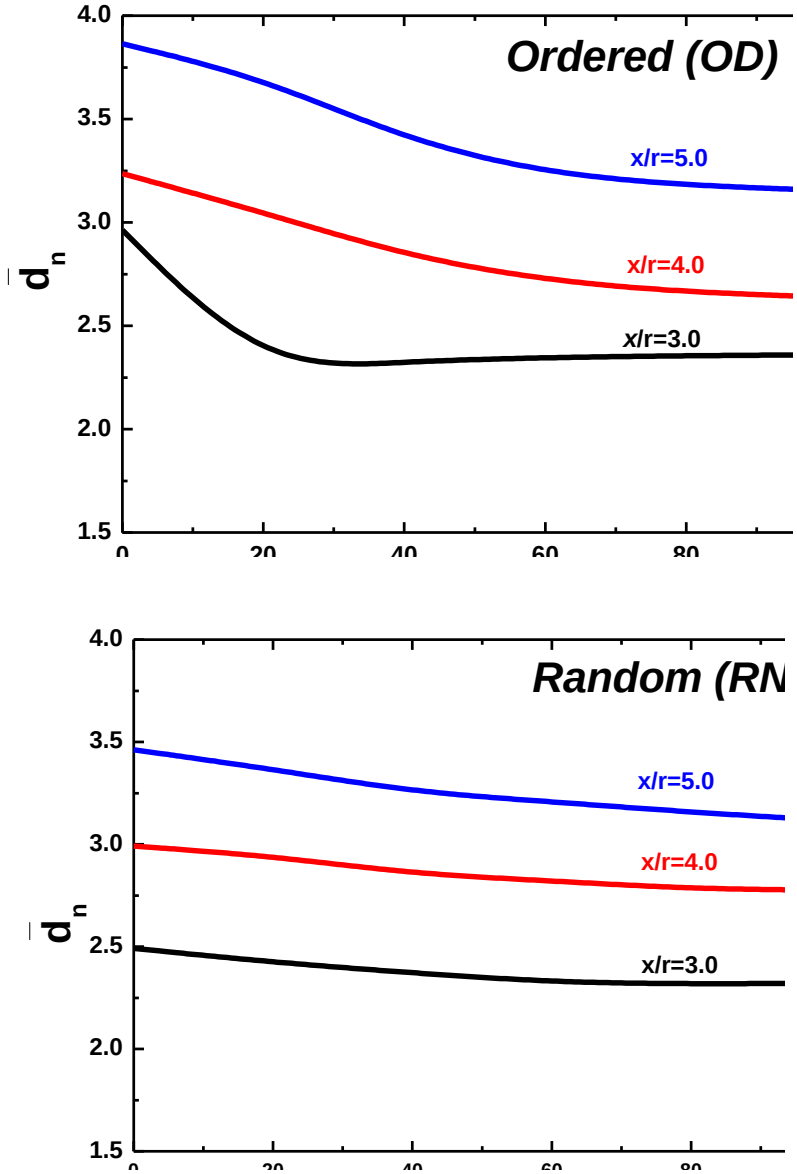

Fig. 5.6. Variation of neighbour distance metric ($\bar{d}_n$) with progression of clustering for OD and RN arrangements

Fig. 5.6 shows the variation of dimensionless parameter normalized dimensionless parameter $\bar{d}_n$ for OD and RN for different cut-off radii (x). It may be noted that $\bar{d}_n$ is proportional to the x/r. As x/r increases the area of the neighbourhood also expands. Thus, fibres that are at

larger distance from the centre are included in the neighbourhood, resulting in higher $\bar{d}_n$. As the clustering progresses the fibres come closer to each other. Understandably, as the clustering proceeds $\bar{d}_n$ gradually reduces for both the configurations. Thus, AND is a true measure of clustering for both OD and RN. The slopes of the curves have reduced as the clustering progressed converging to almost a zero slope in all the cases. This indicates that AND converges with clustering. In the present case the initial $\bar{d}_n$ was higher for OD.
However, as the clustering progressed, both OD and RN converged to values that are close to each other. It can be concluded that OD and RN produced statistically similar clusters.

5.2.2 *Average Cluster Distance (ACD)*

Average Cluster Distance ($\bar{d}_c$) is the mean distance of each fibre from its nearest pole. The distance is non-dimensionalised by dividing it by the diameter of one fibre.

$$\bar{d}_c = \sum d_{ik} / r \tag{5.6}$$

Where d_{ik} is the distance between the i^{th} pole and the k^{th} fibre in a cluster. This measure is applicable only when the clustering is around a point and there is a defined pole. As the clustering proceeds the fibres move closer to the respective poles. Thus, ACD reduces gradually. In this case, there is no neighbourhood. Unlike AND, all the fibres participate in the calculation of ACD. Thus, AND is a local measure of clustering while ACD is a global measure.

Fig. 5.7 shows the variation in ACD with the progression of clustering. As clustering proceeds the fibres move towards their respective poles. Thus, ACD reduces with the progression of clustering. Therefore, ACD is

a true measure of clustering. Both OD and RN had almost equal ACD in the beginning of the clustering process.

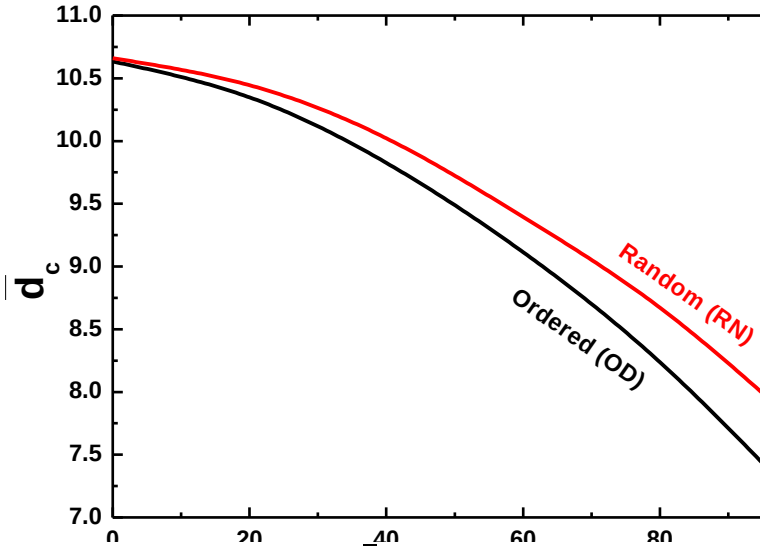

Fig. 5.7. Variation of $\bar{d}_c$ with clustering

The rate of reduction in I is higher in OD than in RN. It was clear from Fig. 5.4 that OD produces more compact clusters than RN. Due to its initial random distribution the clusters of RN are distorted versions of the compact shapes of OD. Thought its distortion the fibres in RN are spread further from the poles than the clusters in OD. This feature of the clusters is quite realistically captured in ACD. It can be concluded that ACD is a good measure of clustering.

It may be noted that the curvature of ACD is opposite of that of AND. Initially, the fibres that are closest to the poles move towards their respective poles. Thus, relatively smaller number of fibres moves by relatively smaller distances. As clustering progresses fibres located further away from the poles move by larger distances towards the pole. As a result, ACD reduces at a higher rate with the progression of clustering. It can be concluded that AND & ACD are complimentary in

nature. While AND emphasises local changes at the core of the clusters ACD highlights the global changes.

5.2.3 *Ripley's K function*

Ripley's-K function (Ripley, 1976 and 1977; Dixon, 2002) is another important tool to perform spatial point pattern analysis. This method has been used extensively in the field of spatial data mining for a wide array of problems (Diggle and Gratton, 1984; Doguwa and Upton 1989; Diggle, 1991; Duncan, 1993; Gaines, 2000). The method gives an insight of the arrangement for various length scales. Relatively fewer studies have been performed on the pattern recognition of 2-D composite materials using this approach (Pyrz, 1994; Myles 1995; Romanov, 2013). From a 2-D composite architecture point of view K-function can be defined as the ratio of number of fibre centres expected to lie within a radial distance x from a randomly chosen fibre centre and the number of fibres (N) per unit domain area (A) (Dixon, 2002):

$$\widehat{\mathrm{K}}(\mathrm{x}) = \hat{\lambda}^{-1} \sum_{\mathrm{i}} \sum_{\mathrm{j}\neq\mathrm{i}} \mathrm{w}\left(\mathrm{l_i}, \mathrm{l_j}\right)^{-1} \mathrm{I}\left(\mathrm{d_{i,j}} \leq \mathrm{x}\right)/\mathrm{N} \qquad (5.7)$$

Where $\hat{\lambda} = N/A$ indicates the number of fibres per unit area; $d_{i,j}$ is the distance between the i^{th} and the j^{th} points. Indicator function $I\left(d_{ij} \leq x\right) = 1$ if the condition within bracket is true (i.e. fibre is within boundary defined by distance x from arbitrarily chosen fibre centre) and 0 if the condition doesn't hold true; $w\left(l_i, l_j\right)$ is a weight term that accounts for the edge effect. It has the value of 1 if fibre *j* is completely inside the boundary of the circle of radius x and centred at randomly chosen fibre i. If part of the neighbouring fibre falls outside the boundary then $w\left(l_i, l_j\right)$ is the proportion of the circumference of the circle within the boundary. With reference to Fig. 5.5, fibres j_1 thru j_5 are within the circle of influence i.e. $d_{i,j} \leq x$. Therefore $w\left(l_i, l_j\right) =$

1. Fibres j_6 thru j_{10} are partially inside the circle. Thus, in their case $0 < w(l_i, l_j) < 1$. For the rest of the fibres the indicator function is zero. Ripley's K-function for a random domain is described by the homogeneous Poisson's point pattern which is also known as complete spatial randomness:

$$K_p(x) = \pi x^2 \tag{5.8}$$

Fig. 5.8 shows $\widehat{K}(x)$ as a function of $\mathrm{x/r}$ when calculated at different stages of clustering for OD (Fig. 5.8a) and RN (Fig. 5.8b) microstructures resp. The dotted curve corresponds to K-function according to Poisson's point pattern. For 0% and 20% clustering levels the K-function curves (Red and Blue) lie below the Poisson's pattern ($K(x)$ is below $K_p(x)$). This indicates the random dispersed nature of microstructures. With the progression in clustering, K-function shifts above the Poisson's curve. Shifting of K-function above the Poisson's curve is an indication of clustering and its severity.

The value of $\widehat{K}(x)$ goes up monotonically with the progression of clustering. Thus, it is a true measure of clustering. The slopes of the curves also increase as clustering progresses. Thus, it is also a global measure of clustering, although some local flavour is brought in through the neighbourhood circle.

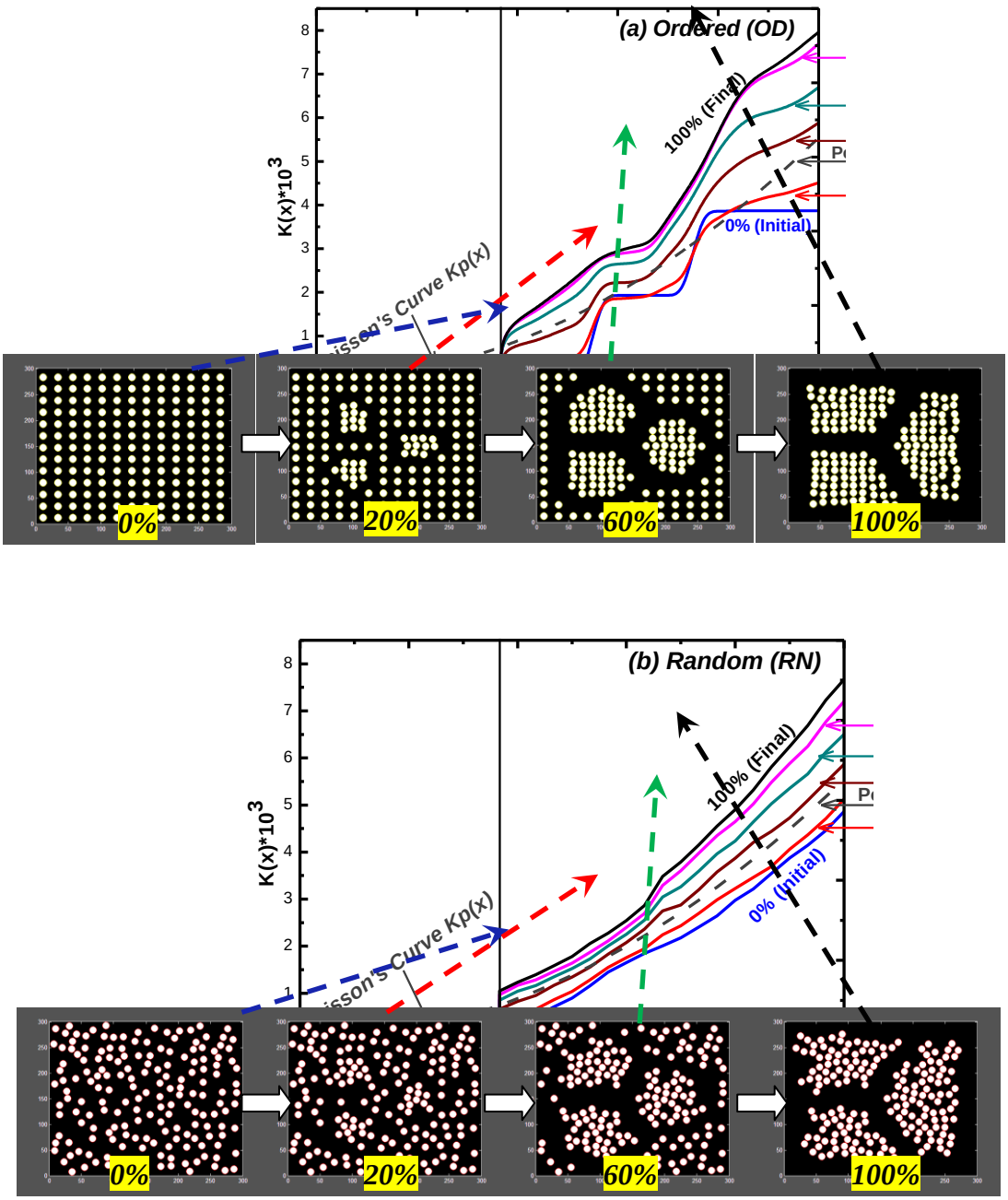

Fig. 5.8. Ripley's K statistics function for different x/r and with progression of clustering

5.3 Moisture diffusion modelling

The moisture diffusion response has been studied through the composites architectures of variable clustering levels under consideration (Fig. 5.4). A proper representative volume element (RVE) must be chosen for such studies. A small RVE may not adequately represent the composite system, while a large RVE may not suitable due to its high computational requirement. Prior research indicates that a square RVE dimension (40 times fibre radius) can represent the constitutive behaviour of a composite material (Shan and Gokhale, 2002). Hence, a 300 µm x 300 µm should be sufficient to represent the composite behaviour for the fibre radius of 7µm.

Majority of the models for diffusion kinetics in composite materials (Vaddadi *et. al.,* 2003; Joliff *et. al.,* 2012 and 2013) are based on Fick's law that states moisture sorption is a diffusion mechanism at a constant rate and constant solubility. The material properties have been chosen to mimic the conditions that were resorted to the laboratory-scale experiments (Joliff *et. al.,* 2012, 2013 and 2014). Table 5.1 presents the properties of the materials used in the numerical examples (Joliff *et. al.,* 2014).

Table 5.1: Properties of fibre and matrix (Joliff et. al., 2014)

Property	Fibre (E-Glass)	DGEBA-based epoxy resin
Young's Modulus (E, transverse)	70 GPa	2.7 GPa
Poisson's Ratio (ν)	0.35	0.35
Density (ρ)	1780 Kg/m^3	1150 kg/m^3
Moisture Diffusivity	0	15 X 10^{-13} m^2/s
Coeff. of moisture expansion (β_h)	0	10^{-3} /%H2O

Fig. 5.9 is an illustration of a cross-section of a uni-directional composite that is studied here. The left edge is exposed to a moist

environment of specified concentration (C_{amb}). At time t=0 the entire representative model including its other three edges had zero moisture content. Boundary moisture concentration (C_{amb}) of 2.29% (Joliff *et. al.,* 2014) has been introduced at the left edge. The moisture concentration C_{amb} is maintained throughout the duration of diffusion. The rest of the edges in Fig. 5.9 are impermeable boundaries with no moisture flux entering or leaving them $(\vec{J} = 0)$ for the entire duration. These are similar to the boundary conditions used in last chapter (Chapter 4, Eq. 4.4(a,b) and Eq. 5)

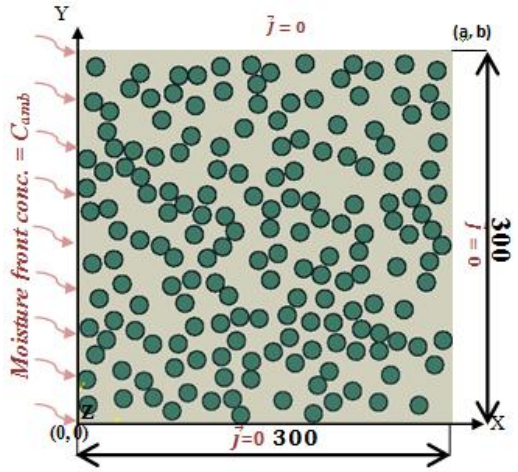

Fig. 5.9. Present diffusion problem

Moisture diffusion is modelled by the Fickian diffusion based finite element code ABAQUS. All models of this work were meshed using quad-dominated (4-noded DC2D4) elements. A prior convergence study was carried out in both neat resin and fibre matrix domains to exclude the influence of meshing. Moisture progression through the resin is observed at distinct time points.

Initially, the left edge is exposed to a moisture concentration(C_{amb}). It may be noted that no point in the domain can attain a concentration

greater than C_{amb}. Thus, it is considered the saturation concentration. Initially the left edge would reach saturation while moisture concentration in the rest of the RVE will be lower. With time larger areas of the RVE will reach saturation. The percentage area of RVE that has reached saturation at different time instants is presented in Fig. 5.10. The first column designates the levels of clustering. The first rows show the initial fibre arrangements both in OD and RN. The next 5 models (20%, 40%, 60%, 80% and 100%) for the same volume fraction correspond to increased levels of clustering. The saturated area is the fraction of total resin area where moisture content reaches the boundary moisture concentration. The isolines depict the moisture progression with time. It is noticed that clustering has a significant effect on the moisture diffusion characteristics. For OD with no clustering the isolines are straight. As the fibres get clustered they affect the isolines and they get curved. The similar phenomenon was observed in study of smaller microstructures with varying spatial distribution of fibres in last chapter. In OD, clustering caused faster progression of moisture through the left half of the RVE. Thus, a larger area of the RVE is coloured red (indicating saturation) in clustered microstructures than the ordered one until 50,000 s. After that moisture progression slows down to a great extent in clustered microstructures. Finally, at 90,000 s the ordered microstructure is completely saturated but the clustered ones are yet to be completely saturated. The clustered microstructures take longer to get completely saturated than the ordered structures.

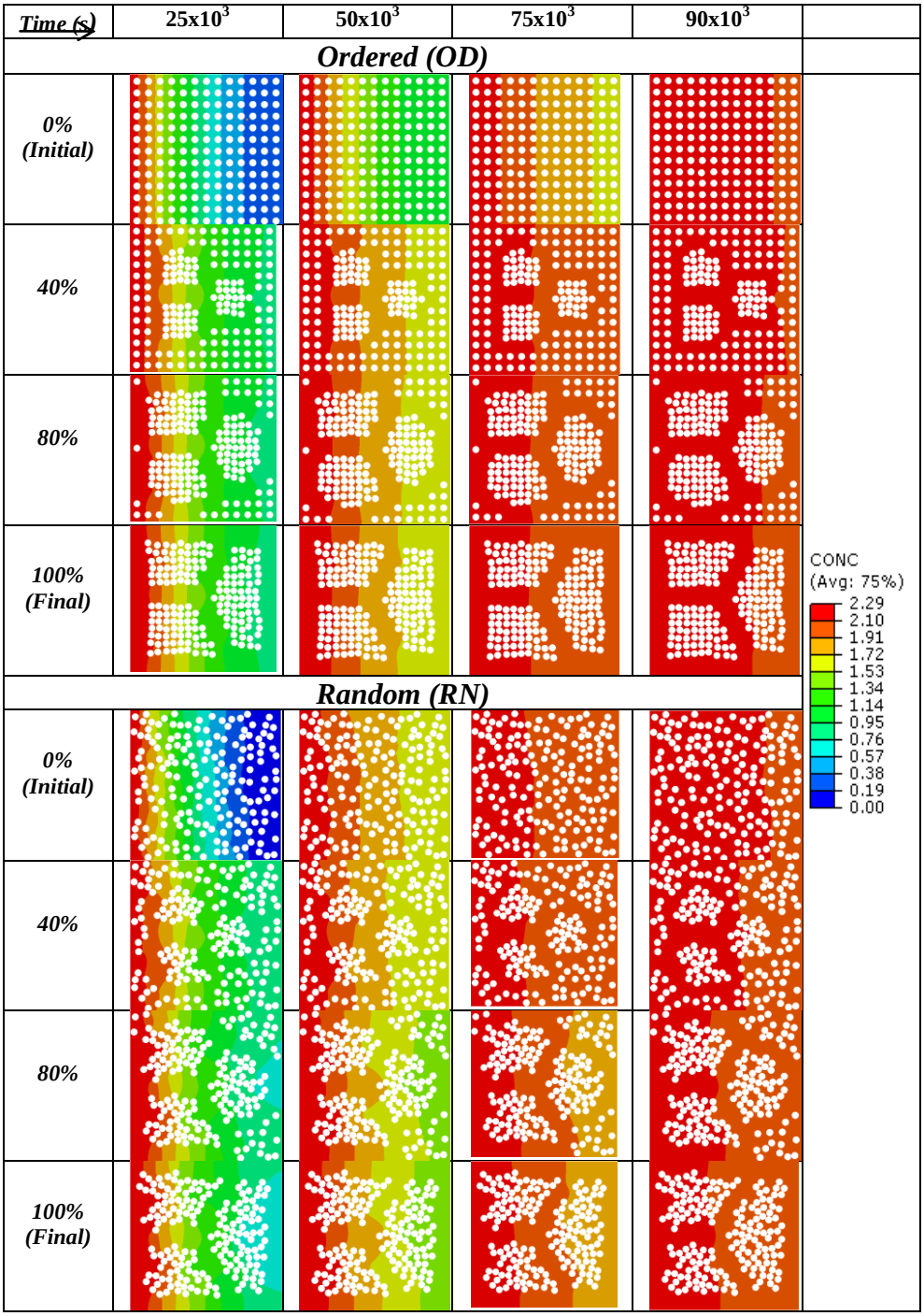

Fig. 5.10. Snapshots of moisture progression for different clustering levels

Comparison of OD and RN reveals that in this case the saturation is faster in OD than in RN. That indicates that the present RN has a more favourable topological distribution than OD for successfully impeding moisture. However, it cannot be concluded as universal truth. Depending on the topological distribution of fibres some RNs may be better than OD while some may be worse. However, clustering had the same effect on moisture progression in RN as in OD. Due to the presence of two clusters in the left half of the RVE moisture progresses faster in the left half of the RVE and slows down in the right half.

To estimate the rate of internal progression of moisture the colour based spatial` calibration technique (J Image) is used. Fig. 5.11 presents the fraction of saturated area measured at different time steps for different microstructures. It can be noted that saturation front moves exponentially in space. On careful observation of the individual curves it can be noticed that during the initial stages moisture transport is faster in the clustered models (20%-100%) as compared to unclustered models (0%). The trend gets reversed at later stages of the diffusion process.

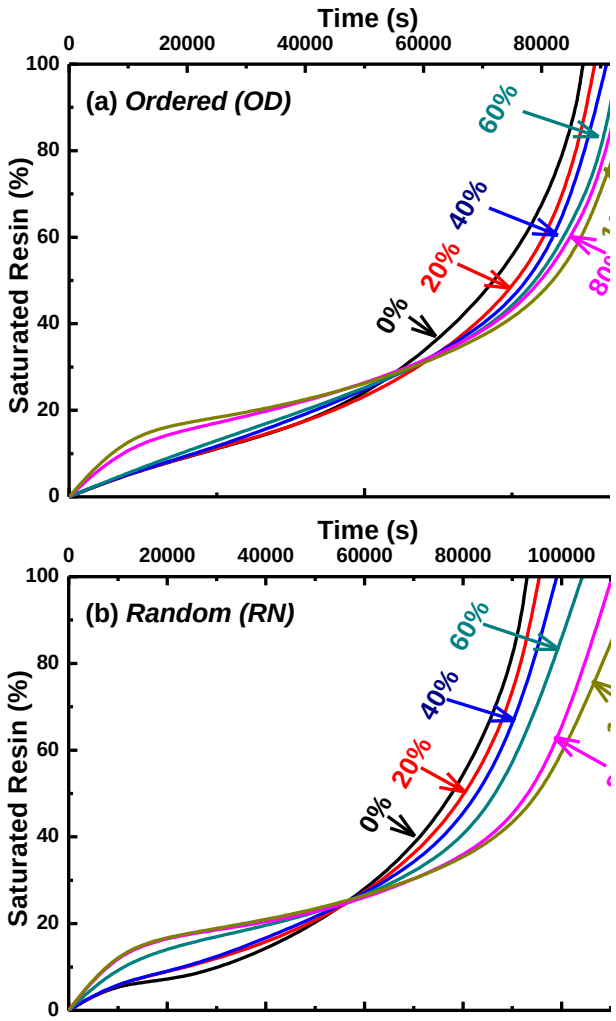

Fig. 5.11. Saturation time for (a) Ordered and (b) Random microstructures

The curves intersected each other at around 60000 s. After that time moisture progression slows down as the fibres get more and more clustered near the poles. As a result, the time to saturate increases monotonically as clustering progresses from 0% to 100%. It is worth mentioning that location of clusters respective to each other plays a key role. In this case two clusters are located in the left half of the RVE. Thus, when the saturation isoline progresses beyond the left half two clusters pull it to the left while only one cluster pulls it towards the

right. As a result, the progression slows down greatly. If the direction of progression is reversed and the moisture is introduced from the right edge an opposite picture will emerge. Clustering will initially slow the moisture progression down and later accelerate it.

On comparing Fig. 5.11a and Fig. 5.11b, it is clear that RN takes longer time to saturate than OD. The gap widens with the degree of clustering. The RN fully clustered microstructure has the highest time to saturation, close to 12,000 s. Clearly, the topological distribution of the fibres in a RVE has greatly affected the moisture diffusion characteristics. In this case saturation time varies from by over 40% from a little over 8,500 s to nearly 12,000 s.

5.4 Correlation study

5.4.1 *AND vs. diffusion response*

The topological entropy based on suggested nearest neighbour metric AND has been correlated microstructural diffusion response. Fig. 5.12 indicates the linear fit R^2 values for various x/r ratios of chosen volume fractions. It may be noted that at low x/r both OD and RN structures correlate poorly with AND. As x/r increases the correlation with AND improves rapidly. It has been pointed out earlier that AND is a local measure of clustering. The saturation time, on the other hand, is a global phenomenon for the entire RVE. Thus, a low x/r the correlation between AND & saturation time is poor. As x/r increases the AND represents more global characteristic of fibre distribution. As a result, the correlation improves.

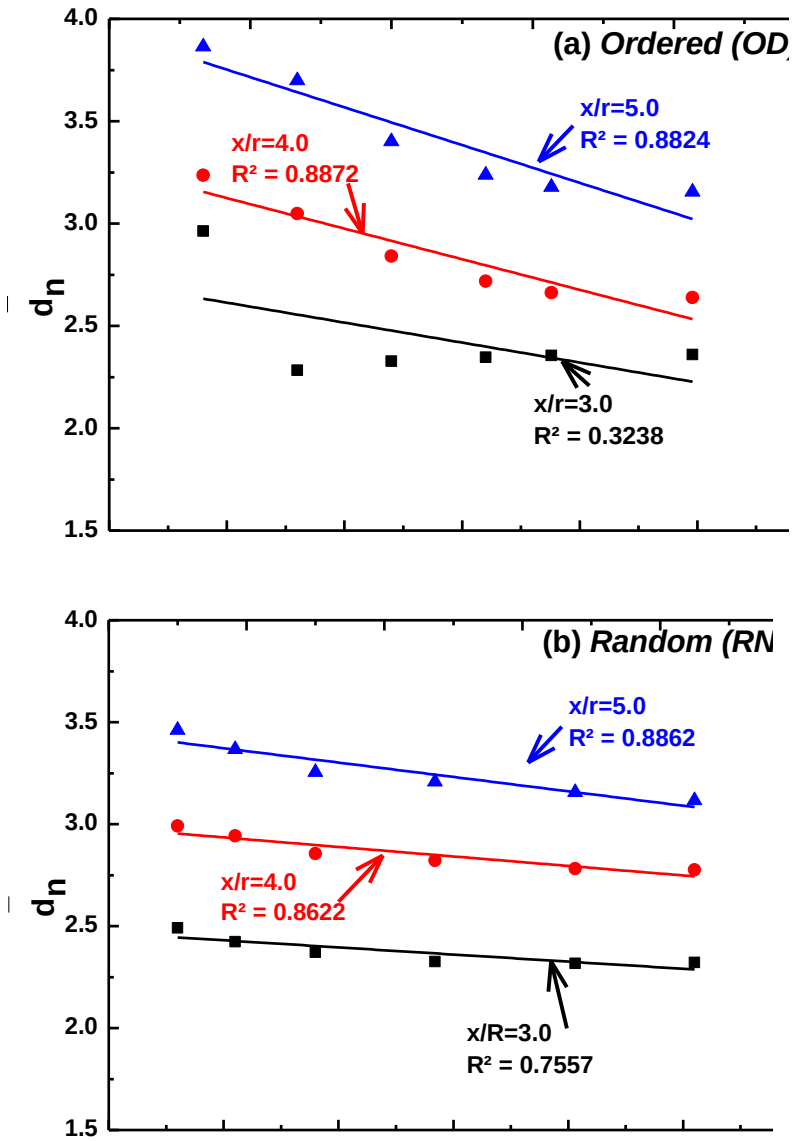

Fig. 5.12. AND vs. saturation time correlation for (a) Ordered and (b) Random microstructures

5.4.2 *ACD vs. diffusion response*

The previous example shows that AND correlates better with saturation time at higher x/r. It indicates that a global measure of fibre distribution would be preferable for correlating with saturation time.

The average cluster distance (ACD) is such a global measure. Fig. 5.13 shows an excellent correlation of this metric with the microstructure saturation time both for OD and RN. The correlation is marginally better in case of RN than OD. It demonstrates that ACD is able to capture the topological characteristics very well for the purpose of moisture diffusion studies.

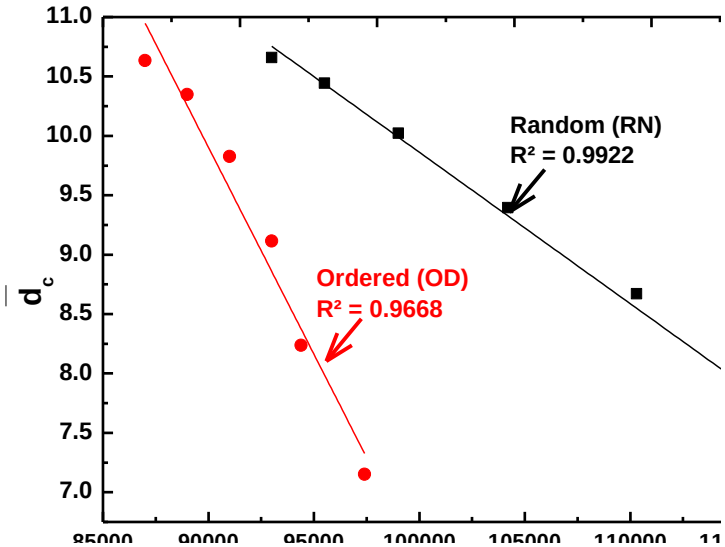

Fig. 5.13. ACD vs. Saturation time correlation

5.4.2 *Ripley's K vs. diffusion response*

ACD is an excellent measure for diffusion studies in composites. However, it is for a pole based clustering. For a general cluster it may not be possible to identify a pole at all times. In such situations Ripley's K metric can be a good alternative. It is demonstrated earlier that Ripley's K represents the global characteristic of the composite. In this section the topological entropy based on Ripley's K metric has been correlated with microstructural diffusion response. Fig. 5.14 shows the correlation parameter (R^2) of linear fit between Ripley's K and saturation time for various x/r cases. A consistently good correlation

can be observed. When compared with AND Ripley's K produced better correlation for the same x/r. In this case too, the correlation improved for higher x/r. Thus, Ripley's K is a good metric for statistical representation of fibre arrangement in composites for assessing moisture diffusion. RN had a better correlation than OD in all the cases. However, both microstructures correlated very well with Ripley's K.

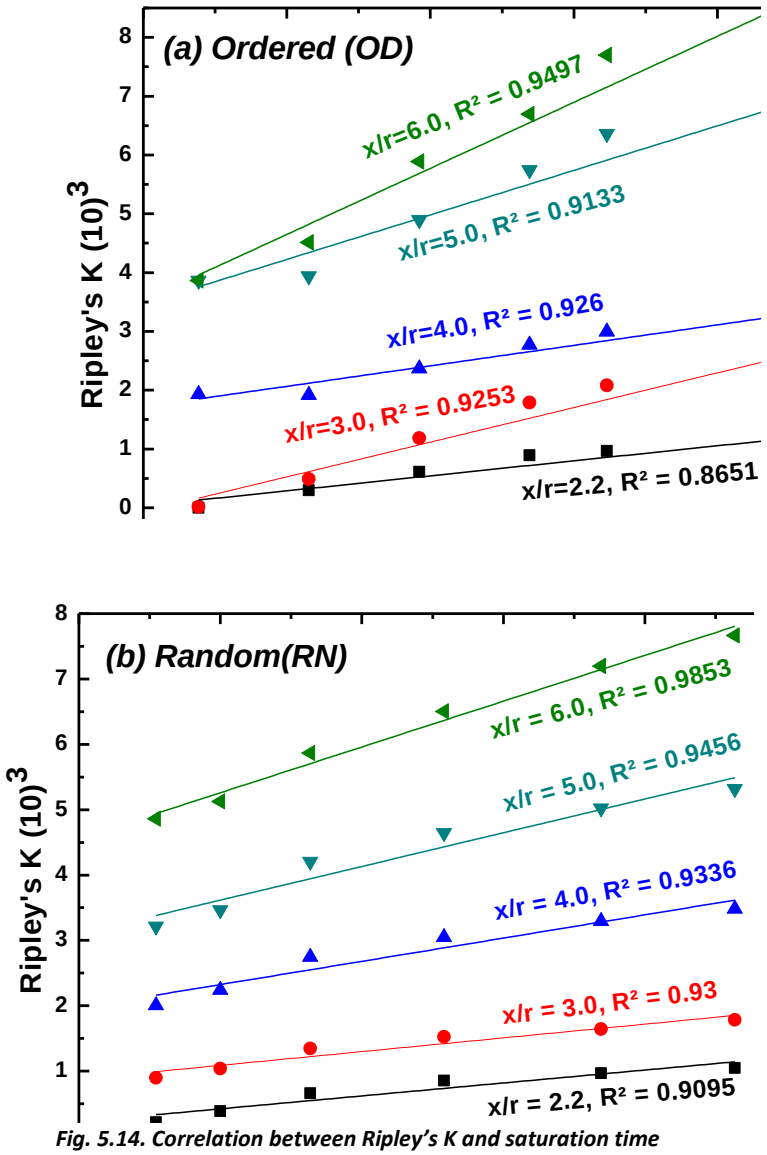

Fig. 5.14. Correlation between Ripley's K and saturation time

Chapter 6: Hygromechanical Response

In this chapter the work is extended to include the moisture induced stresses along with the rate of diffusion in various fibre architectures. A numerical study has been carried out to determine moisture concentrations in the matrix along with the corresponding stresses. Moisture diffusion and the resulting stresses in a fibre-matrix system vary considerably with the topology of the fibres inside the polymer matrix. This chapter reports a numerical study on stress build up in FRP due to moisture diffusion. The Fickian diffusion model is implemented. Stresses due to the transient moisture distribution have been estimated through the finite element modelling. Some fundamental topologies have been studied. Most important topological parameters have been identified. Utilising the results of fibre neighbourhood, interpretation of large microstructures has been discussed. Considerable interactions among neighbouring fibres are observed in the stress build up.

6.1 Numerical model

The present problem deals with diffusion inside unidirectional fibre-matrix composites where fibres are very long compared to their diameter therefore plane strain model is a reasonable approximation. Fig. 6.1 is an illustration of the present UD composite.

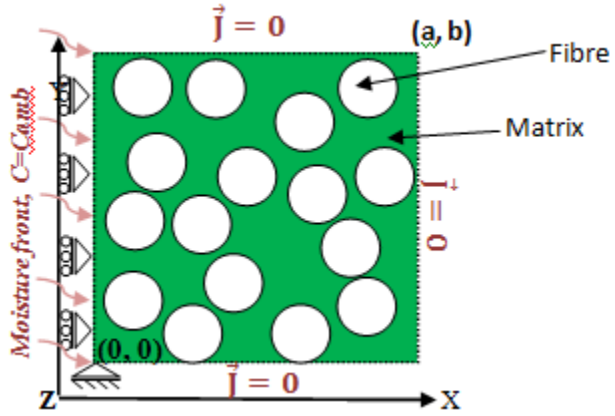

Fig. 6.1. Present diffusion problem in composite and boundary conditions

To model the moisture diffusion response the following boundary conditions are taken:

(a) Moisture boundary conditions:

The initial moisture concentration inside the composite is null. The moisture exposed left edge attains the boundary moisture (C_{amb}) as soon as it is exposed to the environment.

$$C = 0 \qquad (0 < x < a, \forall t = 0) \tag{6.1}$$

$$C = C_{amb} \qquad (x = 0, \forall t > 0) \tag{6.2}$$

(b) Flux boundary condition:

There is no moisture flux $(\vec{J})$ across the other 3 edges (Right, bottom and top) for the entire duration of analysis

$$\vec{J} = 0 \quad (x = a, y = 0, y = b, \forall t \geq 0) \tag{6.3}$$

(c) Displacement boundary conditions:

$$U_1(0, y) = 0 \ \ (0 \leq y \leq b) \tag{6.4a}$$

$$U_2(0,0) = 0 \tag{6.4b}$$

The Moisture boundary conditions and flux boundary conditions are similar to ones used in chapter 4 and 5 to simulate the diffusion response. Whereas displacement boundary conditions are employed to

induce the hygromechanical stresses. Here U_1 and U_2 are the displacement degrees of freedom along *X* and *Y* directions. With the imposed displacement boundary conditions the composite exhibits a controlled expansion in both the directions. In addition to the mentioned boundary conditions the nodes are tied at the fibre matrix interface to model the interfacial behaviour. Once boundary conditions are applied, the resulting linear simultaneous equations of Eq. (3.14) can be solved for nodal displacements and hence, Eq. (3.15) for stresses. In this investigation Eq. (3.4) and Eq. (3.14) have been discretized in a finite element form (ABAQUS/STANDARD, 2011). As the material properties have been assumed to be unaffected during the entire process the two governing equations are uncoupled and they can be solved successively at every time step.

6.2 Numerical examples

The properties of the materials and boundary moisture concentration are taken after the numerical and experimental investigations (Joliff *et. al.,* 2014). These are similar to the ones used in chapter 5 (Table 5.1). The boundary moisture concentration is 2.29% (Joliff *et. al.,* 2014). A finite element model of the composite was developed based on 2D plane strain assumption. The convergence of the mesh used in this study has been reported earlier in chapter 4. At first, simple cases of neat resin and resin with a single fibre is presented to illustrate the composite effect. The effect of fibre topology is presented in the end of this chapter.

6.2.1 *Resin only model*

A square domain of side 54 µm has been considered to model the stress build up due to transient moisture diffusion inside the resin in absence of fibre. The Von Mises stress at the centre of the right hand edge is presented in Fig. 6.2. Understandably, the stress is zero in the beginning. It asymptotically converges to around 6 MPa. It may be noted that the resin freely expands in *XY* plane, but plane strain condition imposes the condition $\varepsilon_{ZZ} = 0$. Due to the condition of isotropic free expansion in *XY* plane, shear stress σ_{XY} is zero at all time and normal stresses σ_{XX} and σ_{YY} are non-zero only when moisture concentration varies in the XY plane. In the end of the diffusion process all points in the domain reach the maximum moisture concentration (2.29%). At that instant, the in-plane strains reach their theoretical limit. The limiting value of the in-plane strains ε_{XX} and ε_{YY} for the present material is 0.309%. At that time, the in-plane stresses are zero because the moisture concentration is uniform in x and y. However, the out-of-plane stress (σ_{ZZ}) would exist due to the imposition of plane strain condition. Using the plane strain relation (σ_{ZZ}) for at the saturation can be evaluated. For the resin matrix of the Von Mises stress at saturation is 6.183 MPa $(\sigma_h = \beta_h CE)$. It can be seen from Fig. 6.2 that Von Mises stress indeed converges to that value in this example.

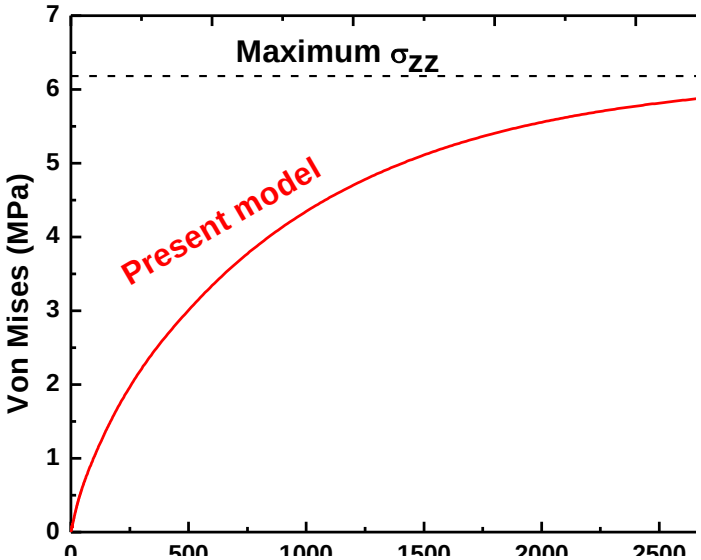

Fig. 6.2. Mises variation within neat resin

Fig. 6.3a shows ε_{XX} along the centre of the domain from left to right and at different time points. *X=0* corresponds to left edge that is exposed to moisture. Understandably, the strain is maximum there. The strain gradually reduces as we move from the left to the right edge. As the diffusion progresses the moisture concentration approaches the maximum value throughout the domain. As a result, the difference of strains across the domain goes down and the entire domain approaches the uniform strain (0.309%). In Fig. 6.3b the Von Mises stress along the same line has been plotted. In the initial stages when the variation of moisture concentration is high, normal stresses σ_{XX} and σ_{YY} are present. As the diffusion progresses, due to free expansion in *XY* plane, σ_{XX} and σ_{YY} diminishes and in the end only σ_{ZZ} dominates. Thus the Von Mises stress converges to the theoretical value of σ_{ZZ}.

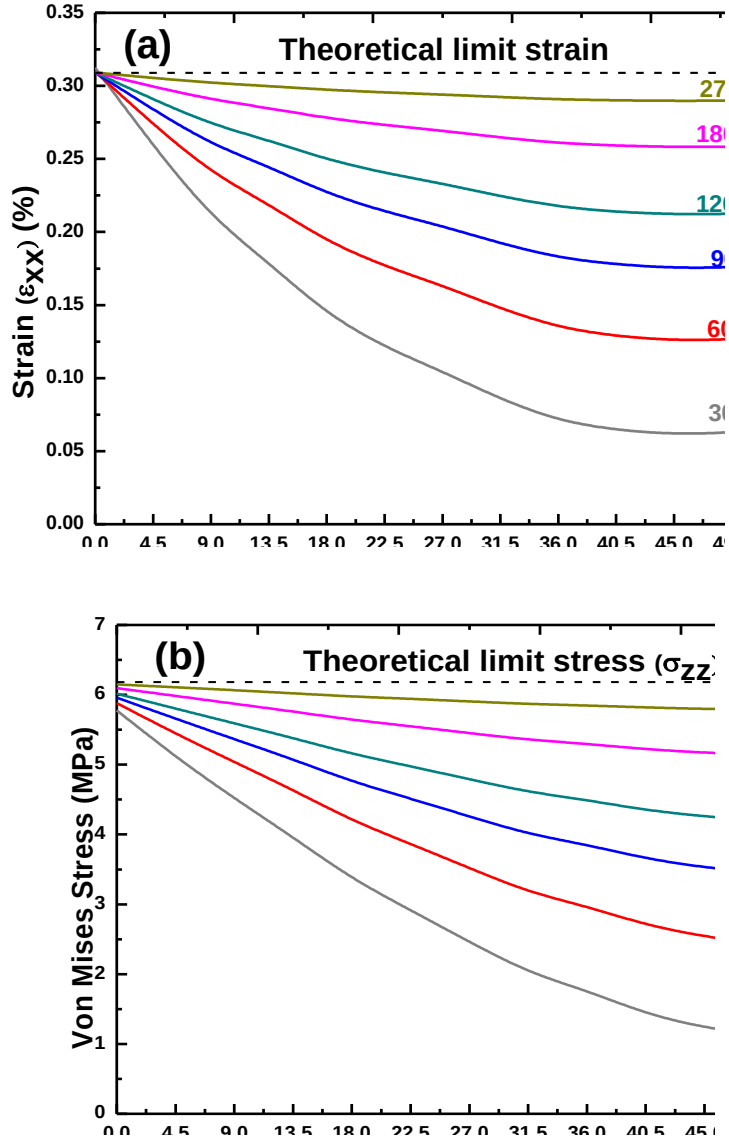

Fig. 6.3. Spatial and temporal variations of (a) Strain (ε_{xx}), and (b) Von Mises stress inside neat resin

6.2.2 One fibre in resin

To understand the effect of fibre, one fibre is introduced at the geometric centre of the domain of resin. The diameter of the fibre is 18 µm which is a third of the edge dimension of the resin domain. All

other parameters remain the same as the previous example. It may be remembered that no moisture diffuses into the fibre and its elastic constant is more than 20 times higher than that of the resin. As a result, its deformation will be marginal. This is discernible in the plot of ε_{XX} (Fig. 6.4a). As a result of introduction of the fibre the interface between the fibre and the matrix experiences a surge in ε_{XX}. The strains are higher at higher moisture concentrations. With the progress of diffusion the strains away from the fibre approach that of free expansion strain of the resin. But the strain in the vicinity of the fibre remains almost double of the free expansion strain. This example illustrates the strain build up at the interface of two mechanically dissimilar materials (glass and epoxy resin). The inset shows the strain contours at saturation. The concentration of strain around the fibre is clearly illustrated.

The build up of strain around the interface makes it imperative to study its effect on stresses (Fig. 6.4b). Clearly, the Von Mises stress in the matrix close to the fibre is nearly two times that away from it. This clearly demonstrates the distress of the interfacial region. The inset shows the stress contours at moisture saturation. It is clear that a sharp concentration of stress exists around the fibre. Understandably, this phenomenon makes the interfacial region far more vulnerable to failure and ageing. Especially, in cyclically varying moisture concentration the interfacial region is likely to fatigue far more rapidly than the rest of the composite. In combination with mechanical stresses, this region is more likely to reach the material limits and crack. The cracks may increase diffusion and soften these regions. That in turn can cause fibre pull out and mechanical failure of the composite.

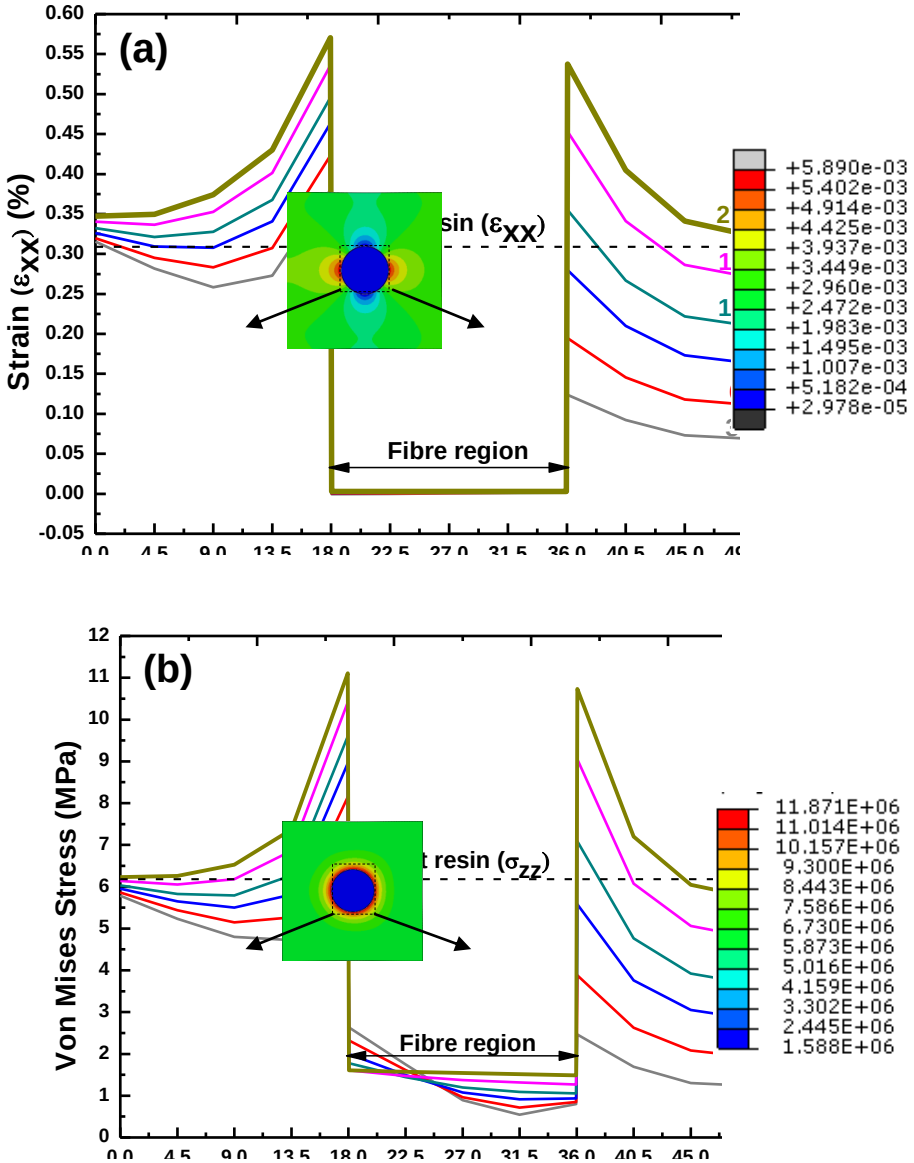

Fig. 6.4. Single fibre problem (a) Strain (ε_{xx}) (b) Von Mises stress (x=18μm-36μm is the fibre region)

Moreover, the increased diffusion can cause flow of deleterious ions that attack the fibre. Thus, the stresses at the fibre-matrix interface are of paramount importance in determining the capacity and life of composites.

6.3 A fibre neighbourhood in resin

The previous section illustrated the effect of one fibre in resin. In a composite there are many fibres and their topological arrangement can influence the mechanical response of the composite. This section illustrates the effect of fibre neighbourhood. The effect on the overall stress due to the introduction of other filaments in the vicinity of the reference filament is reported. The filaments surrounding reference filament are named as neighbourhood filaments. The neighbourhood is characterized by three parameters – angle (θ), distance (*d*) and density (*N*) (Fig. 6.5).

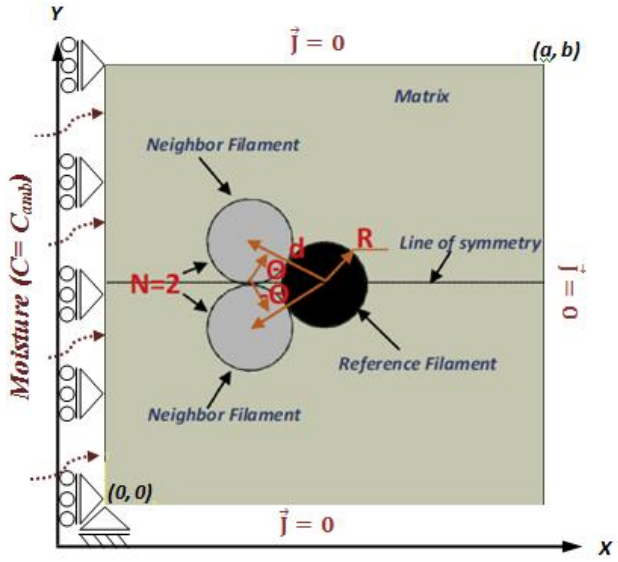

Fig. 6.5. Present diffusion problem

The neighbourhood filaments are located in a symmetrical fashion across the horizontal line bisecting the reference filament. Thus, neighbourhood filaments are introduced in a pair at ±θ at the same distance (*d*) from the reference filament. The angle (θ) is varied in a range of 30° – 150° with an increment of 30°. Five inter-fibre distances (*d*) are chosen in the range 2.05R - 3.0R, where R is the radius of the filament. The considered distance range covers a theoretical fibre

volume fraction range (35%-75%). Although the theoretical minimum distance between fibres is 2.0R some gap between the fibres is inevitable. Therefore 2.05R is chosen as the minimum gap.

The stresses are estimated for the same moisture condition described in the previous examples. The models were meshed using 4-node plane strain quadrilateral elements (CPE4T) (ABAQUS/STANDARD, 2011). A convergence study was conducted to decide the meshing. Approximately 12,000 elements were used to represent each model. Time step is chosen according to Eq. 4.6. Fig. 6.6 illustrates the moisture concentrations and the corresponding Von Mises stress distribution at different time points for one of the configurations (θ = 30° and d/R = 2.2). The phenomenon of moisture progression has already been reported in chapter 4. This discussion explains the stresses caused by the moisture ingress. At all times the moisture concentrations and Von Mises stress are symmetric about the central horizontal axis due to symmetry. The stresses are higher near the fibres and they rapidly go down away from the fibre region. Within the fibre region the resin sandwiched between two fibres experiences the maximum stress. Thus, this area is most susceptible to failure and degradation.

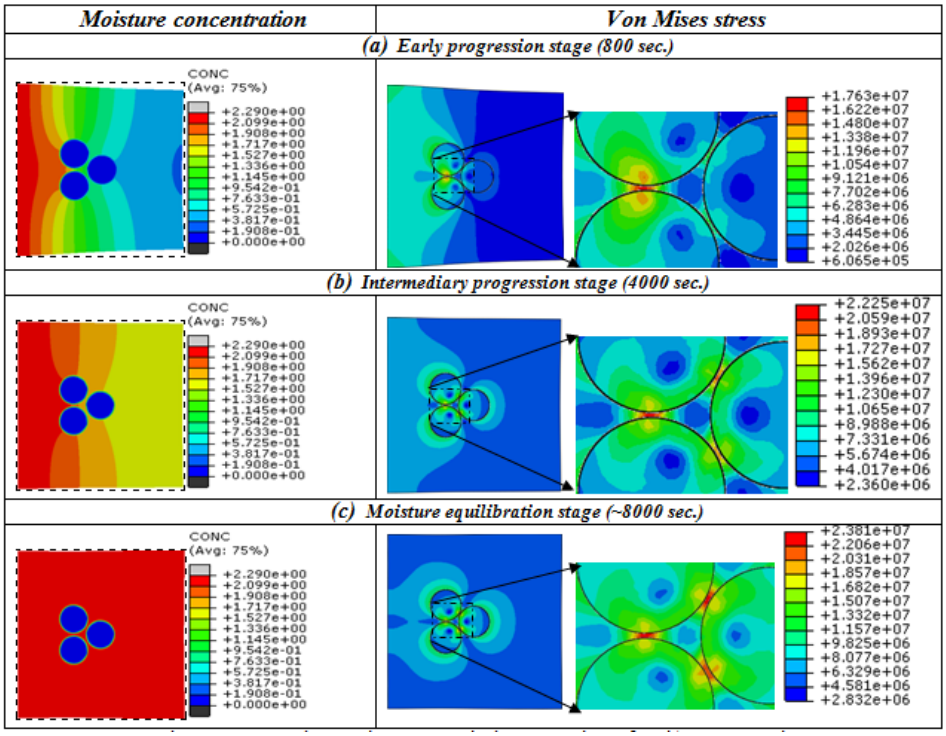

Fig. 6.6. Moisture progression and stress evolution snapshots for d/R=2.05 and ϑ=30°

At 800s the stresses are largest at the interface of the two leading fibres. It can be seen that a sharp concentration occurs in the region where the distance between the two fibres is minimum. Due to ingress of moisture the resin tends to expand. However, the two stiff fibres constrain the expansion of the resin between them causing stress concentration. Stress concentration of a lesser degree can be discerned between the leading fibres and the back (reference) fibre. However, as the diffusion progresses even those interfaces reach the same level of stress concentration as the leading fibre interface. The value of the maximum stress is considerably higher than that in the single fibre case. Eventually, at t = 4,000s. The stress concentration in this neighbourhood is more than two times of that of the single fibre case. This example illustrates the effect of fibre neighbourhood on stress

concentration. An analysis of the effect of fibre topology on stress concentration follows.

The subsequent sections demonstrate the influence of the parameters θ, *d* and *N*. The transient variations are plotted against two independent variables- moisture content (Fig. 6.7) and time (Fig. 6.8).

6.3.1 Influence of θ

This section reports the effect of the angle between the neighbouring fibres and the reference fibre on the mechanical stress behaviour. Neighbourhood filaments are introduced in a pair at ±θ angle and at the same distance (*d*) from the reference filament. Two cases of d = 2.05R and 2.5R are presented. The orientation (θ) is varied in a range of 30° – 150° with an increment of 30°. Fig. 6.7 illustrates the maximum Von Mises stress at different states of moisture ingress. At d = 2.05R (Fig. 6.7a) the fibres are closest to each other and the stress concentration is maximum. The curve for 150° is almost linear and has the lowest stresses. The 30° curve has higher initial values but later follows the 150° curve closely. It may be noted that at 30° the neighbouring fibres are closest to the left edge. Thus, moisture reaches them early creating initial high stress. The 60° curve has the highest stresses followed by 120°. Thus, in 60° to 120° angle highest stresses are expected. The rest of the curves are bunched together. At 2.5R (Fig. 6.7b) the trends are the same but the stress values are far lower (almost half) than that at 2.05R. The results show that stress concentration is far more sensitive to inter-fibre distance than the angle between the fibres.

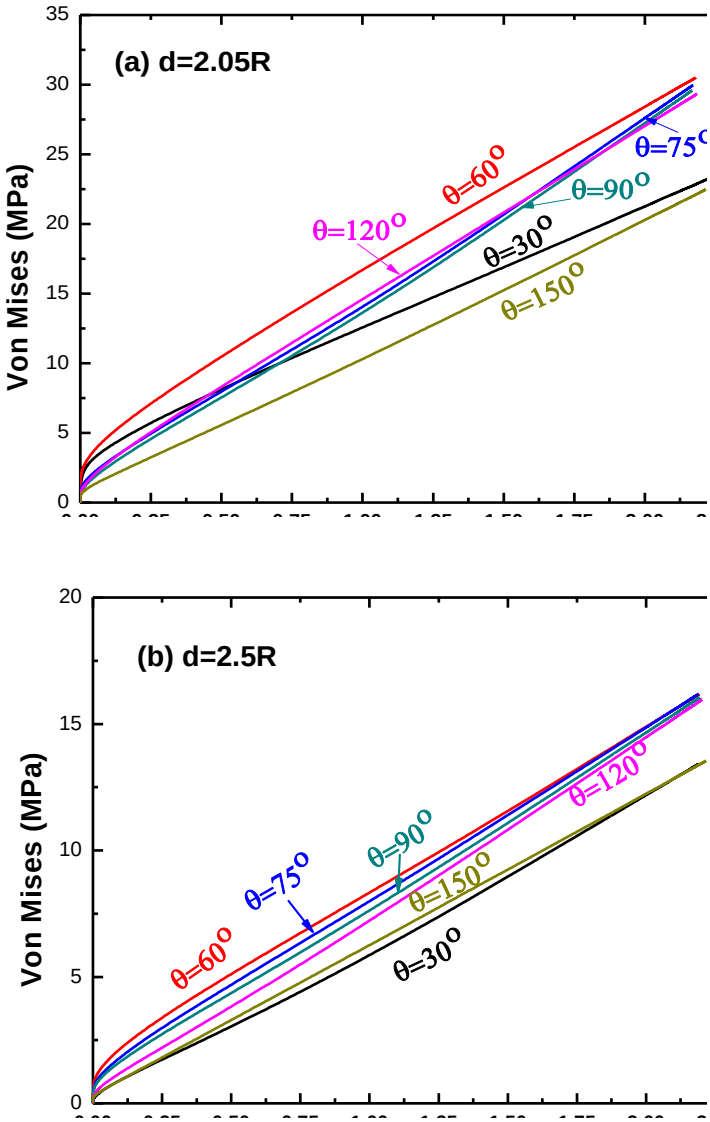

Fig. 6.7. Mises vs moisture plots for (a) d=2.05R and (b) d=2.5R

6.3.2 Influence of *d*

The effect of inter-fibre distance (*d*) is analysed by placing the neighbouring fibres at varying distances from the reference fibre. Fig. 6.8 demonstrates the maximum Von Mises stress at different stages of diffusion. The stresses build up early and then reach a plateau. It may

be noted that in case of 30° the neighbourhood fibres are in front the reference fibre. Therefore, the moisture reaches the fibre earlier than other configurations. Thus, there is a rapid rise of stress. In case of 90° the neighbourhood fibres are in line with the reference fibre. The stress build up in this case is slower than 30°, but faster than 150°, where the neighbourhood fibres are behind the reference fibre. The maximum stresses at d = 3.0R are the same level for all the angles. If we compare these values with that of the single fibre case in Fig. 6.4b we would observe that they are very close. Thus, it can be concluded that at d ≥ 3.0R the neighbourhood effect is negligible. The corresponding fibre volume fraction is about 35%. Therefore, for composites with fibre volume fraction less than 35% fibre neighbourhood has no effect on stress intensification due to moisture ingress. It is also clear that the maximum stress rises exponentially as the inter-fibre distance reduces. It is maximum when the inter-fibre gap is minimum at 2.05R. It is about 2.5 times more than that for d=3.0R. Thus, the inter-fibre distance needs to be carefully controlled to avoid premature failure of the composite. It is also imperative to choose the fibre volume fraction wisely. It is quite common to closely pack fibres and increase the fibre volume fraction to achieve high strength and stiffness of the composite in the direction of the fibre. However, as the fibre volume fraction increases the inter-fibre distance would reduce and the stress induced by moisture diffusion would rise exponentially. At around 75% the volume fraction would be highest and so would be the stresses. Comparison of the three stress patterns reveals that the stresses are at their peak for d=2.05R and 90°. This configuration has been further investigated to pinpoint the areas of stress concentration.

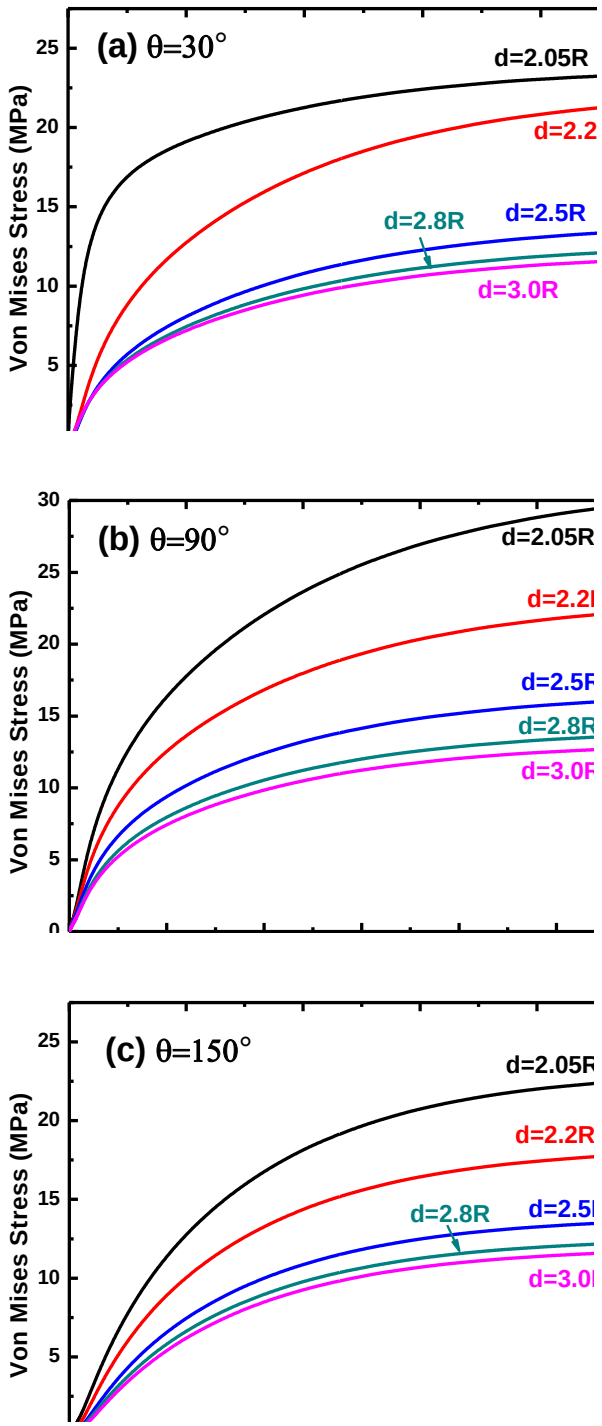

Fig. 6.8. Von-Mises stresses vs. time plots for (a) ϑ=30° (b) ϑ=90° and (c) ϑ=150°

To demonstrate the variation of stress concentrations with inter-fibre distance the stress snapshots at 90° have been plotted (Fig. 6.9). It is seen that the stress concentration occurs in the gap between two fibres. Due to moisture ingress the resin tends to expand. That exerts expansive pressure on the fibres. However, the fibres remain dry and they are stiff as well. Therefore, they impede the expansion causing stress concentration. The body strain in the inter-fibre region is proportional to the moisture concentration gradient. For the same moisture gradient the body stain is independent of the inter-fibre distance, but as the fibres come closer there is less room for the resin to expand and as a result, the stress builds up.

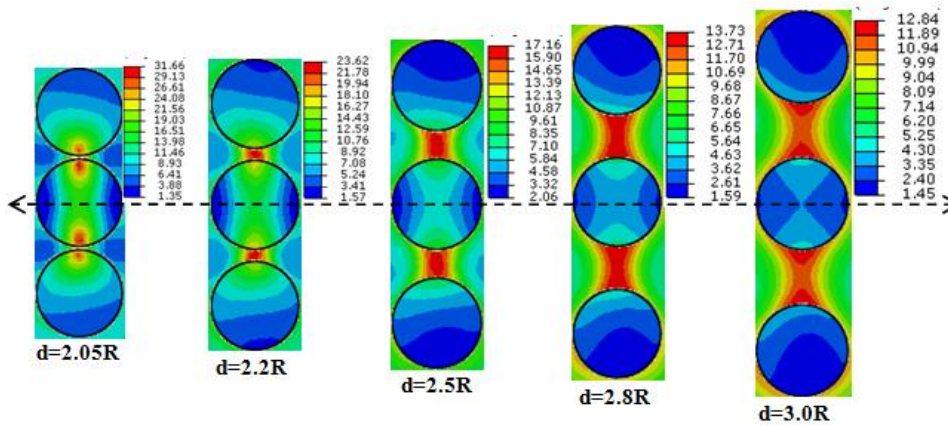

Fig. 6.9. Variation of Mises near the interface zone with increase in inter-fibre gap (θ=90° case).

Fig. 6.10 summarizes the peak stresses for the entire range of θ and d. There is one reference fibre and two neighbourhood fibres in all the samples. At d = 3.0R the stress concentration is negligible. The stresses rise rapidly with reducing d. All the curves are flat in the region 60° to 120°. These conclusions have been used later to propose hypotheses on the stress concentration in fibre composites due to moisture diffusion.

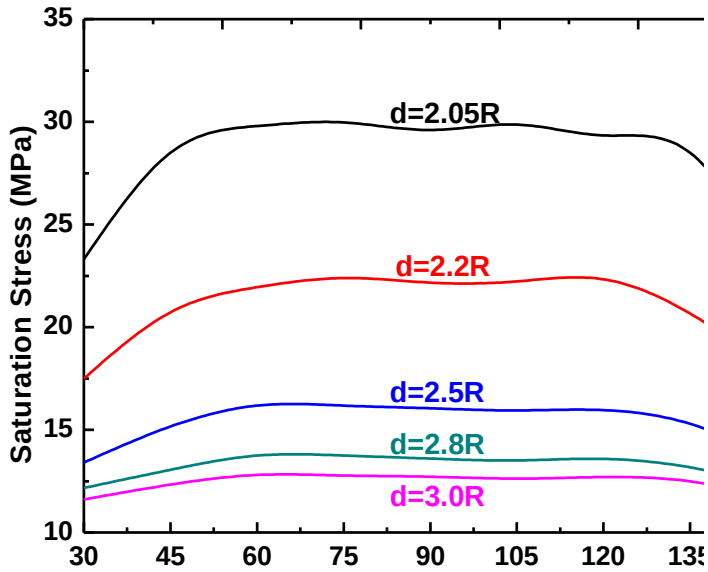

Fig. 6.10. Saturation stresses vs. neighbourhood orientation

6.3.3 Influence of N

In this Section the effect of the number of fibres in a neighbourhood is studied. We have seen earlier that a closely packed fibre topology at 90° had the maximum stress concentration. Effect of adding more fibres at the back and front of this neighbourhood has been studied (Fig. 6.11). Cluster C1 is the neighbourhood of three fibres at 90° (N = 3). C1 is a reference configuration. In C2 the two more fibres have been added in front of C1 (N = 5). In case of C3 two more fibres have been added at the back of C1 (N = 5). C4 has two fibres each at the front and the back of C1 (N = 7). The effect of these neighbourhoods on moisture diffusion has already been reported in chapter 4. The influence of additional neighbourhood fibres on the mechanical stresses has been reported here. For this purpose, peak stress at the same point where it was maximum in case of C1 has been observed for all the configurations. It can be seen that addition of new fibres in the

neighbourhood has reduced the peak stress in varying degrees. C3, with two fibres at the back of C1 has lower stress than C1 but higher than C2. It has been observed earlier that adding fibres in front of the base configuration influences moisture diffusion more. Thus, C3 leads to higher flux and higher stresses than C2. In case of C4 the least stresses are observed. Thus, we note a beneficial effect in addition of fibres in the neighbourhood. It may be noted that these solutions are in plane-strain with ε_{ZZ} as zero. With the addition of new fibres stiffness in that direction increases and as a result, the differential stresses in that direction reduces.

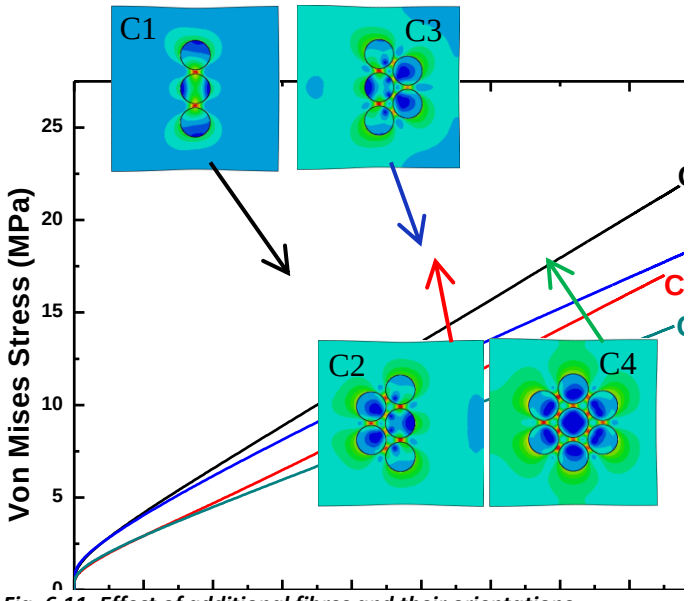

Fig. 6.11. Effect of additional fibres and their orientations

6.3.4 Comparison with large microstructure

This Section utilises three conclusions of the previous sections to make three hypotheses that would enable us to extend the present results to large microstructures. They are:

- There is no neighbourhood effect at $d \geq 3.0R$. Therefore, fibres lying beyond that distance from the reference fibre may be neglected.

- Addition of new fibres in the neighbourhood does not change the solution dramatically and the stress concentration reduces with introduction of new fibre. Thus, a minimal neighbourhood will yield conservative solution but not far away from the large neighbourhood model.
- Neighbourhood angles between 60° and 120° have largely the same stress concentration. Thus, we can choose an angle between these two values without sacrificing much accuracy.

In this Section the comparison is for the 90° neighbourhood (C1) result with that of previously reported large microstructures. In (Joliff *et. al.,* 2014) a random microstructure was generated and its stresses have been studied. The maximum stresses and their locations have been reported. This example compares the stress build up predicted by the large model vis-à-vis the present neighbourhood 90° model. It is worthwhile to note that the size of the present neighbourhood model is small fraction of the whole microstructure model. The volume fraction of the present neighbourhood models is similar to that of the large microstructure.

Fig. 6.12 presents the Von Mises stress of the large microstructure with the present C1. The stresses in the region encircled red are presented here. The trends in all the three curves are same. At the initial stages the neighbourhood models predict higher stresses than the whole microstructure. In case of neighbourhood models the moisture inducing edge (left edge) is very close from the fibres. Thus, moisture flux reaches the fibres early. However, in case of the whole microstructure the sampling point is further away from the edge. Thus its initial stresses are lower.

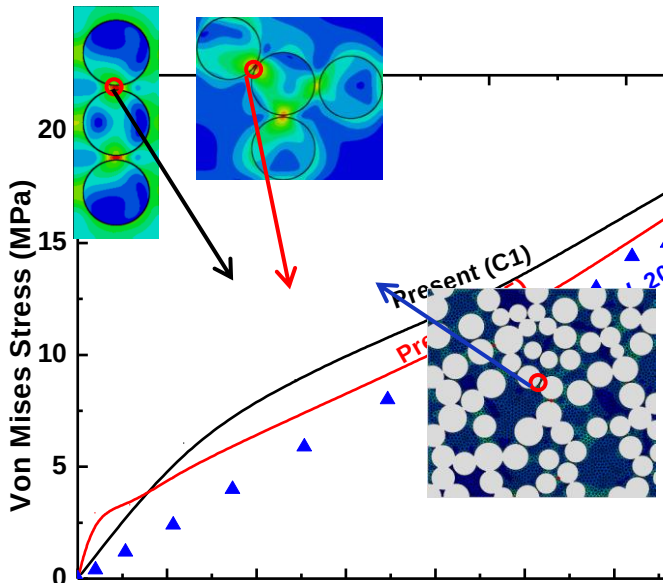

Fig. 6.12. Von Mises stress in C1, C5 and the whole domain

As time progresses all the curves become parallel to each other. C1 predicts about 12% higher maximum stress than the full model. This result supports all the three hypothesis mentioned earlier and demonstrates the utility of the present neighbourhood analysis. It can be concluded that the present neighbourhood analysis can be applied to any microstructure. The area with the closest inter-fibre gap may be selected from the microstructure and the results of the corresponding neighbourhood can be applied to obtain an upper bound of stresses.

As we represent the neighbourhood more accurately we should get closer to the solution of the whole domain. To test this hypothesis the local topology of fibres is modelled as C5. It can be seen that C5 predicts the stresses between those of C1 and whole microstructure. The maximum difference reduces to 8%. These results should facilitate rapid characterization of microstructures without having to resort to tedious modelling and analysis.

Chapter 7: Three Dimensional Analysis

The work presented in chapter 4, 5 and 6 was restricted to studies on diffusion and hygromechanical behaviour by taking two dimensional (2D) models. The stresses due to the expansion of the matrix caused by moisture diffusion are evaluated. A three-dimensional (3D) micromechanical model is developed to study diffusion both across and along the fibre. The well-known 2D plane strain condition is modelled and validated as a special case of the 3D model. The utility of 3D modelling is further demonstrated to analyse the stress along the fibre length. It is demonstrated that the variation of boundary conditions along the fibre length has a dramatic effect on the stresses. The stresses along fibre length computed through finite element analysis (FEA) are compared against an analytical solution obtained from axi-symmetric composite cylinder assemblage (CCA) model. This chapter demonstrates the importance of 3D diffusion kinetics in unidirectional reinforced polymer composites. The moisture progression is reported along the fibre length and time taken for moisture equilibration are analysed for different fractions of surface exposure. Moreover, in 3D models different boundary conditions at the fibre ends can be applied. In addition, when Von-Mises criterion is used in conjunction with plane strain assumption the stress along fibre (z) direction becomes a function of stresses along the xy plane. In the present work, the plane strain condition is reported as a special case of 3D modelling by constraining the transverse (xy) planes. It is noted that plane strain assumption predicts lower stresses at the interface than the fixed-free condition solved in the 3D case. The stresses along the

fibre directions are validated against the results obtained by the analytical concentric cylinder model approach. The importance of 3D analysis for certain boundary conditions is highlighted.

7.1 Three dimensional model and geometry

The three-dimensional model of a single fibre within a polymer matrix is created to analyse the moisture diffusion and hygromechanical response. Fig. 7.1 shows the matrix with a single, long and circular embedded fibre. The fibre diameter is 18µm and the dimensions of square section along the XY plane are 54µm x 54µm. The overall length in the third (Z) direction is 540µm. Hence the aspect ratio of the fibre is 30:1. The complete domain is defined by 8 corners. The origin is at situated at corner O(0, 0, 0). The XY plane O-1-2-3 is termed as reference plane. The moisture boundary condition is applied on the plane O-3-7-4.

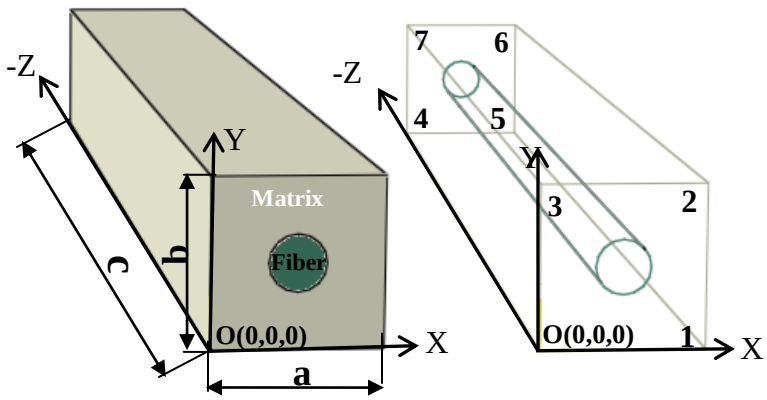

Fig. 7.1 Three dimensional single fibre in resin model

Different sets of boundary conditions are employed in order to estimate the states of diffusion through the domain at different instants. The stresses caused by the swelling of the matrix as a result of moisture diffusion are calculated.

7.2 Moisture diffusion analysis

The 3D moisture diffusion is performed by choosing Fick's law described in chapter 3. The boundary moisture content (C= 2.29%) and fibre matrix properties are adopted from experimental investigations (Joliff *et. al.,* 2014). The material properties are similar to the ones described in chapter 5 (Table 5.1).

7.2.1 Three-dimensional vs. two-dimensional models

The diffusion response is compared for two and three dimensional models under the similar boundary moisture content. Fig. 7.2 shows the moisture boundary conditions employed on both 3D and an equivalent 2D model. There is no moisture influx or outflux through any other surfaces/edges except the moisture exposed surface/edge.

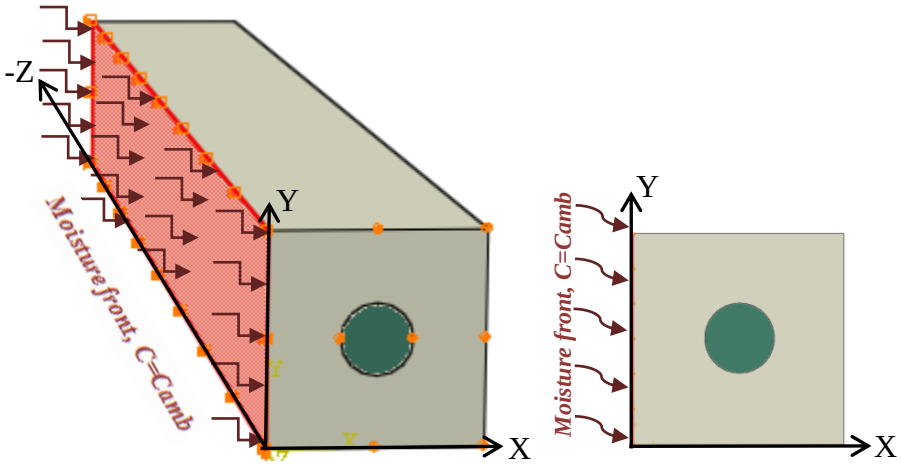

Fig. 7.2. Moisture diffusion boundary condition in (a) 3-D (b) 2-D

To model the moisture diffusion inside the composite following boundary conditions are taken:

(d) Moisture boundary:

The initial moisture concentration (c) inside the composite is null. The moisture exposed *YZ* plane (*i.e. x = 0*) attains the boundary moisture (c_{amb}) as soon as it is exposed to the moist environment.

$$c = 0 \qquad (0 \leq x \leq a, \forall t = 0) \tag{7.1}$$

$$c = c_{amb} \qquad (x = 0, \forall t > 0) \tag{7.2}$$

(e) Flux boundary:

There is no moisture flux $(\vec{J})$ across the other five planes for the whole duration

$$\vec{J} = 0 \qquad (x = a, y = 0, y = b, z = 0, z = -c, \forall t \geq 0) \tag{7.3}$$

The analysis is conducted on FE code Abaqus with the available mass diffusion procedure based on Fick's law. The models were meshed using 8 noded brick (*C3D8P*) in 3D and 4 noded (*DC2D4*) elements for 2D analysis.

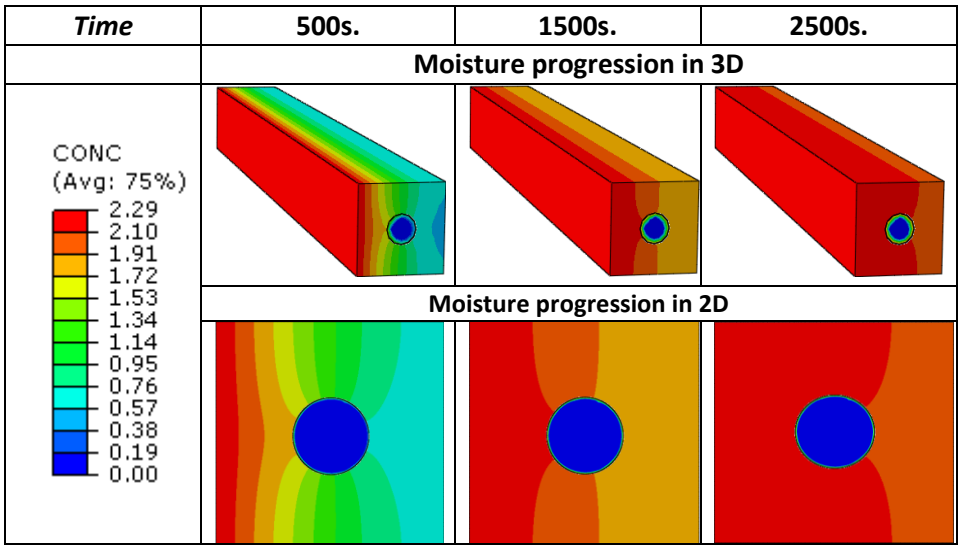

Fig. 7.3 Analogous moisture concentration profiles in 2D and 3D models.

Fig. 7.3 shows the moisture diffusion snapshots taken at different time instances. The moisture progresses from the moisture exposed face to the opposite face. It can be noticed that the profiles are identical for both the models. The effect of mesh quality is clearly visible in 3D model. The fibre although has zero diffusivity, the snapshots shows the moisture concentration contour inside the fibre for 3D model. This is due to the edge effect that arises due to the continuity condition for the nodes at the interface.

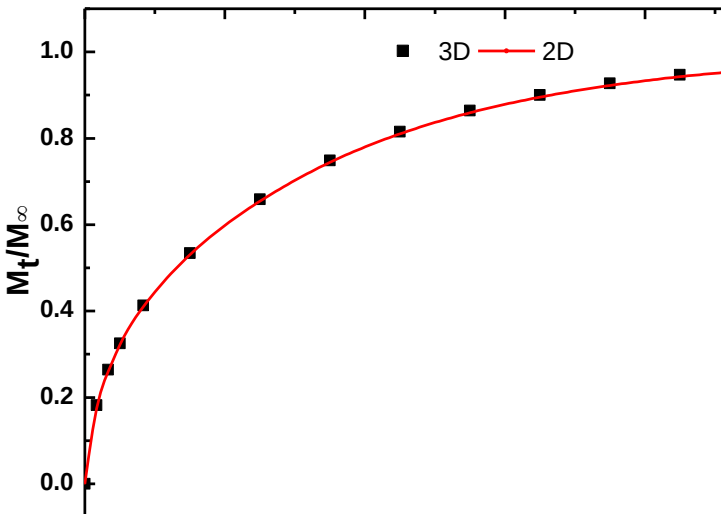

Fig.7. 4. Mass gain with time

Fig. 7.4 shows the mass gain curves for both 2D and 3D models with the progress of moisture. The rate of mass gain is maximum during the initial period of absorption. A high initial moisture uptake is followed by a saturation plateau. M_t and M_∞ denote the mass at time t and mass at time infinity respectively. At that time all points of the domain will attain the moisture concentration same as that of the applied moisture (2.29%). This can be understood from the solution of Fick's law in Eq. (3.9). The equation indicates that a saturation state will be approached asymptotically. This is the reason why the curve drawn for

fractional mass uptake (M_t/M_∞) asymptotes to unity. Thus, it is important to define a point of saturation. The saturation stage corresponds to a moisture level > 2.10% (it is > 92% of boundary moisture which is 2.29%). This exercise demonstrates that 2D model is sufficient for problems where the moisture load does not vary with z.

7.2.2 Partial (patch) moisture exposure

The moisture progression is analysed when a part of the face is exposed to moisture. In this case moisture will diffuse both across and along the fibre. Fig. 7.5 shows the moisture boundary condition to emulate the partial moisture exposures. Five different cases of partial moisture exposure along path ratios (*l/L* = 0.1, 0.25, 0.5, 0.75 and 1) are reported.

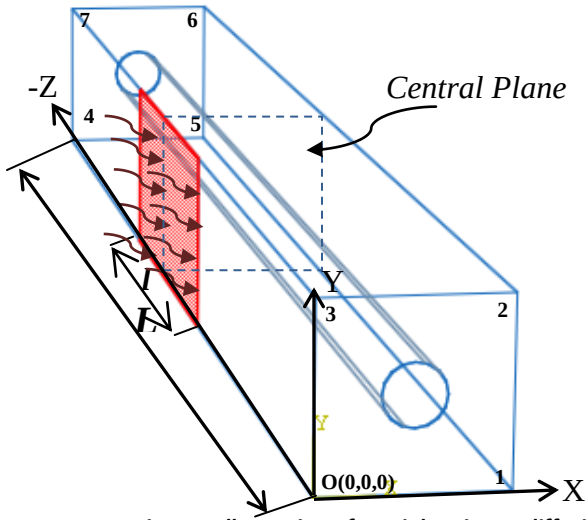

Fig.7. 5. Illustration of partial moisture diffusion

Here *l* is the length of moisture patch and *L* is the length of the composite along fibre (*Z)* direction. The patch is symmetric on both sides of central plane that is situated in mid-way between plane O-1-2-3 and 4-5-6-7. Fig. 7.6 illustrates the moisture progression both across the fibre direction (*XY plane*) and along the fibre direction at different time instances. The fibre remains dry because it has no diffusivity. In

chapter 4 while performing diffusion across the fibre it demonstrated that the dry fibre creates a high moisture gradient. As a result, the moisture isolines bend towards the fibre (Fig. 7.3). In case of 3D moisture diffuses simultaneously both across and along the fibre.

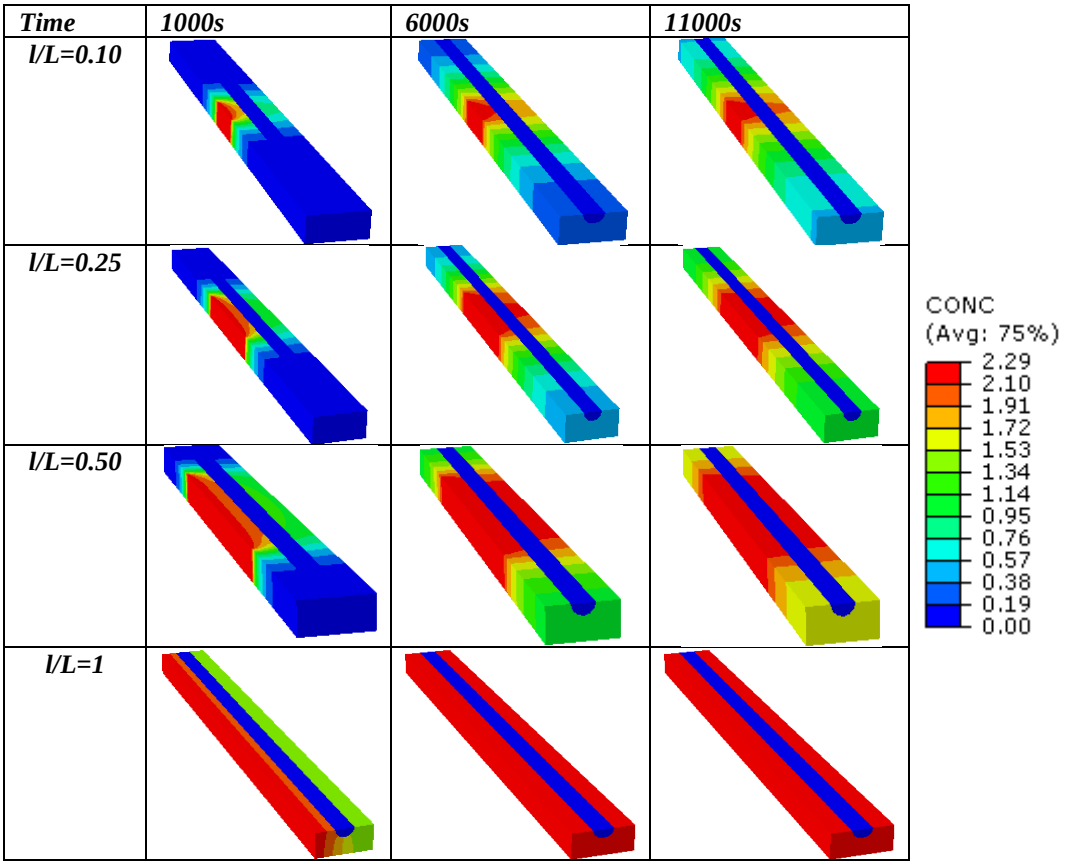

Fig. 7.6 Cut section views of moisture progression along the xz plane

In the case of diffusion along the fibre the isolines are not curved towards the fibre. This is expected as in this case the effect of fibre is identical both upstream and downstream of the moisture front. Fig. 7.7 shows the mass gain curves. It can be noticed that the rate of mass gain is affected by the patch width. The saturation time is gets exponentially higher as the patch length gets smaller.

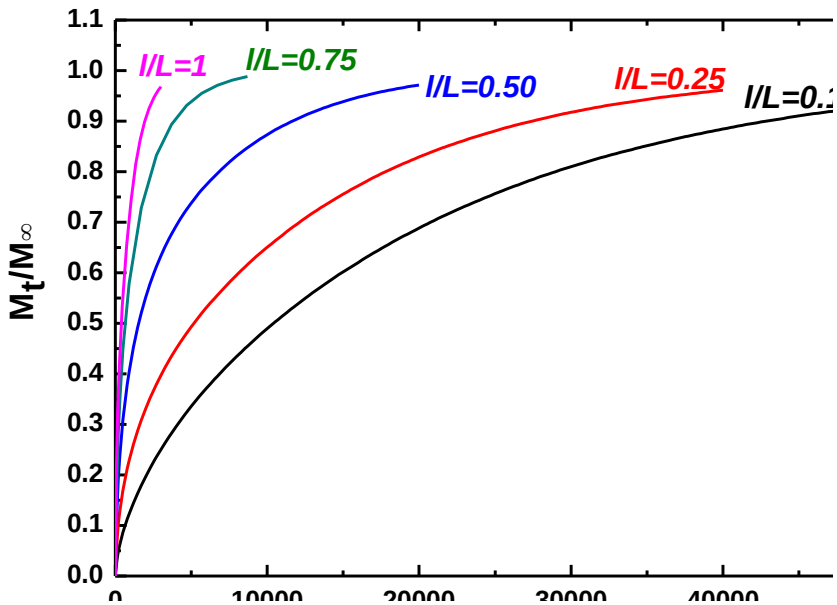

Fig. 7.7 Mass gain curves for different percentile of moisture exposed surface

Fig. 7.8 shows the moisture progression for a patch exposure of *l/L* = 0.5. Three different section views along the principle plains (*XZ, YZ and XY*) are used to illustrate the diffusion kinetics. Moisture progression along the fibre direction can be noticed from first two views whereas third view along section XY can be used to visualise the progression across the fibre. This view shows the section along the central plane (described in Fig. 7.5). It can be noticed that moisture isoareas spread out as they approach the fibre. It is due to the high moisture gradient that exists due to the presence of dry fibre. This results in a faster rate of moisture progression at the fibre-matrix interface.

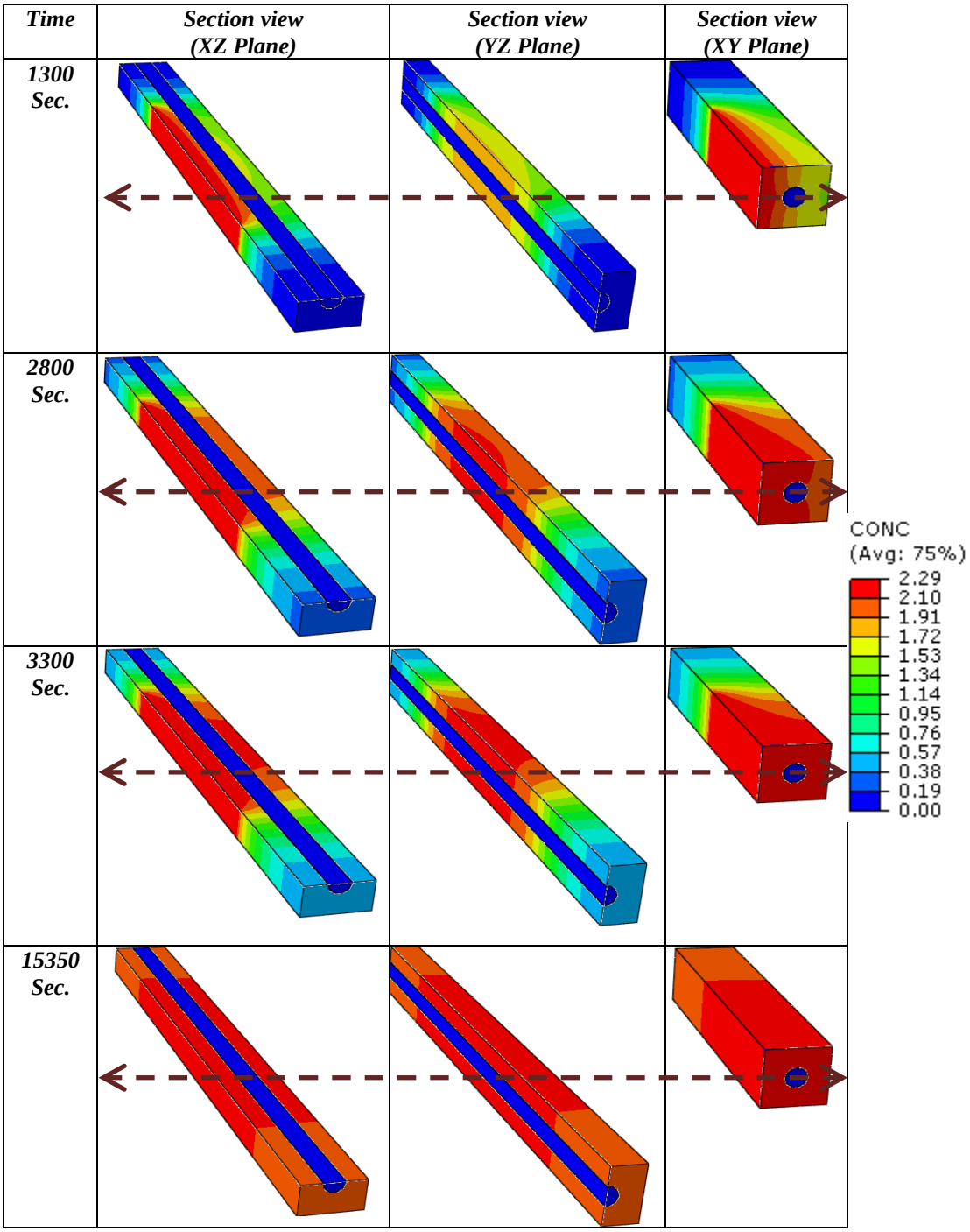

Fig. 7.8. Snapshots of moisture progression along different planes for l/L=0.5

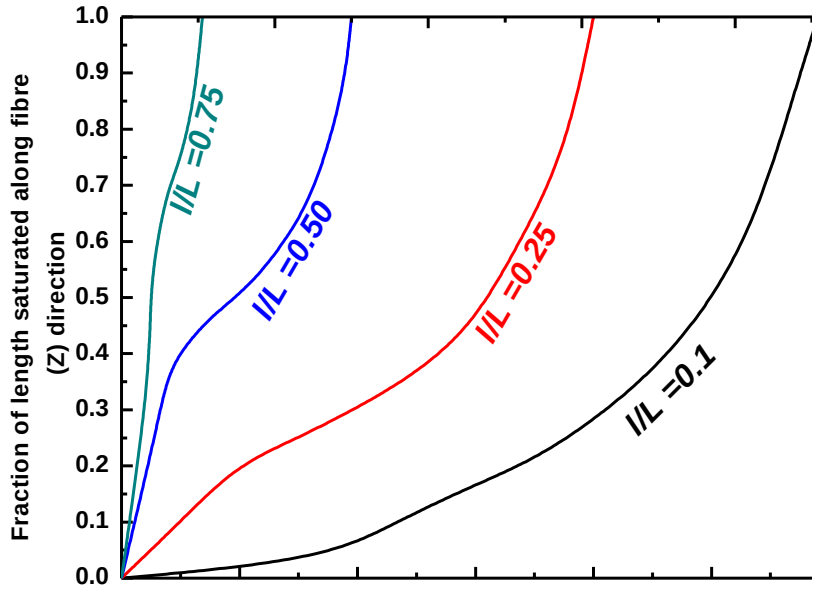

Fig. 7.9. Fractions of saturated length along fibre direction for different l/L.

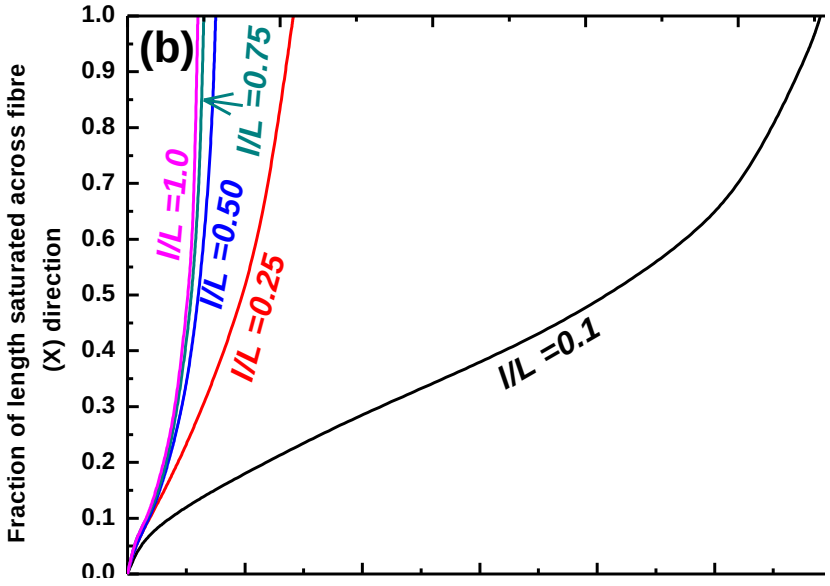

Fig. 7.10. Fractions of saturated length across fibre direction for different l/L.

The rates of propagation across the fibre (*X*) (Fig. 7.9) and along the fibre (*Z*) (Fig. 7.10) direction are compared. The fraction of saturated

length along the fibre and across the fibre is measured from the section views *YZ* and *XY* respectively at different time instances. The saturation time is obviously high for small patch lengths. The moisture saturation is attained first across the fibre and then along the fibre. This is due to the fact that dimensions across fibre are much smaller as compared to the length of the fibre. Fig. 7.9 shows that there are three distinct regions in each graph. Initially, the slope of the graph is high indicating fast rate of saturation. It continues until the fraction of length which is exposed to moisture gets saturated. In other words, for *l/L* = 0.25 the initial high slope continues until it reaches an l/L of 0.25 in y axis, as there is flow of moisture from the exposed face up to that length. The diffusion slows down from this point. Then it increases continuously until the entire length is saturated. This trend is expected, as Eq. 3.9 shows quadratic rate of change in moisture concentration.

The present analysis emphasises the importance of 3D modelling to represent the physics of diffusion kinetics.

7.3 Hygromechanical analysis

This section reports the hygromechanical stress-stain behaviour of the composite. The geometry considered is similar to the one reported for the diffusion response. The mechanical boundary conditions are imposed by constraining the displacements. U_1,U_2, U_3 denotes the displacement degrees of freedom along *X*, *Y* and *Z* directions respectively. Two different sets of boundary conditions are reported for three-dimensional models. These are referred as *Fixed-Fixed* and *Fixed-Free* boundaries.

7.3.1 Condition 1: Fixed-Fixed boundaries

The *Fixed-Fixed* boundaries refer to the constraints applied on the planes where the fibre terminates. This is done by constraining planes (O-1-2-3) and (4-5-6-7) so that the displacement along the fibre direction (U_3) is zero. Fig. 7.11 shows the 2D and 3D geometries. Plane O-1-2-3 and 4-5-6-7 may be referred as $Fixed_{Z0}$ and $Fixed\ _{Zmax}$ planes respectively. Applying these constraints prevents the axial movement of the fibre. It is close to a plane strain condition that is generally used while modelling in 2D. The boundary conditions for the 3D modelling can be summed up as follows:

$$U_1 = 0 \ \ (on\ left\ plane\ i.e. x = 0) \tag{7.4}$$

$$U_3 = 0\ (on\ Fixed\ _{Z0}\ plane\ i.e.\ z = 0, and\ Fixed\ _{Zmax}\ plane\ i.e. z = -c) \tag{7.5}$$

$$U_1 = U_2 = U_3 = 0 \ \ (at\ corner\ O(0,0,0)\ and\ corner\ 4((0,0,-c)) \tag{7.6}$$

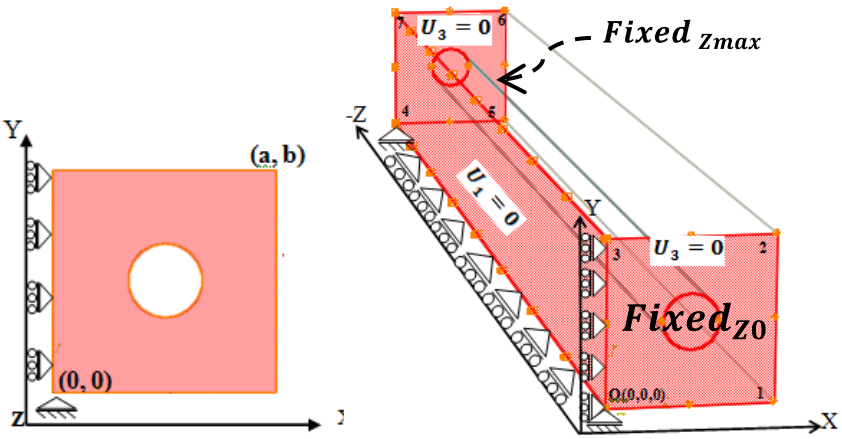

Fig. 7.11. Boundary conditions 2D and 3D (Fixed-Fixed) models

The composite exhibits a controlled expansion with the imposed displacement conditions. In addition to the above boundary conditions, the moisture boundary conditions are same as those applied during the diffusion analysis (Eq. 7.1-7.3). The problem is modelled using the 2D plain strain conditions as well. The displacement along the fibre (*Z*) direction is zero. Hence the strain components

$$\varepsilon_z = \gamma_{xz} = \gamma_{yz} = 0 \tag{7.7}$$

$\gamma_{xz} = \gamma_{yz} = 0$ means τ_{xz} and τ_{yz} are zero, and $\varepsilon_z = 0$ means

$$\varepsilon_z = \frac{\sigma_z}{E} - \mu\frac{(\sigma_x+\sigma_y)}{E} = 0 \quad => \sigma_z = \mu(\sigma_x + \sigma_y) \tag{7.8}$$

In the 3D finite element framework Eq. (3.8) is solved for the basic solution variable of nodal concentration (c). The hygral strain ($\boldsymbol{\epsilon_h}$) is calculated from nodal concentration $\boldsymbol{\epsilon_h} = \beta_h c$ and the stresses are computed using constitutive stress-strain relationships. From the hygroelastic properties given in Table 5.1, the theoretical stress inside the resin at the moisture saturation is calculated from the relation:

$$\sigma_{matrix} = \beta_h c E \tag{7.9}$$

The hygromechanical behaviour is analysed using coupled temperature displacement procedure available on Abaqus. The moisture diffusivity (D_m) is defined in terms of equivalent thermal diffusivity (D_t). Using the combination of thermal conductivity (k), the mass density (ρ) and the specific heat (c_p), the thermal diffusivity can be defined as $D_t = k/(\rho c_p)$. However, it is the ratio that is important rather than the values of the individual parameters. The domains were meshed using displacement and thermally coupled elements C3D8T and CPE4T respectively for 3D and 2D simulations.

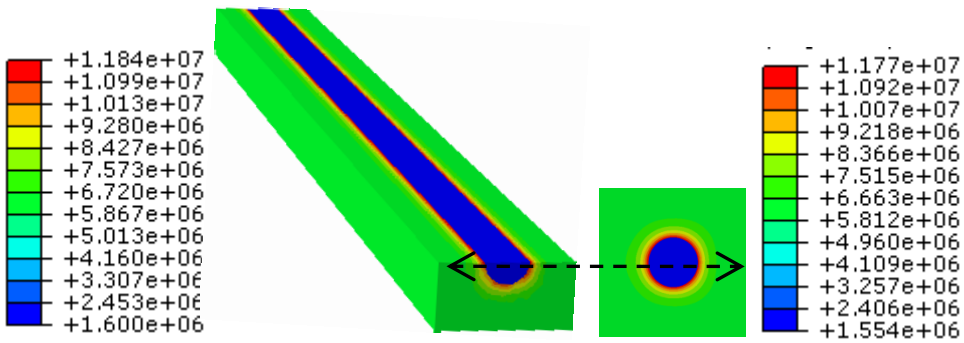

Fig. 7.12. Von-Mises distribution in 3D and corresponding 2D plane strain model

Fig. 7.12 shows the Von-Mises stress contours in 3D and corresponding 2D plane strain models. The stresses at the moisture saturation are illustrated. The stress magnitudes in the matrix, fibre and at interface are almost identical for both the models. The peak interfacial stresses are encountered near the fibre edges where the free expansion of the matrix is prevented.

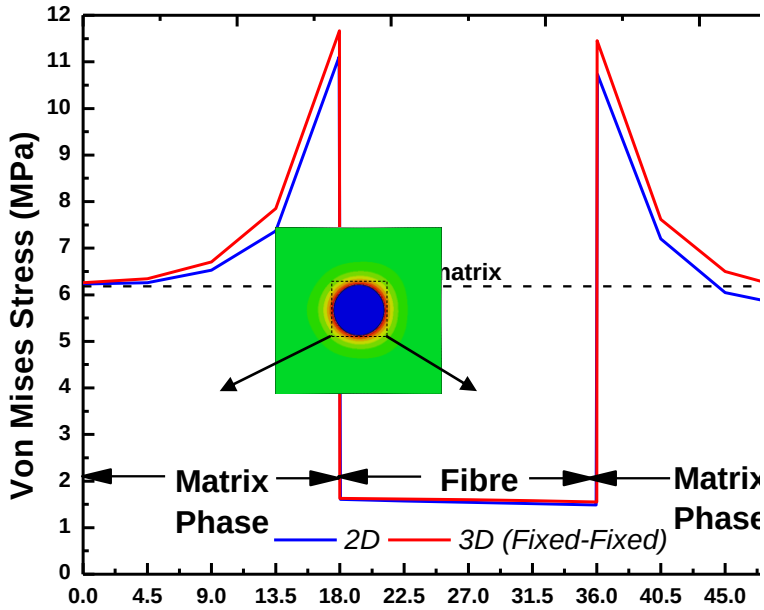

Fig. 7.13 Von-Mises stresses variations for 3D (Fixed-Fixed) and 2D plane strain model

Fig. 7.13 shows the variation of Von-Mises stress in the central plane across the fibre. The stress in neat resin as per Eq. 7.9 is plotted for reference. The stresses inside matrix away from the fibre-matrix interface are close to the applied stress. The stresses rise rapidly as the interface is approached peaking at the interface, which is almost double of the stress in the matrix. It demonstrates the importance of bond between the fibre and the matrix. Also this region of high stress

concentration is susceptible to deterioration due to fatigue and matrix softening. Clearly, 2D plane strain analysis, as has been widely reported, captures the phenomenon well and 3D analysis is not warranted in case of the fibre ends are restrained from motion. However, the fibre ends seldom have such condition. Therefore, *fixed-free* condition is modelled in 3D.

7.3.2 Condition 2: Fixed-Free boundaries

The *Fixed-Fixed* boundary condition emulates the condition that exists far away from the ends of the fibre, where the longitudinal strain (ε_z) is negligible. At the free surface the fibre is free to move. Thus, *Fixed-Fixed* condition does not hold good. The 3D analysis allows us to apply different boundary conditions at the two ends of the fibre and investigate the stresses close to its free edge. For this purpose, the *Fixed-Free* boundary condition is applied to allow the free expansion along the fibre axis (*-Z direction*). This is achieved by removing the displacement boundary constraint $(U_3 = 0)$ from plane *4-5-6-7*. Plane *4-5-6-7* is referred as $Free_{Zmax}$ plane this time. The boundary conditions remain same for plane *O-1-2-3* and it is referred as $Fixed_{Z0}$ plane. The boundary conditions are:

$$U_1 = 0 \ \ (on\ left\ plane\ i.e.\ x = 0) \tag{7.10}$$

$$U_3 = 0\ (on\ Fixed_{\ Z0}\ plane\ i.e.\ z = 0) \tag{7.11}$$

$$U_1 = U_2 = U_3 = 0 \ \ \ (at\ corner\ O(0,0,0)\ ) \tag{7.12}$$

Fig. 7.14 illustrates the *Fixed-Free* conditions. Apart from the displacement boundary condition, the moisture boundary conditions remain similar (Eq. 7.1-7.3).

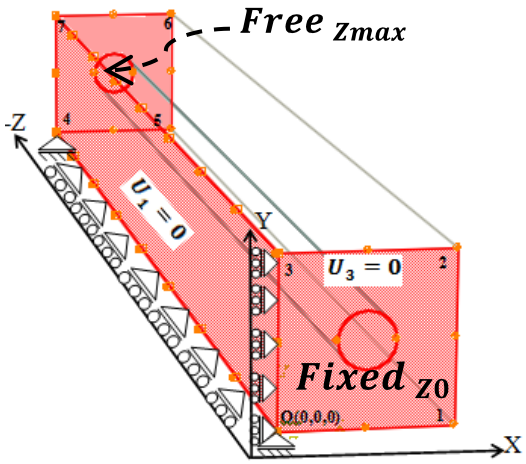

Fig. 7.14 Fixed-Free Boundary condition

The Fixed-Free boundary conditions resulted in a dramatic variation of stress-strain behaviour when compared with Fixed-Fixed boundary conditions. Graphs in Fig. 7.15 shows the Von-Mises stresses at the fixed edge across the central plane of the fibre from moisture exposed plane (*X=0*) to the opposite plane (*X=54*) on $Fixed\ _{Z0}$ plane.

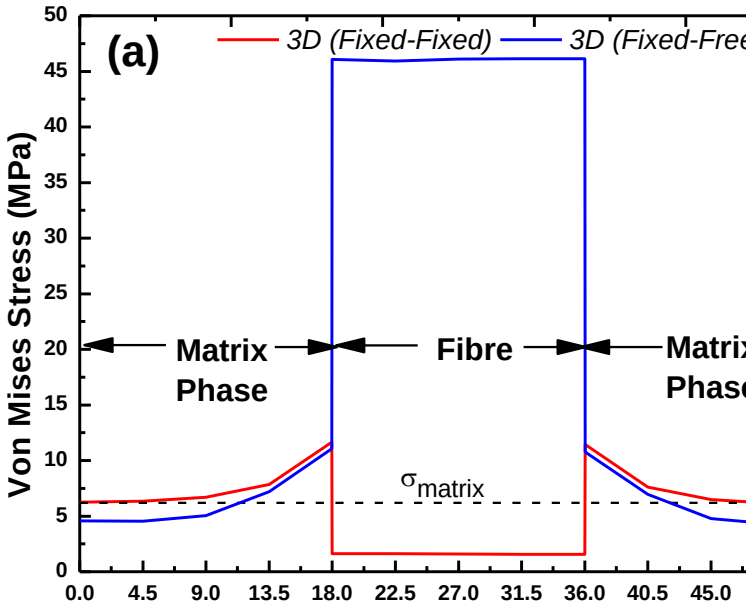

Fig. 7.15 Von-Mises stress (Fixed-Fixed and Fixed-Free conditions)

In the *Fixed-Free* case the stresses away from the fibre were marginally lower than that in the *Fixed-Fixed* case. As one end of the composite is allowed to move the resin is able to release stress. In fact in neat resin there would be no stress in this case. However, interfacial stresses develop due to the presence of the fibre that does not expand due to moisture diffusion. While the matrix tends to expand in the *Z*-direction the fibre impede that expansion. This is illustrated in the deformation of the $Free\ _{Zmax}$ plane in Fig. 7.16. As a result, the fibre experiences a pull from the matrix, while it in turn pushes the matrix back. This gives rise to interfacial stresses. Due to this a steep rise in the Von-Mises stresses in the fibre can be noticed for *Fixed-Free* condition in Fig. 7.15. The rise in Von-Mises stresses can be attributed to high magnitude σ_z that resulted from the free expansion along the fibre direction

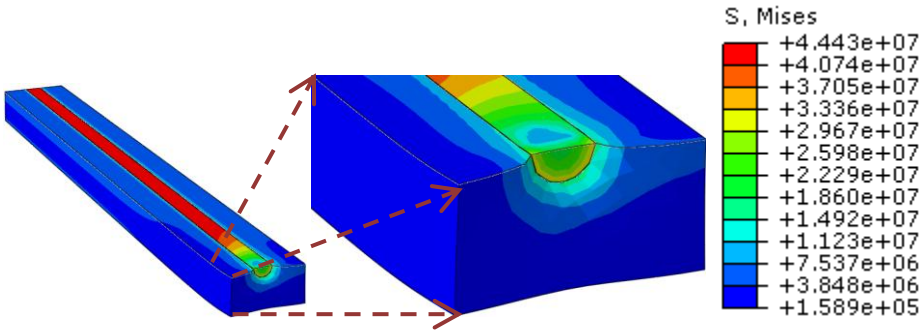

Fig. 7.16. Deformation of Free Plane

It is clear from the graph that the interfacial stresses in the fixed-free case are more than four times larger than that in the fixed-fixed case. Thus, failure in the interface is far more likely near the free edge. This phenomenon has not been captured in the analyses reported so far.

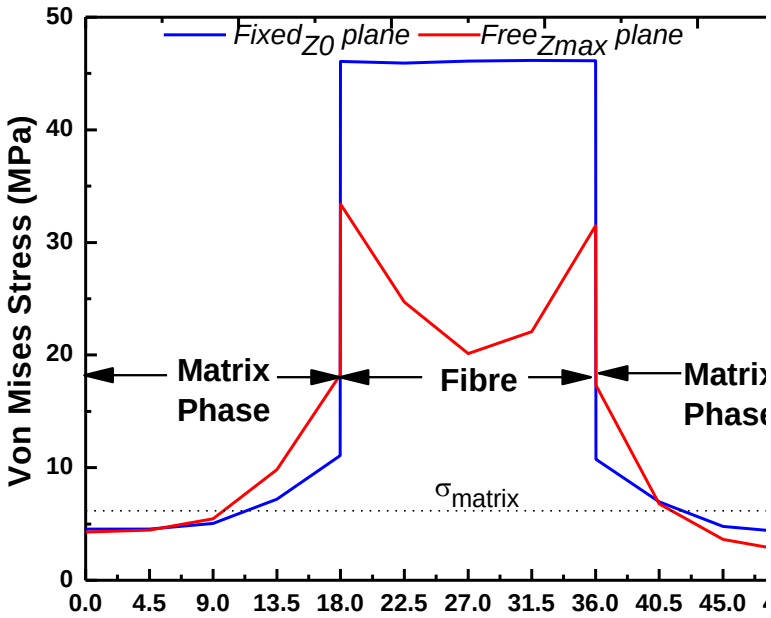

Fig. 7.17. Von-Mises stress on Fixed and Free planes (Fixed-Free condition)

Fig. 7.17 compares the Von-Mises stresses close to the $Fixed_{Z0}$ and $Free_{Zmax}$ planes. There is a considerable variation in the stresses. As we approach the free edge the Von-Mises stresses come down. This is expected as the free boundary must be stress free. It is seen in the stress contours of Fig. 7.16 that the Von-Mises stress for the most length of the fibre is around 40MPa. The stress reduces rapidly within the 10% distance from the free edge. As the enhanced stresses in the fixed-free condition are not reported hetherto it is important to validate these results with another method. The finite element simulation results `with a simple concentric cylinder assemblage approach.

7.3.3 Concentric cylinder assemblage (CCA) model of free expansion

The concentric cylinder assemblage CCA approach (Hashin and Rosen, 1964; Jacquemin *et. al.,* 2006; Ramezani *et. al.,* 2014) analyses the composite as a micro-model of two co-axial cylinders of different constituent properties. The simplified model allows the stress strain variations calculated using the formulations based on the linear elastic theory.

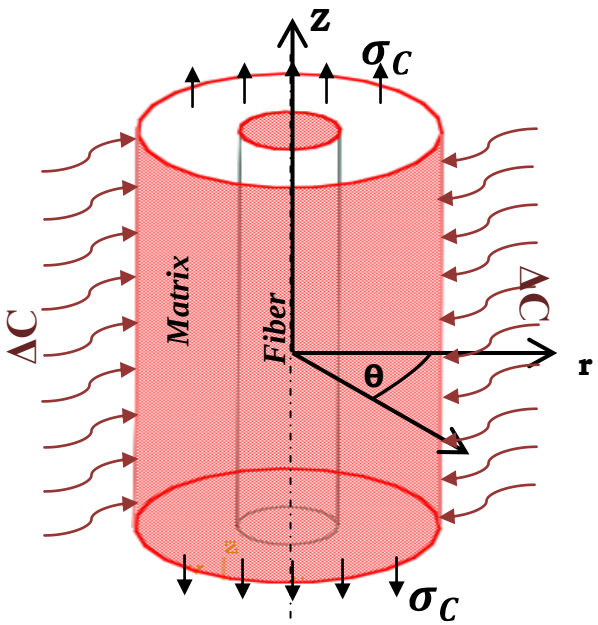

Fig. 7.18 Schematic of concentric cylinder assemblage (CCA) model

It is assumed that a stress-free composite is subjected to a moisture concentration change (ΔC). The concentration is assumed uniform throughout the matrix while the fibre remains dry. Fig. 7.18 is the detailed schematic of the CCA analytical model. This is an axisymmetric condition and the equilibrium equations in the *r*-, θ-, *z*-coordinate system reduce to:

$$\frac{d\sigma_r}{dr} + \frac{\sigma_r - \sigma_\theta}{r} = 0 \qquad (7.13)$$

The two independent displacements are u and w in the r- and z-directions, respectively. The strains are given by:

$$\varepsilon_r = \frac{du}{dr}, \varepsilon_\theta = \frac{u}{r}, \varepsilon_z = \frac{dw}{dz} \tag{7.14}$$

Note that only ordinary derivatives are used, because *u* cannot be a function of *z* due to the infinitely long cylinders, and *w* cannot be a function of *r*, otherwise iso-strain conditions in the z-direction are violated. The displacement field given by Eq. 7.14 can be used to write the compatibility condition for strains. The resultant compatibility condition is:

$$\frac{d\varepsilon_\theta}{dr} + \frac{\varepsilon_\theta - \varepsilon_r}{r} = 0 \tag{7.15}$$

Eq. 7.13 and Eq. 7.15 forms the basis of elastic-plastic-viscoplastic analysis. Eq 7.14 provides the strains, and generalized Hooke's law is used to determine the stresses from the strains. When hygral strains are present, they must be subtracted from the total strains derived from Eq 7.14, in order to determine the stresses. Thus the stress components become:

$$\sigma_r = \lambda(\varepsilon_r + \varepsilon_\theta + \varepsilon_z - 3\beta_h \Delta C) + 2G(\varepsilon_r - \beta_h \Delta C) \tag{7.16}$$

$$\sigma_\theta = \lambda(\varepsilon_r + \varepsilon_\theta + \varepsilon_z - 3\beta_h \Delta C) + 2G(\varepsilon_\theta - \beta_h \Delta C) \tag{7.17}$$

$$\sigma_z = \lambda(\varepsilon_r + \varepsilon_\theta + \varepsilon_z - 3\beta_h \Delta C) + 2G(\varepsilon_z - \beta_h \Delta C) \tag{7.18}$$

λ is Lame's constant and G is shear modulus. *E, λ, G,* and β_h are material specific. For a purely hygral loading, i.e. $\sigma_c = 0$, and when Poisson's ratio (ν) of constituents are equal a simpler solution is obtained (Tandon GP, 1995) and the axial stresses in the matrix and fibre are:

$$\sigma_z^{matrix} = (\beta_f - \beta_m)\Delta C E_m \left[\frac{\lambda_1}{\lambda_2}\right]\left[\frac{E_f}{E_C}\right]\left[\frac{V_f}{1-\nu_m}\right] \tag{7.19}$$

$$\sigma_z^{fibre} = -\frac{V_m}{V_f}\,\sigma_z^{matrix} \tag{7.20}$$

Where, $\lambda_1 = \left(1 - \frac{1}{2}\left\{\frac{1-2\nu}{1-\nu}\right\}\left\{\frac{1-E_c}{1-E_f}\right\}\right)$ $and\ \lambda_2 = \frac{1}{2}\left[1 - \frac{E_c}{E_f}\right]$ (7.21)

Here, E_C is the longitudinal modulus of the composite and can be computed using the rule of mixture; v refers the volume fraction. The constants for material are designated by subscripts f and m for fibre and matrix respectively. The stress behaviour observed using the finite element method is compared with CCA approach. Fig. 7.19 depicts the results for stress along the axial (fibre) direction.

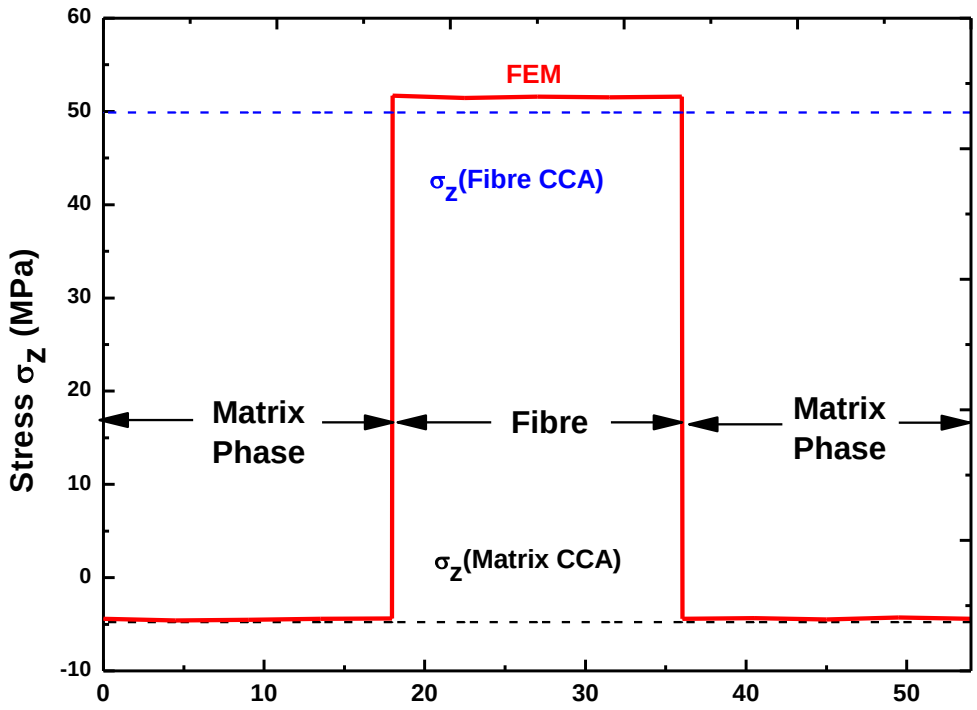

Fig. 7.19 Axial stress along fibre direction (FEM vs. CCA)

The results of finite element modelling are in accordance to the results predicted by concentric cylinder model for both the constituents (*i.e.* fibre and matrix). Evidently, the agreement between the two analyses is very close.

Chapter 8: Conclusions

The research reported in this dissertation can be divided into four main parts:

In the first part diffusion of moisture through a polymer matrix composite is modelled in finite element using Fickian diffusion law. Basic diffusion kinetics of a single filament in resin is illustrated. Effect of neighbourhood filaments is studied along transverse direction through analysis of a number of microstructures with varying number of filaments and inter-filament angle distance. Effect of cluster configuration on diffusion kinetics is presented.

In the second part microstructures of various levels of clustering have been generated. Three different statistical metrics have been presented for characterization of the clustered microstructures. The time to saturate an RVE is considered as a measure of diffusion characteristics and it is correlated with the statistical measures.

In the third part Hygro-mechanical response of polymer matrix composites is reported. Stresses resulting due to moisture ingress are evaluated using a plane strain finite element model. The effect of introducing a fibre in resin is demonstrated by comparing it with the resin only analysis. The effect of neighbouring fibre on the reference fibre is studied through a parametric analysis varying the neighbourhood fibre angle, distance and number.

Finally a comprehensive three-dimensional analysis is performed to evaluate the hygromechanical behaviour of unidirectional fibre reinforced polymer composites. The 2 stage finite element analysis is performed by taking single fibre insertion model first to evaluate the diffusion and then hygromechanical stress-strain behaviour.

The finite element analysis results are further validated by numerical and analytical investigations. The presented research has led to the following specific conclusions:

- The progression of moisture is affected by the presence of filaments and their layout in space. Any addition of the non diffusing filament disturbs moisture evolution that should have been exponential in its absence (in neat resin).
- Filaments act as attractor of moisture. Thus, they hasten the progress of moisture fronts that have not reached them. They impede the progression of moisture front and retard its progress once it has hit the filament.
- Filaments, although not diffusive themselves, do not always lead to an overall lower effective composite diffusivity and reduce the rate of moisture progression.
- Addition of filaments beyond 90° from the reference filament leads to faster moisture progression and higher composite diffusivity. Adding filaments at less than 90° reduces diffusion rate. Filaments at a distance up to 4 times their diameter interact with each other. Filaments with larger distance have little interaction.
- It is not essential to add or reduce filaments in a composite to control its diffusivity. Composites with identical filament

density possessed dramatically different diffusivities depending on their spatial configuration.

- The shape of a clustered configuration heavily influenced the diffusivity of a composite. By carefully designing the cluster configuration a highly durable composite can be developed.
- As time to saturate is a global indicator, AND, that highlights local characteristics, correlated poorly. ACD happens to be a global indicator of spatial distribution of fibres. Understandably, it correlated very well with the time to saturate and showed a very good coefficient of correlation (0.99).
- Ripley's K method is also found to represent the global characteristics of a microstructure but it had a marginally lower correlation (In a variable range 0.86 to 0.98) with time to saturate than ACD depending on the radius of circle of influence (x/r). It can be used as a general measure for diffusion kinetics in fibre matrix composites.
- Stress concentration increases exponentially as the fibres come closer than 3.0R. Thus, in a microstructure the neighbourhood with the closest fibres determine its stress concentration. The angle, on the other hand, is far less sensitive. Thus, any angle between 60° and 120° yields stress concentration close to one another.
- Addition of new fibres in the neighbourhood reduces the peak stress. Thus, it is concluded that a minimal neighbourhood can be studied to gain insight into a large and complex microstructure.

- The diffusion characteristics along fibre direction are notably different from the characteristics across the fibre direction; therefore it becomes imperative to use three dimensional modelling procedures to evaluate the moisture progression characteristics.
- The diffusion results in sharp stress concentration field around the fibre. This distress in the region ultimately softens the matrix in the region that leads to subsequent failure depending on the interfacial strength.
- The 2D plane strain models predict the interfacial stresses accurately in the interiors of the composite where longitudinal stress (σ_z) is negligible. This condition does not hold good near the surface of the composite where expansion due to moisture is expected. The stresses in that region are found to be a few times higher than those obtained based on the plane strain analysis. Thus, interfaces close to the surface are much more prone to degradation than the interior region. Hence 3D analysis is necessary to realistically evaluate the peak interfacial stresses. This is demonstrated by the results of 3D finite element models with two different sets of boundary conditions along the transverse planes.

The microstructural moisture diffusion determines the long term behaviour of FRPs and their durability in humid environments. Any microstructural analysis should begin from the smallest entity. The novelty of this study is the bottom up analytical procedure commencing from the hygromechanical response of smallest entity (single fibre), scaled to its surroundings and then the clustered neighbourhood has been reported. The plane strain theory has been

questioned for its straightforward applicability in depicting 3-dimensional stress behaviour. In addition new statistical measures have been proposed. These statistical measures should be useful in predicting the diffusion kinetics of microstructures with variable clustering and hence predict the lifetime at the structural scale.

The detailed computational experiments propose the new and original industrially relevant results which can be used to improve the reliability and lifetime of FRP structures (e.g. wind turbines, outdoor applications) subjected to humid environments.

In the present investigation the conclusions have been arrived from the study of models with a restricted volume fraction. Therefore applicability of the measures for a range of volume fractions (dilute to dense) must also be explored. The future scope of this work includes the detailed experimental investigations.

References

ABAQUS/STANDARD 6.11; 2014. http://www.simulia.com.

ABAQUS/STANDARD Analysis User's Manual - Vol. II, Dassault Systemes; 2011.

Abhilash AS, Joshi SP, Mukherjee A, Mishnaevsky L Jr. Micromechanics of Diffusion Induced Damage Evolution in Reinforced Polymers. Compos Sci Technol. 2011;3(71):333.

Alger M. Polymer Science Dictionary (2nd ed.). Springer Publishing. ISBN 0412608707; 1997.

Askeland D, Fulay P, Wright W. The Science and Engineering of Materials (6th ed.). Cengage Learning. ISBN 9780495296027; 2010.

Benzarti K, Cangemi L and Dal Maso F. Transverse properties of unidirectional glass/epoxy composites: influence of fibre surface treatments. Compos. A: Appl. Sci. Manuf. 2001; 32(2): 197.

Biwa S, Yamamoto S, Kobayashi F, Ohno N. Computational multiple scattering analysis for shear wave propagation in unidirectional composites. Int. J. Solids Struct. 2004;41:435.

Böhm HJ, Rammerstorfer FG, Micromechanical models for investigating fibre arrangements in MMC's. Proceedings of International Seminar Micromechanics of Materials (MECAMAT). 1993a:383.

Böhm HJ, Rammerstorfer FG, Weisenbek E. Some simple models for micromechanical investigations of fiber arrangement effects in MMCs, Comput. Mater. Sc. 1993b:177.

Böhm HJ. A short introduction to basic aspects of continuum micromechanics. ILSB (Vienna University of Technology) Report [Several important modelling strategies in the field of continuum micromechanics are discussed in this report]. (2012).

Bond DA. Moisture diffusion in a fiber-reinforced composite: Part I – nonfickian transport and the effect of fiber spatial distribution. J. Compos. Mater. 2005;39:2113.

Bonora N, Ruggiero A. Micromechanical modeling of composites with

mechanical interface – Part 1: Unit cell model development and manufacturing process effects. Compos. Sci. Technol. 2006;66(2):314.

Boualem N, Sereir Z. Accelerated aging of unidirectional hybrid composites under the long-term elevated temperature and moisture concentration. Th. App. Fract. Mech. 2011;55(1):68.

Boukhoulda BF, Adda-Bedia E, Madani K. The effect of fiber orientation angle in composite materials on moisture absorption and material degradation after hygrothermal ageing. Compos. Struct. 2006;74:406.

Carter HG, Kibler HG. Langmuir-Type Model for Anomalous Moisture Diffusion In Composite Resins. J. Compos. Mater. 1978;12:118.

Chawla, N., Sidhu, R.S., Ganesh, V.V. Three-dimensional visualization and microstructure-based modelling of deformation in particle-reinforced composites. Acta Mater. 2006; 54:1541.

Clark PJ, Evans FC. Distance to nearest neighbour as a measure of spatial relationships in populations. Ecology 1954;35(4):445.

Clough RW. The finite element method in plane stress analysis. Proceedings of the Second ASCE Conference on Electronic Computation, Pittsburgh, PA. (1960).

Courant R. "Variational methods for the solution of problems of equilibrium and vibrations". Bulletin of the American Mathematical Society. 1943;49:1.

Crank J. The mathematics of diffusion. Oxford University Press, London (1956).

Curtin WA, Takeda N. Tensile Strength of Fiber-Reinforced Composites: I. Model and Effects of Local Fiber Geometry. J Compos. Mater. 1998;32(22):2042.

Diggle PJ, Chetwynd AG. Second-order analysis of spatial clustering for inhomogeneous populations. Biometrics 1991;47:1155.

Diggle PJ, Gratton RJ. Monte Carlo methods of inference for implicit statistical models. Journal of the Royal Statistical Society, Series B 1984;46:193.

Dixon PM. Ripley's K Function. Encyclopedia of Environmetrics. John

Wiley & Sons Ltd. (2002); ISBN: 0471-899976.

Doguwa SI, Upton GJG. Edge-corrected estimators for the reduced second moment measure of point processes. Biometrical Journal 1989;31:563.

Du DX, Zheng QS. A further exploration of the interaction direct derivative (IDD) estimate for the effective properties of multiphase composites taking into account inclusion distribution. Acta Mechanica. 2001;157:61.

Duncan RP. Testing for life historical changes in spatial patterns of four tropical tree species in Westland New Zealand. J. Ecol. 1993;81:403.

Edeson R, Aglietti GS, Tatnall ARL. Conventional stable structures for space optics: The state of the art. Acta Astron. 2010;66(1-2);13.

Eshelby JD. The determination of the elastic field of an ellipsoidal inclusion. Proc. R. Soc. Lond. A. 1957;241:376.

Eslami S, Honarbakhsh-Raouf A, Eslami S. Effects of moisture absorption on degradation of E-glass fiber reinforced Vinyl Ester composite pipes and modelling of transient moisture diffusion using finite element analysis. Corr. Sc. 2014, doi: http://dx.doi.org/10.1016/j.corsci.2014.10.009

Fiedler B, Gojny FH, Wichmann MHG, Nolte MCM, Schulte K. Fundamental aspects of nano-reinforced composites. Compos. Sci. Technol. 2006;66:3115.

Gaines KF, Bryan ALJr, Dixon PM. The effects of drought on foraging habitat selection in breeding wood storks in coastal Georgia. Waterbirds 2000;23:64.

Gamstedt EK, Andersen SI. Fatigue Degradation and Failure of Rotating Composite Structures – Materials Characterisation and Underlying Mechanisms. Risø Report Risø-R-1261 (EN) Risø National Laboratory, Roskilde, Denmark [This report reviews the fatigure damage mechanisms in rotating structures] (2001).

Gamstedt EK, Sjögren BA. Micromechanisms in tension–compression fatigue of composite laminates containing transverse plies. Compos. Sci. Technol. 1999;59(2):167.

Ghosh S, Bai J, Raghavan P. Concurrent multi-level model for damage

evolution in microstructurally debonding composites. Mech. Mater. 2007;39(3):241.

Ghosh S, Nowak Z, Lee K. Quantitative characterization and modeling of composite microstructures by voronoi cells. Acta Mater. 1996;45(6):2215.

Haj-Ali R and Kilic H. Nonlinear constitutive models for pultruded FRP composites. Mech. Mater. 2003; 35:791.

Halpin JC and Kardos JL. The Halpin–Tsai equations: A review. Polym. Engg. Sci. 1976;16:344.

Halpin JC. Primer on composite materials: analysis. Lancaster, PA: Technomic. (1984).

Hashin, Z, Rosen BW. The elastic moduli of fiber-reinforced materials. J. Appl. Mech. 1964;31(2):223.

Hashin Z, Shtrikman S. A variational approach to the theory of the elastic behavior of multiphase materials. J. Mech. Phys. Solid. 1963;11:127.

Hrach R, Novak S, Svec M. Correlation between morphology and transport properties of composite films: Charge transport in composites. Appl. Surf. Sc. 2006;252:5516.

Image J Analyzer; 2013. http://rsbweb.nih.gov/ij/docs/intro.html.

Jacob A, Steven MA, Brett AB. Micromechanics of Composite Materials: A Generalized Multiscale Analysis Approach. Elsevier (2013).

Jacquemin F, Fréour S, Guillén R. Analytical Modeling of Transient Hygro-elastic Stress Concentration - Application to embedded optical fiber in a non-uniform transient strain field. Compos. Sci. Technol. 2006;66:397.

Jiang M, Jasiuk I, Ostoza-Starzewski M. Apparent thermal conductivity of periodic two-dimensional composites. Comput. Mater. Sc. 2002;25(3):329.

Jiang X, Kolstein H, Bijlaard FSK. Moisture diffusion in glass–fiber-reinforced polymer composite bridge under hot/wet environment. Compos. Part B - Engg. 2014;45:407.

Joliff Y, Belec L, Heman MB, Chailan JF. Experimental, analytical and numericalstudy of water diffusion in unidirectional composite

materials – interphase impact. Comput. Mater. Sci. 2012;64:141.

Joliff Y, Belec L, Chailan JF. Modified water diffusion kinetics in an unidirectional glass/fibre composite due to the interphase area: Experimental, analytical and numerical approach. Compos. Struct. 2013;97:296.

Joliff Y, Rekik W, Belec L, Chailan JF. Study of the moisture/stress effects on glass fibre/epoxy composite and the impact of the interphase area. Compos. Struct. 2014;108:876.

Jost, W. Diffusion in Solids, Liquids, Gases. Academic Press, New York (1960).

Karalekas D, Cugnoni J, Botsis J. Monitoring of hygrothermal ageing effects in an epoxy resin using FBG sensor: A methodological study. Compos. Sci. Technol. 2009;69:507.

Karbhari VM, Chin JW, Hunston D, Benmokrane B, Juska T, Morgan R, Lesko JJ, Sorathia U, Reynaud D. Durability Gap Analysis for Fiber-Reinforced Polymer Composites in Civil Infrastructure. J. Compos. Construct. 2003;7;238.

Klusemann B, Böhm HJ, Svendsena B. Homogenization methods for multi-phase elastic composites with non-elliptical reinforcements: Comparisons and benchmarks. Eu. J. Mech. 2012;34:21.

Kondo K, Taki T. Moisture diffusivity of unidirectional composites. J Compos. Mater. 1982;16:82.

Kuna M, Zun DS. Three-dimensional cell model analyses of void growth in ductile materials, Int. J. Fract. 1996;8:235.

Kundu CK, Maiti DK, Sinha PK. Nonlinear Finite Element Analysis of Laminated Composite Doubly Curved Shells in Hygrothermal Environment. J. Reinf. Plast. Compos. 2007;26(14):1461.

Lebensohn R, Rollett A, Suquet P. Fast Fourier Transform-based modelling for the determination of micromechanical fields in polycrystals. J. Min. Met. Mater. Soc. 2011;63:1318.

Lee MC, Peppas NA. Models of moisture transport and moisture induced stresses in epoxy composites. J. Compos. Mater. 1993;27(12):1146.

Lee S, Chiang H, Lin C, Huang H, Dong D. Finite element analysis of

thermo-debonding mechanism in dental composites. Biomaterials 2000;21:1315.

Li S, Lee LJ, Cartro J. Effective mass diffusivity in composites. J. Compos. Mater. 2002;36(14):1709.

Li X, Binienda WK and Goldberg RK. Finite Element Model for failure study of two-dimensional triaxially braided composite NASA/TM—2010-216372. Available electronically at http://gltrs.grc.nasa.gov.

Lin MW, Berman JB, Khoshbakht M, Feickert BA, Abatan AO. Modeling of moisture migration in an FRP masonary structure. Building and Environment 2006;41:646.

Loh WK, Crocombe AD, Wahab MMA, Ashcroft IA. Modelling anomalous moisture uptake, swelling and thermal characteristics of a rubber toughened epoxy adhesive. Int. J. Adhes. Adhes. 2005;25:1.

López Jiménez F, Pellegrino S. Folding of fiber composites with a hyperelastic matrix. Int. J. Sol. Struct. 2012;49(3-4):395.

MacSleyne JP, Simmons JP, Graef MD. On the use of 2-D moment invariants for the automated classification of particle shapes. Acta Mater. 2008;56(3):427.

MATLAB 7.13; 2013. http://www.mathworks.com.

Melro AR, Camanho PP, Pinho ST. Generation of random distribution of fibres in long-fibre reinforced composites. Compos. Sci. Technol. 2008;68(9):2092.

Mishnaevsky L Jr, Brøndsted P. Micromechanical Modeling of Strength and Damage of Fiber Reinforced Composites. Annual Report on EU FP6 Project UpWind Integrated Wind Turbine Design (WP 3.2). Risø National Laboratory, Roskilde, Denmark [This report overviews the micromechanical modelling concepts in FRP composites] (2007).

Mishnaevsky L Jr, Schmauder Siegfried. Continuum mesomechanical finite element modeling in materials development : A state-of-the-art review. Appl. Mech. Rev. 2001;54.

Mukherjee A, Arwikar SJ. Performance of GFRP rebars in tropical environment-I. Structure scale tests, ACI Struct. J. 2005a;102:745.

Mukherjee A, Arwikar SJ. Performance of GFRP rebars in tropical

environment-II. Microstructural tests, ACI Struct. J. 2005b;102:816.

Murthy PLN, Mital SK, Shah AR. Probabilistic Micromechanics and Macromechanics for Ceramic Matrix Composites Probabilistic Micromechanics and Macromechanics for Ceramic Matrix Composites. NASA Technical Memorandum 4766 (1997).

Myles JP, Flenley EC, Fieller NRJ, Atkinson HV, Jones H. Statistical tests for clustering of second phases in composite materials. Philosophical Magazine A 1995;72(2):515.

Noda N, Nisitani H, Takase Y and Shukuwa Y. Two-dimensional and axisymmetric unit cell models in the analysis of composite materials. Compos. Struct. 2005; 69: 429.

Nogales S, Böhm HJ. Modeling of the thermal conductivity and thermomechanical behavior of diamond reinforced composites. Int. J. Engg. Sc. 2008;46(6):606.

Okabe T, Takeda N. Size effect on tensile strength of unidirectional CFRP composites— experiment and simulation. Compos. Sci. Technol. 2002;62(15):2053.

Pindera MJ, Bednarcyk BA. An efficient implementation of the Generalized Method of Cells for Unidirectional, Multi-Phased Composites with Complex Microstructures. Compos. B: Engg. 1999;30:87.

Pyrz R, Bochenek B. Topological disorder of microstructure and its relation to stress field. Int. J. solids struct. 1998;35:2413.

Pyrz, R. Quantitative description of the microstructure of composites .1. Morphology of unidirectional composite systems. Compos. Sci Technol. 1994;50(2):197.

Pyrz, R., Correlation of microstructure variability and local stress-field in 2-phase materials. Mater. Sc. Engg: A. 1994;177(1-2):253.

Raghavan P, Li S, Ghosh S. Two scale response and damage modeling of composite materials. Finite Elem. Anal. Des. 2004;40:1619.

Ramamurty U, Seshacharyulu T. Effect of spatial inhomogeneity in fibre packing on the strength variability of Al–matrix composites. Mater. Sc. Engg.: A. 1999;268:97.

Ramezani Dana H, Jacquemin F, Fréour S, Perronnet A, Casari P, Lupi C.

Numerical and experimental investigation of hygromechanical states of glass fiber reinforced polyester composites experienced by FBG sensors. Compos. Struct. 2014;116:38.

Ray BC Effects of Changing Environment and Loading Speed on Mechanical Behavior of FRP Composites. J. Reinf. Plast. Compos. 2006;25(12):1227.

Reuss A. Berechnung der Fliesßgrenze von Mischkristallen auf Grund der Plastizitätsbe dingung für Einkristalle. ZAMM 1999;9:49.

Ripley BD. The second-order analysis of stationary point processes. J. Appl. Prob. 1976;13:255.

Ripley BD. Modelling spatial patterns. J. Royal Stat. Soc.: B 1977;39:172.

Romanov V, Lomov SV, Swolfs Y, Orlova S, Larissa G, Verpoest I. Statistical analysis of real and simulated fibre arrangements in unidirectional composites. Compos. Sci. Technol. 2013;87:126.

Sahimi M. Applications of percolation theory. Taylor & Francis London. (1994).

Segurado J and LLorca J. Computational micromechanics of composites: The effect of particle spatial distribution. Mech. Mater. 2006; 38: 873.

Segurado J, Gonzalez C, LLorca J. A numerical investigation of the effect of particle clustering on the mechanical properties of composites. Acta Mater. 2003;51:2355.

Sevostianov I, Kushch V.Effect of pore distribution on the statistics of peak stress and overall properties of porous material. Int. J. Solids Struct. 2009;46:4419.

Shan Z, Gokhale AM. Representative volume element for non-uniform microstructure. Comput. Mater. Sci. 2002;24(3):361.

Shen CH, Springer GS. Moisture absorption and desorption of composite materials. J. Compos. Mater.1976;10:2.

Singh BN, Verma VK. Hygrothermal Effects on the Buckling of Laminated Composite Plates with Random Geometric and Material Properties. J. Reinf. Plast. Compos. 2009;28(4):409.

Springer GS. Environmental effects on composite materials. Technomic

Lancaster (PA). (1984).

Steglich D, Siegmund T, Brocks W. Micromechanical modelling of damage due to particle cracking in reinforced metals. Comput. Mater. Sci. 1999; 16:404.

Tandon GP, Use of Composite Cylinder Model as Representative Volume Element for Unidirectional Fiber Composites, J. Compos. Mater. 1995;29(3):385.

Tang X, Whitcomb JD, Li Y, Sue HJ. Micromechanics modeling of moisture diffusion in woven composites. Compos. Sci. Technol. 2005;65:817.

Tang X. Micromechanics of 2D woven composites. Ph.D. Dissertation, Department of Aerospace Engineering, Texas A&M University; 2001.

Thomas M, Boyard N, Perez L, Yarny J, Delaunay D. Representative volume element of anisotropic unidirectional carbon–epoxy composite with high-fibre volume fraction. Compos. Sci. Technol. 2008;68:3184.

Torquato S. Nearest-neighbour statistics for packings of hard spheres and disks. Phy. Rev. E 1995;51:3170.

Tsai Jia-Lin, Chi Yang-Kai. Investigating thermal residual stress effect on mechanical behaviours of fiber composites with different fiber arrays. Compos. B: Engg. 2008;39:714.

Tsai YI, Bosze EJ, Barjasteh E, Nutt SR. Influence of hygrothermal environment on thermal and mechanical properties of carbon fiber/fiberglass hybrid composites. Compos. Sci. Technol. 2009;69:432.

Turner MJ, Clough RW, Martin HC, Topp L. Stiffness and deflection analysis of complex structures. J. Aero. Sc. 1956;23(9):805.

Vaddadi P, Nakamura T, Singh RP. Inverse analysis for transient moisture diffusion through fiber-reinforced composites. Acta. Mater. 2003a;51:177.

Vaddadi P, Nakamura T, Singh RP. Transient hygrothermal stresses in fibre reinforced composites: a heterogeneous characterization approach. Compos. A: Appl. Sci. Manuf. 2003b;34:719.

Vaughan TJ and McCarthy CT. Micromechanical modelling of the

transverse damage behaviour in fibre reinforced composites. Compos. Sci. Technol. 2011;71: 388.

Vlahinić Ivan, Thomas Jeffrey J, Jennings Hamlin M, Andrade José E. Transient creep effects and the lubricating power of water in materials ranging from paper to concrete and Kevlar. J. Mech. Phy. Solids. 2012;60(7):1350.

Voigt W. Uber die Beziehung zwischen den beiden Elasticitäts-Constanten isotroper Körper. Ann. Phys. 1889;38:573.

Wang W, Sain M, Cooper PA. Study of moisture absorption in natural fiber plastic composites. Compos. Sci. Technol. 2006;66:379.

Wenbin Y, Tian T. Variational asymptotic method for unit cell homogenization of periodically heterogeneous materials. Int. J. Solids Struct. 2006;44:3738.

Whitney JM. Moisture effects in epoxy matrix composites. TECHNICAL REPORT AFML-TR-77-17:Mechanics and Surface Interactions Branch Nonmetallic Materials Division. (1978).

Wilding SE, Fullwood DT. Clustering metrics for two-phase composites. Comput. Mater. Sci.2011;50:2262.

Wilt TE. On the finite element implementation of the generalized method of cells micromechanics constitutive model, NASA Technical Report NASA-CR-195451. (1995).

Wu M, Johannesson B, Geiker M. A study of the water vapor sorption isotherms of hardened cement pastes: Possible pore structure changes at lowrelative humidity and the impact of temperature on isotherms. Cement and Concrete Research 2014;56:97.

Yagoubi JE, Lubineau G, Roger F, Verdu J. A fully coupled diffusion-reaction scheme for moisture sorption-desorption in an anhydride-cured epoxy resin. Poly. 2012;53:5582.

Yang Q, Cox B. Cohesive models for damage evolution in laminated composites. Int. J. Fract. 2005;133:107.

Youssef Z, Jacquemin F, Gloaguen D, Guillen R. A multi-scale analysis of composite structures: Application to the design of accelerated hygrothermal cycles. Compos. Struct. 2008;82:302.

Zangenberg J, Larsen JB, Østergaard RC, Brøndsted P. Methodology for

characterisation of Glass Fibre Composite Architecture. Plast. Rub. Compos. 2012;41(4-5):187.

Zhang H, Ericson M, Varna J and Berglund L. Transverse single-fibre test for interfacial debonding in composites: 1. Experimental observations. Compos. A: Appl. Sci. Manuf. 1997; 28: 309.

Zheng QS, Du DX. An explicit and universally applicable estimate for the effective properties of multiphase composites which accounts for inclusion distribution. J. Mech. Phys. Solids. 2001;49(11):2765.

Zienkiewicz OC. The Finite Element Method (3rd ed.) McGraw-Hill: New York. (1977).

Zulkifli R. Surface Fracture Analysis of Glass Fibre Reinforced Epoxy Composites Treated with Different Type of Coupling Agent. European Journal of Scientific Research 2009; 29:55.

Publications

Jain D, Mukherjee A, Kwatra N. Local Micromechanics of Moisture Diffusion in Fiber Reinforced Polymer Composites. *International Journal of Heat and Mass Transfer* 2014;**76**:199-209.

Jain D, Mukherjee A, Kwatra N. Topological Disorder of Microstructure in Fibre-Reinforced Polymer Composites: Diffusion Response. *Journal of Reinforced Plastics and Composites* 2015;**34(1)**:49-59.

Jain D, Mukherjee A, Kwatra N. Effect of Fibre Topology on Hygro-Mechanical Response of Polymer Matrix Composites. *International Journal of Heat and Mass Transfer* 2015;**86**:787-795.

Jain D, Mukherjee A, Kwatra N. Numerical Modelling of Moisture Diffusion in FRP with Clustered Microstructures. *Applied Mathematical Modelling* 2015. doi:10.1016/j.apm.2015.09.021.

Jain D, Mukherjee A. Three-Dimensional Hygromechanical analysis of fibre polymer composites: Effect of Boundary Conditions. *Composites Part-B: Engineering* 2015. Revision Submitted (R1).

Jain D, Mukherjee A. Stresses in FRP Composites due to Moisture Diffusion. Sixth International conference on Theoretical, Applied, Computational and Experimental Mechanics *(ICTACEM 2014)*. Indian Institute of Technology, Kharagpur (Dec. 29-31, 2014).